TRANSIENT SIMULATION OF RADIATION-INDUCED CHARGE TRAPPING AND INTERFACE TRAP FORMATION USING A PHYSICALLY-BASED, THREE-CARRIER TRANSPORT MODEL IN SILICON DIOXIDE

By

Randall J. Milanowski

Dissertation

Submitted to the Faculty of the

Graduate School of Vanderbilt University

in partial fulfillment of the requirements

for the degree of

DOCTOR OF PHILOSOPHY

in

Electrical Engineering

December, 1999

Nashville, Tennessee

Approved:

Lloyd Massengill, Chair
Robert Weller
Sokrates Pantelides
Ron Schrimpf
Ken Galloway

For Shania

ACKNOWLEDGEMENTS

First, I want to thank Lloyd Massengill for acting courageously to create the place for this project at Vanderbilt. If not for him, I would certainly have pursued those other opportunities in country music or songbird biology; and thank-you Chris Nicklaw for getting me started that summer of '95 in Boston and for not telling me then how crazy most people thought you were. Also, barring any more skydiving accidents, I'm sure we will all be thanking Manish Pagey for years to come for always knowing how to do everything in record time. He has worked miracles.

I also thank the RHTCAD program manager Jeff Johann and sponsors Jim Howard and Andy Weber for their support and continued confidence in the project and my committee members Sokrates Pantelides, Robert Weller, Ron Schrimpf and Ken Galloway for their numerous insights and suggestions.

Thanks to Sam, Max, Glenda, Ken, and Pointy Lingo for taking care of me all these years. Thanks to Laura, Janet, and Amy at South Beach for their support during the development of the proton release kinetics.

TABLE OF CONTENTS

LIST OF FIGURES

LIST OF TABLES

CHAPTER I

INTRODUCTION

Overview of Radiation-Induced Failure Modes

Ionizing radiation poses a serious threat to semiconductor integrated circuits (ICs) that are required to operate reliably in radiation environments, for example, circuits used in space vehicles and satellites. Damage due to ionizing radiation, e.g., X-rays, γ-rays, energetic electrons and ions, begins with the generation of electron-hole pairs in device materials, e.g., regions of silicon and silicon dioxide (SiO_2). Energetic particles can produce electron-hole pairs in silicon and SiO_2 regions simultaneously. It is convenient, however, to categorize IC radiation response into Total Ionizing Dose (TID) effects, which are characterized by charge generation in the oxide, and Transient Radiation (TR) effects, which are typically associated with charge generation in silicon.

Charge generation in oxide regions causes temporary as well as long-lasting changes in device parameters that can prevent ICs from functioning properly. The temporary component of device parameter shift is a direct consequence of transient imbalances in mobile charge density in the oxide; this type of response is observable under high dose-rate, pulsed-irradiation conditions. The long-lasting parameter shift results from electrically-active defects, specifically trapped charges and interface traps that are created by interactions between these mobile carriers and pre-existing imperfections in the SiO_2 network. The build-up of these defect populations is cumulative with dose; consequently, permanent parameter shift can be observed after long exposures at low dose-rates as well as after high dose-rate, pulsed exposures as long as enough total dose is delivered to the oxide. This behavior is reflected in the label "Total Ionizing Dose" effects and constitutes a primary failure mode for satellites subjected to low dose-rate, background radiation in space. Although transient device parameter shift due to pulsed-irradiation of device oxides can be important, transient charge generation processes in silicon, in particular due to energetic ions and nuclear fission events, account for two additional radiation-induced failure modes, termed "Single Event" effects and "Dose-Rate" effects. These are often referred to collectively as "Transient Radiation" effects.

Project Summary

Focus: Radiation Effects on Silicon Dioxide

Because Single Event and Dose-Rate effects are primarily defined by carrier transport in silicon, standard device simulators provide the basic capability, i.e, semiconductor carrier transport models, to study these effects. Analogous capabilities for Total Ionizing Dose effects, however, have not been available because standard device simulators do not provide models for carrier transport and defect formation in oxide regions. A significant barrier to achieving such a model has been the lack of an integrated approach accounting for the coupled nature of the carrier transport and defect generation processes that occur in irradiated oxides. This dissertation describes the development of a such an approach.

Motivation: Simulation-Based Hardness Optimization

It has become standard practice in current commercial semiconductor industry to reduce empiricism in performance optimization using Technology Computer Aided Design (TCAD). Traditional TCAD practices integrate the activities of numerical process and device simulation, device model parameter extraction, and circuit simulation [1]. Formal methods for Design of Experiments (DOE) can be carried out using this simulation framework to create and calibrate Response Surface Models (RSM) that can be used to search large, multi-variable design spaces for regions that satisfy performance, yield, and manufacturing constraints [2]. The ability to simulate large numbers of process variations can reduce the number of experimental split lots, and therefore cost and time, required to develop and advance process technologies [3]. Given the advantages of TCAD approaches to performance optimization, it is logical to pursue their application for radiation response optimization. Numerical device simulation methods for analyzing Single Event effects are relatively well-established [4, 5, 6, 7]. Because of their highly global nature, Dose-Rate effects must be addressed using circuit-level simulation [8, 9]. However, device simulation has been applied to help verify analytical photocurrent models needed to simulate Dose-Rate effects in circuits [10]. The underlying motivation for the present work is the need for improved device simulation methods for analyzing Total Ionizing Dose effects, i.e., models for the radiation

response of device oxides.

Approach: Electron, Hole, and Proton Continuity Equations

This dissertation presents a novel solution to modeling the effects of ionizing radiation on semiconductor device oxides, specifically, a coupled model for electron, hole, and proton transport in silicon dioxide (SiO_2) suitable for transient device simulation-based prediction of the buildup of both major types radiation-induced defects: trapped oxide charge and interface traps. This model provides two fundamental "firsts" in physically-based TID effects simulation: (1) the representation of hole-trapping-induced proton release in a self-consistent system of electron, hole, and proton continuity equations, and (2) the application of a continuity equation-based model for dispersive proton transport.

Methods for representing electron and hole generation, recombination, transport and trapping in SiO_2 in a system of continuity equations are fairly well-established (though not as widely used as similar semiconductor transport models). However, these methods have not addressed interface trap formation which is a significant, sometimes dominant determinant of radiation response. Chapter II reviews the physical mechanisms that have been previously accommodated in numerical simulation of radiation effects in SiO_2 and identifies hydrogen chemistry as the basic issue that must be addressed in order to account for interface trap formation processes. Chapter III focuses specifically on this hydrogen chemistry and concludes with the specification of proton release kinetics in the form of a generation rate. Chapter IV outlines the complete numerical approach to integrating proton release kinetics and transport calculation methods.

Overview of Simulation Studies

Chapters V-VII report several simulation studies that address both the basic scientific aspects of the research as well as the engineering/design motivation behind this project. Chapter V focuses on the primary novel scientific aspect of the research, specifically, the numerical approach to modeling hydrogen-mediated interface trap formation. In this study, the three coupled continuity equations and dispersive proton transport equations are applied (in one spatial dimension) in a study of a pulsed-irradiation/switched bias experiment. In Chapters VI and VII, a two-dimensional

implementation of the electron and hole continuity equations is applied to clarify two types of MOS technology hardening problems that are dominated by hole trapping in SiO_2. Chapter VI considers edge-effects in Mesa-isolated, Silicon-On-Insulator (SOI) nMOSFETs using both process and device simulation; Chapter VII applies the same two-carrier transport model in a study of the the dependence on field implant parameters of radiation-induced leakage in parasitic nMOSFETs associated with LOCal Oxidation of Silicon (LOCOS) isolation.

CHAPTER II

PHYSICAL MECHANISMS

Overview

The major physical mechanisms underlying radiation-induced device parameter shift are organized, roughly in order of occurrence as follows:

1. Electron-hole pair generation and geminate recombination
2. Electron transport and free carrier recombination
3. Hole transport, trapping, and hydrogen release
4. Trapped hole annealing/compensation, hydrogen transport, and interface trap formation

Device parameter shift associated with charge generation in SiO_2 can be transient in nature (due to generation/recombination and transport processes) but is also uniquely characterized by permanent or semi-permanent parameter shift due to the gradual buildup of electrically active defects (charge trapping and interface trap formation). Under steady-state, low dose-rate conditions, the instantaneous concentrations of free carriers are insufficient to directly cause parameter shifts and only the long-term defect formation processes can be observed. On the other hand, because these different mechanisms are characterized by widely varying time scales, their different effects on metal-oxide-semiconductor structures can be separately identified under high dose-rate, pulsed-irradiation conditions. This is illustrated in Figure 1 which indicates the contributions of different physical mechanisms to the time-dependent response of transistor threshold voltage to a pulsed exposure to ionizing radiation (a similar discussion of this type of experiment is found in [11]).

The basic elements of a pulsed exposure of an nMOS transistor are illustrated in Figure 2. A short pulse of radiation generates electron-hole pairs throughout the device material. The pulse is delivered with the gate biased positively relative to the substrate and the source and drain grounded. By monitoring the threshold or flatband voltage as a function of time after a short pulse of radiation, the underlying physical mechanisms can be observed somewhat separately and in the order listed above. Here it must be the case that the $I_D - V_G$ measurement indicated in

Figure 2 can be performed rapidly compared to the response times. The following discussion of physical mechanisms is aided by references to specific features of Figure 1. Particular attention is devoted in this chapter to identifying the basic calculational methods applicable to these mechanisms that are required for physically-based numerical simulation.

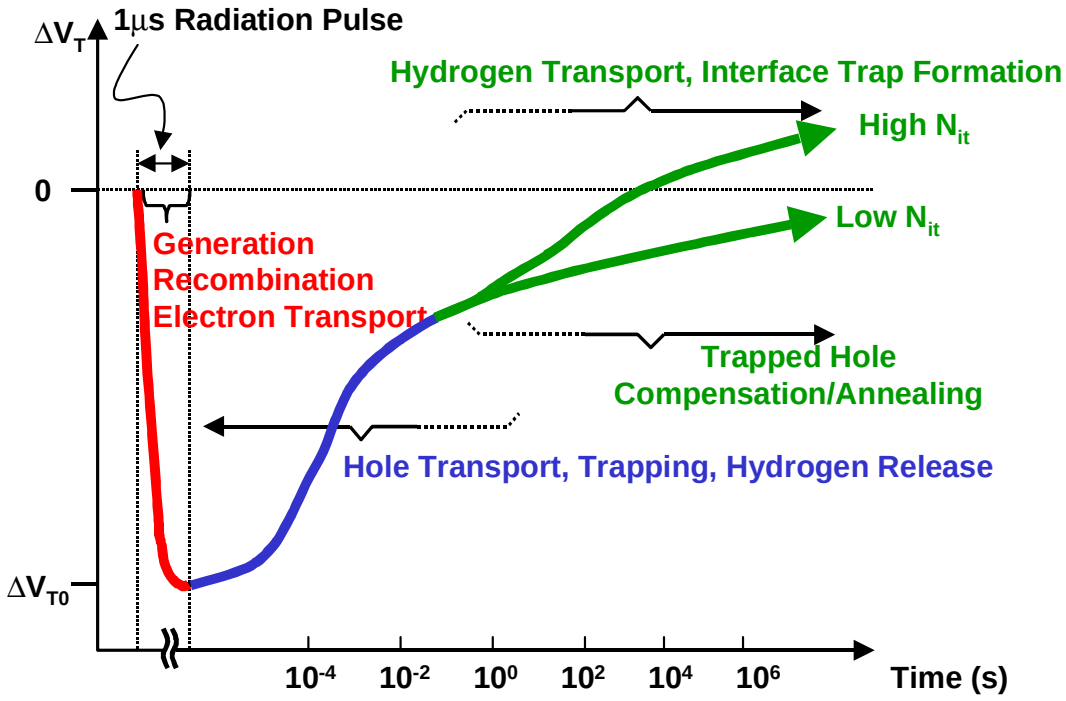

Figure 1: Typical time-dependent response of nMOSFET threshold voltage to pulsed irradiation at 300 K. The initial negative shift, ΔV_{T0}, is due to mobile holes remaining in the oxide after rapid recombination and electron transport processes are complete. The subsequent recovery period is due to slower transport of holes out of the oxide. The initial recovery in V_T is incomplete because some holes are trapped at defect sites before escaping. The more gradual recovery observed after about 1 second is due to slower trapped hole neutralization and interface trap formation processes.

Carrier Generation and Geminate Recombination

Free carriers are introduced in the oxide through the generation of electron-hole pairs when energetic particles (photons, electrons, protons, etc.) pass through device layers. Figure 3 illustrates this ionization process. The intensity of electron-hole pair generation in a given oxide layer depends on how much energy is deposited in that layer. The reader is referred to the review in [12] and references therein for discussions of methods for calculating "dose vs. depth"

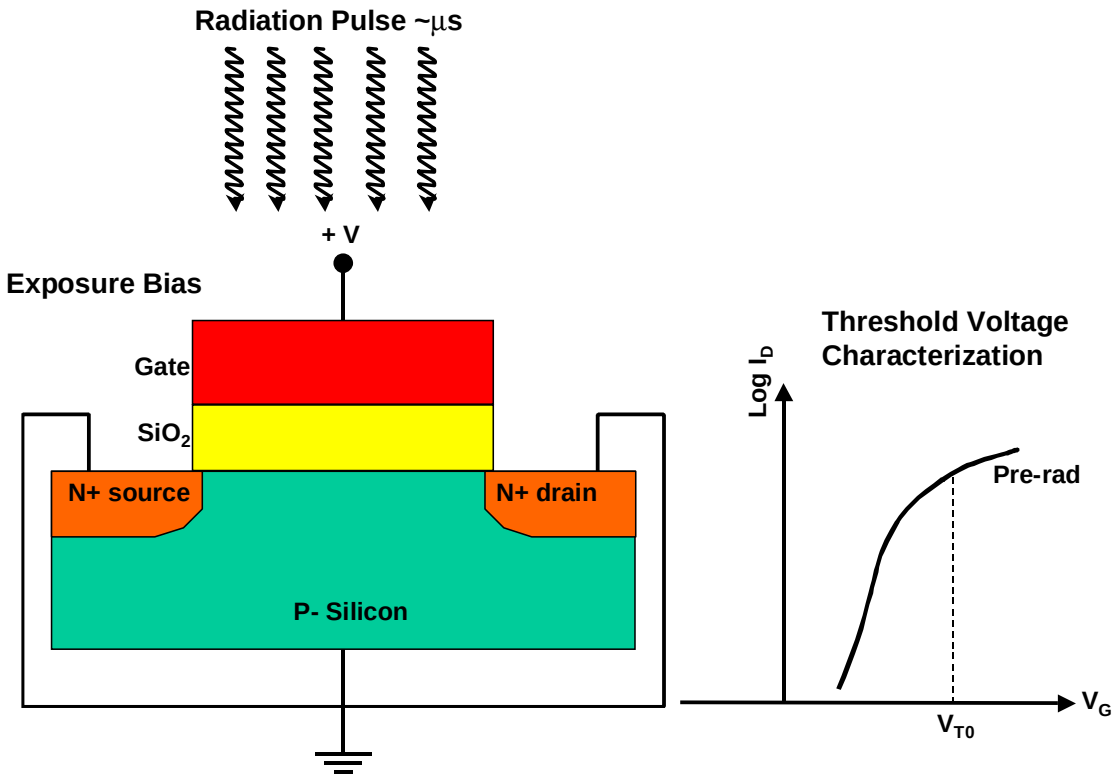

Figure 2: Illustration of typical pulsed-irradiation exposure of nMOSFET and $I_D - V_G$ measurement for monitoring radiation-induced threshold voltage shift.

curves for different device topologies, radiation sources, packaging, and shielding scenarios. Here it is sufficient to state that once the instantaneous dose-rate, $\dot{D}$ (rad(SiO_2)/s), at a given position in the oxide is known, the rate of electron-hole pair generation at that location and time, G(ehp/$cm^3 \cdot s$), is obtained by multiplying by the electron-hole pair generation factor for SiO_2, g_{ox}:

$$G = \dot{D} g_{ox} \tag{1}$$

where, using the average electron-hole pair creation energy for SiO_2 ($\sim 18 \pm 3$eV) [13], g_{ox} can be obtained as:

$$g_{ox} = \left(\frac{1 \quad \text{Gy}}{100 \quad \text{rad}}\right)\left(\frac{1 \quad \text{J}}{\text{kg} \cdot \text{Gy}}\right)\left(\frac{1 \quad \text{eV}}{1.6 \times 10^{-19} \quad \text{J}}\right)\left(\frac{2.2 \quad \text{g}}{\text{cm}^3}\right)\left(\frac{1 \quad \text{ehp}}{18 \quad \text{eV}}\right) \tag{2}$$

$$= 7.6 \times 10^{12} \frac{\text{ehp}}{\text{cm}^3 \cdot \text{rad}(SiO_2)} \tag{3}$$

Some of the electron-hole pairs instantly recombine, i.e., before any transport in a macroscopic sense has occurred. This view of recombination is most appropriate under conditions where the electron-hole pairs are sufficiently isolated that they can be considered non-interacting. Under these so-called "geminate" conditions, the recombination probability is determined by the competing effects of Coulomb attraction between the electron and hole (which tends to bring them together) and the electric field, E (which acts to separate them). The geminate recombination probability is quantified in a field-dependent fractional yield, Y(E). The derivation of Y(E) first provided by Onsager [14] to explain recombination in ionized gases is based on Brownian motion in a potential representing the effects of coulomb attraction and the applied field. The same basic explanation has been accepted for experimentally observed Y(E) in irradiated SiO_2 [15, 16]. Figure 4 illustrates the field-dependence typical of geminate recombination probability in oxide.

The condition that electron-hole pairs are non-interacting is not, in practice, always absolutely satisfied. Strictly speaking, for two different electron-hole pairs to be considered "non-interacting" the mean distance separating those pairs, λ, should be greater than the average separation distance between an electron and its sibling hole [17]. The former quantity is a decreasing function of the incident particle stopping power, i.e., pairs are created closer together for particles with high stopping power. The latter quantity, known as the electron-hole pair thermalization distance, r_t, is thought to be around 5 or 10 nm for SiO_2 [17]. For incident radiation with

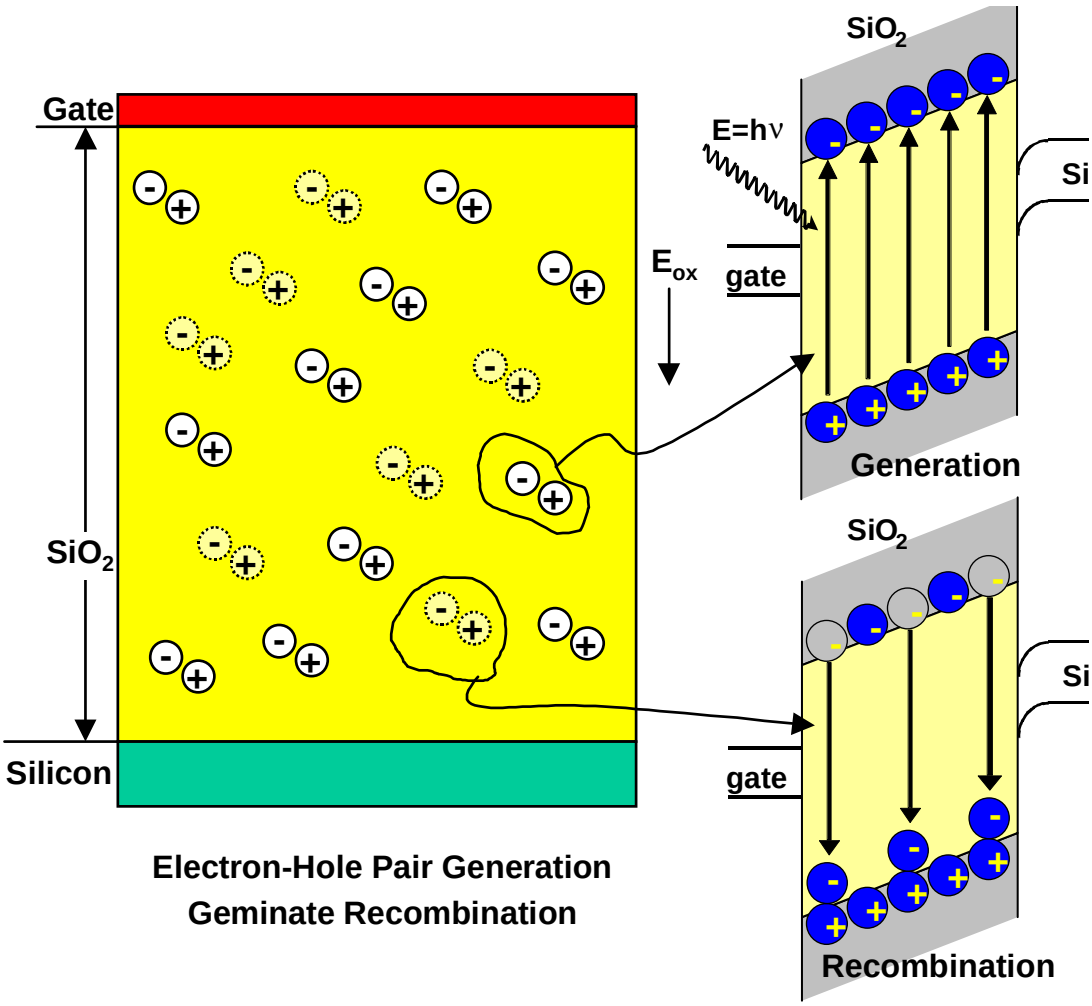

Figure 3: Ionizing radiation produces electron-hole pairs in the oxide. Some of these pairs are instantly lost to geminate recombination.

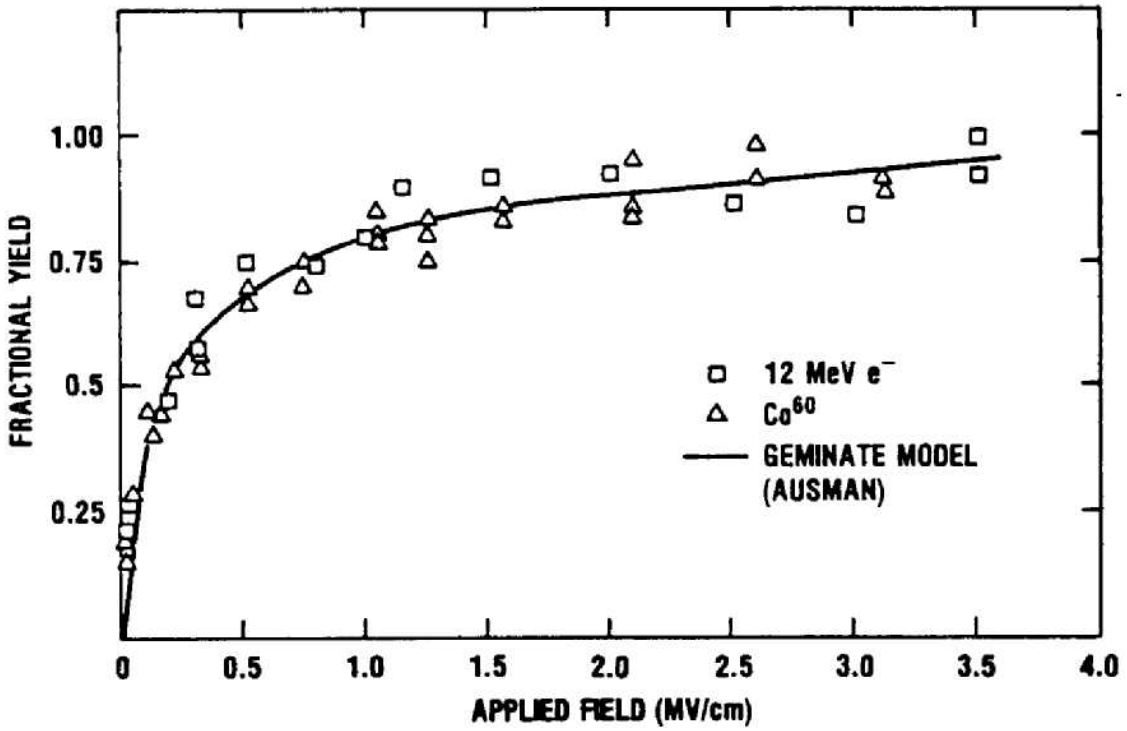

Figure 4: Typical field dependence of the fractional electron-hole pair yield associated with geminate recombination

stopping power less than 10 MeV/g·cm^2, e.g., high energy electrons, $\lambda > 10$ nm and the idealized picture of non-interacting pairs can be considered valid [17]. Practically speaking, however, exposure environments may contain particles, such as protons, whose stopping power exceeds 10 MeV/g·cm^2. Although the idealized picture of non-interacting pairs is violated under these conditions, the geminate model provides reasonable predictions up to about 100 MeV/g·cm^2. This is understandable if one considers that even under conditions where the pairs are not truly isolated, the overall competition between Coulomb force and applied field that is postulated in analyses like that of Onsager may still be established. In any case, the most important aspect of the geminate recombination concept is that it applies specifically to initial recombination, i.e., before carrier transport begins. This view justifies the use of Y(E) as a scaling factor to obtain a field-dependent net generation rate, $G' = G \cdot Y(E)$, required in continuity equation-based approaches to modeling carrier transport in SiO_2. Carrier transport mechanisms are best discussed after making a few comments about the relative mobilities of electrons and holes in SiO_2.

Electron and Hole Mobilities

There is a vast difference in the mobilities of electrons and holes in SiO_2 [17, 18, 19, 20]. Hole motion is governed by effective mobilities that vary from 10^{-11} up to 10^{-4}cm^2/V·s. This extremely wide range derives from the strong dependence on temperature, field, and also, due to unique features of dispersive transport, an apparent dependence on time and oxide thickness [17]. The mobility of electrons is much higher under virtually all conditions - approximately 20 cm^2/V·s at room temperature and rising to 40 cm^2/V·s at lower temperatures; at high fields the electron velocity saturates at about 10^7 cm/s [17, 19].

Electron and Hole Transport

As a result of the high mobility of electrons, they are swept toward the positively biased gate and either escape the oxide or recombine with a hole well before holes have moved from the point of origin. Both these possibilities are illustrated in Figure 5. The electrostatic effects of the holes that are left behind produce the initial negative shift in V_T after pulsed irradiation (Figure 6). The $I_D - V_G$ curves shown in Figure 6 illustrate an important aspect of positive charge located in the

bulk of the oxide; specifically, a given charge distribution in the oxide produces the same effect as an applied gate voltage, and thus results in a fixed, lateral translation in current vs. gate voltage measurements. This will be contrasted later with the "stretchout effect" of interface traps. It must be understood that, in case of mobile positive charge, i.e., free holes, the measurement time must be rapid compared to hole transport times in order to observe this ideal, undistorted translation.

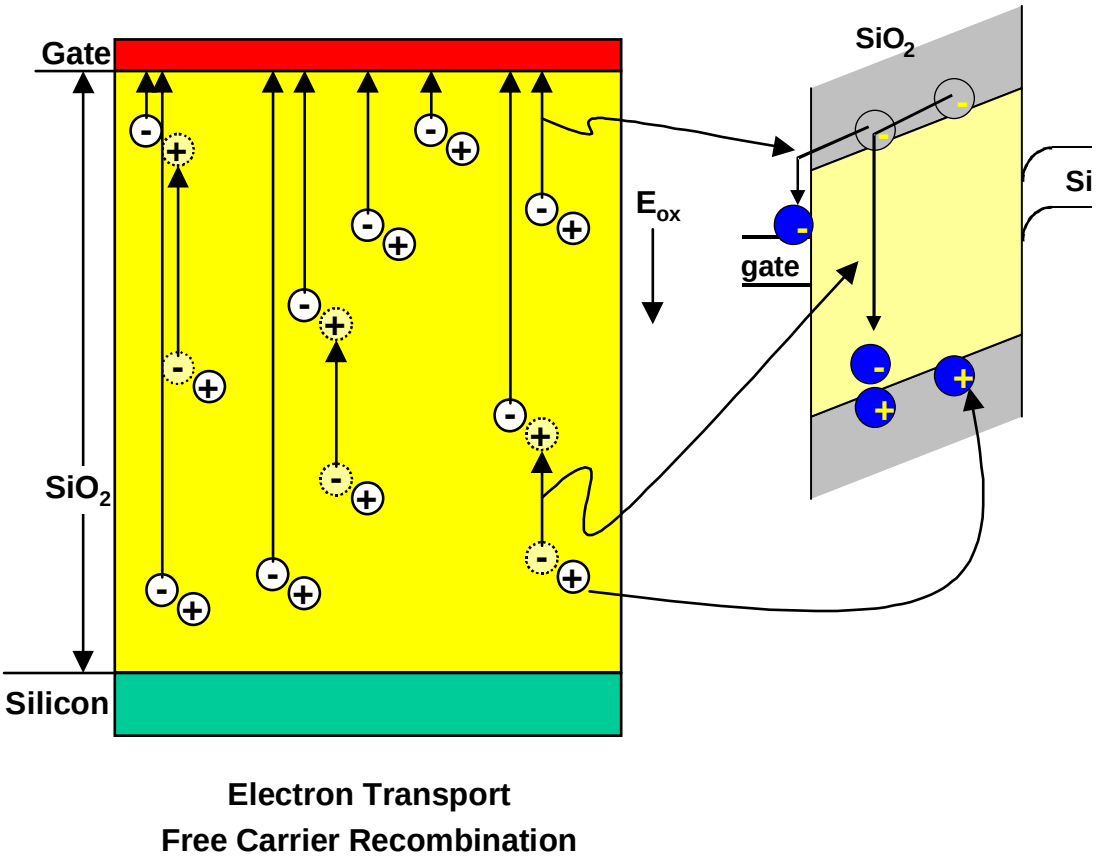

Figure 5: Transporting electrons either escape the oxide or recombine with a hole; holes remaining in the oxide following these processes cause a lateral shift in $I_D - V_G$ measurements toward more negative gate voltages.

As mentioned, there is a possibility that some electrons may recombine with holes before escaping the oxide (Figure 5). This results in a smaller apparent fractional yield and, consequently, initial threshold shift. Here we are speaking of a recombination process involving carriers that have already survived the period of geminate recombination. As such, it is not explicitly accommodated in the fractional yield concept described above. This recombination process is often

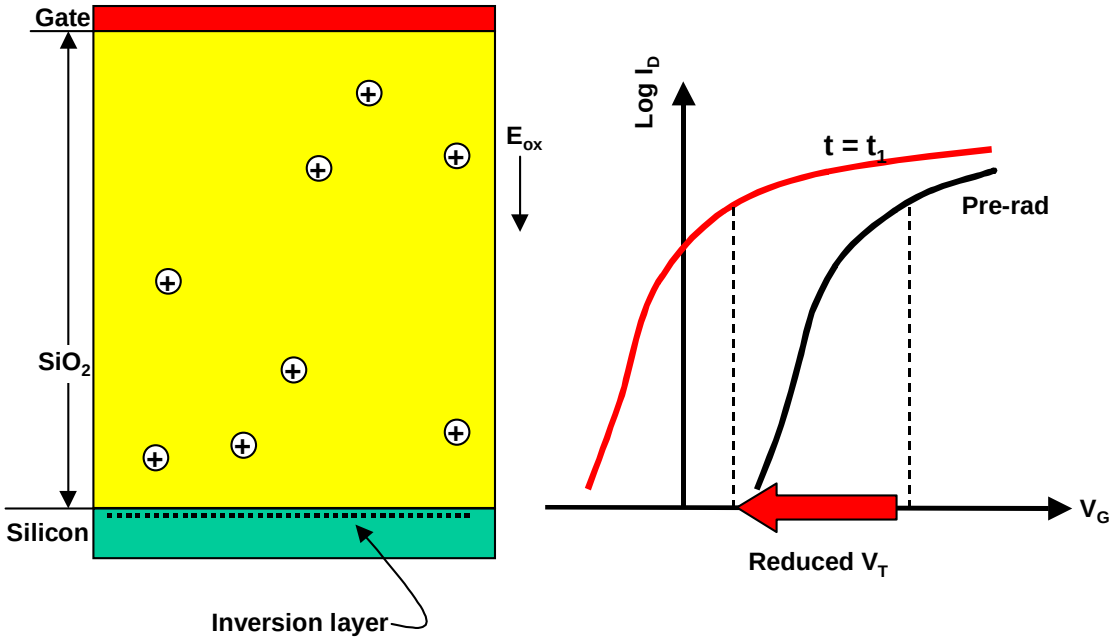

Figure 6: Following the radiation pulse, the holes that survive all recombination processes attract substrate electrons to the Si-SiO_2 interface. A given distribution of holes produces a fixed negative translation in $I_D - V_G$ measurements, thus reducing threshold voltage and increasing leakage current.

neglected in analyses of exposure conditions in which geminate conditions are satisfied; specifically, with electron-hole pairs distributed sparsely throughout the oxide, electrons that survive initial recombination have a small chance of encountering holes as they travel through the oxide. There are, however, several problems with this view that have particular relevance to the present work.

First, hole trapping processes can eventually produce space-charge effects which may draw electrons toward the interior regions of the oxide [21]. Under these conditions it may become important to account for recombination between electrons and transporting (as well as trapped) holes.

Second, at sufficiently high dose-rates, similar space-charge effects can be caused directly by large densities of free holes. In this case, recombination between mobile holes and electrons must be considered to avoid predicting unphysically high instantaneous densities of mobile electrons as well as holes.

Third, recombination between transporting electrons and holes has also been found to be important in cases of incident radiation with very high-stopping power, specifically, heavy ion strikes [22, 23, 24]. Although failure modes due to ion strikes are usually associated with charge generation in active semiconductor regions, the trend toward smaller device dimensions has motivated the investigation of possible failure modes associated with ionization of SiO_2 by heavy charged particles. One of these studies [24], in fact, constitutes a significant precedent in the area of interest in the present work, i.e, the application of numerical solutions of coupled electron and hole continuity equations for simulating carrier transport and trapping in SiO_2.

Continuity Equation Approach to Carrier Transport in SiO_2

Electron-hole pair recombination in ion-induced charge tracks in SiO_2 has previously been considered in the context of a carrier transport problem described by differential equations containing terms for drift, diffusion, and recombination processes [22, 23, 24]. For a dense column of charge the problem has been expressed as follows:

$$\frac{\partial n_{\pm}}{\partial t} = D_{\pm}\nabla^2 n_{\pm} \mp \mu_{\pm} E \sin\theta \frac{dn_{\pm}}{dt} - \alpha n_{+} n_{-} \tag{4}$$

where:

$n_{\pm}$ is the density of positive (or negative) charge,

D is the diffusivity ($D/\mu = kT/q$),

μ is the mobility of the carriers,

E is the applied field (assumed to lie in the x-direction),

θ is the angle between the electric field and the initial charge track, and

α is the recombination coefficient ($\alpha = q(\mu_+ + \mu_-)/\varepsilon\varepsilon_0$ [25, 26])

In early studies [22, 23], analytical solutions for fractional hole yield associated with ion strikes were obtained from this equation by imposing as an initial condition a cylindrically symmetrical charge density distribution,

$$n_{\pm}(\mathbf{r}, 0) = \frac{N_0}{\pi b^2} \exp\left(-\frac{r^2}{b^2}\right) \tag{5}$$

where N_o is the total number of electron-hole pairs generated per unit length, b is the characteristic width of the charge cylinder, and $\mathbf{r}$ is the position coordinate relative to the center of the track. In [24], however, numerical simulation methods were applied to solve this problem without the approximations made in previous analytical solutions. Here, Equation 4 is properly recognized as a standard system of continuity equations for electrons and holes in which drift-diffusion equations are assumed to describe the carrier current densities. Applying this method for more general-purpose analyses requires a number of modifications. For example, rather than represent electron-hole pair generation through an initial condition, $G' = G \cdot Y(E)$ must be used as a generation term in the continuity equations. The transport equations must also be coupled to Poisson's equation and trapping equations; the necessity of these and several other additions is clarified in the following sections on hole transport and trapping. Some of these improvements can be found in several reports of numerical simulation of transient photoconductivity and charge trapping SiO_2 [27, 28, 29, 30, 31, 32, 33]. However, the distinction cited in the above discussion between initial recombination processes and those occurring after transport begins is not clearly acknowledged in previous work and is crucial to proper physical interpretation of the equations, specifically, in understanding the precise physical interpretation of the two different mathematical representations of electron-hole pair recombination, i.e., Y(E) covers *initial* recombination and αnp covers recombination *after* transport begins.

Dispersive Transport

A typical approximation in the continuity equation approach to carrier transport is the use of drift-diffusion equations for the carrier flux densities [27, 28, 29, 30, 31, 32, 33]. Simple drift-diffusion methods are acceptable in cases where transport is governed by a well-defined mobility. This is observed to be the case for bulk-limited electron transport. However, hole transport in SiO_2 defies predictions based on the usual concept of mobility. This is easily demonstrated in transient photoconductivity measurements like that depicted in Figure 7 [34, 35].

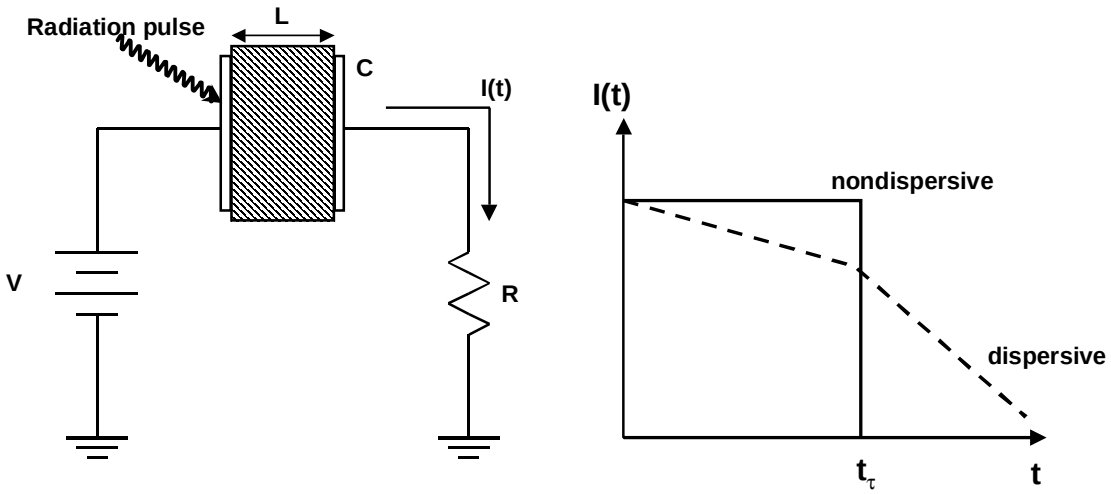

Figure 7: Schematic illustration of non-dispersive and dispersive behavior in a transient photoconductivity experiment.

In this experiment, a flash of light generates electron-hole pairs at the positively biased surface of an MOS capacitor. The motion of the holes across the oxide produces a transient current in the external circuit. In Figure 7, the dashed line labeled "dispersive" represents the experimentally observed behavior. The solid line labeled "nondispersive" represents the result expected for a sheet of carriers transporting according to a well-defined mobility. In this case, the motion of the initial surface charge is described by a propagating Gaussian wave packet, i.e., the mean displacement is proportional to the elapsed time, the ratio of the dispersion to the mean decreases with time as $t^{-1/2}$, and an unambiguous transit time can be related to the mobility according to $\mu = L^2/(t_\tau V)$ [35].

In dispersive transport, however, there is a wide distribution in the transit times of different carriers, giving the appearance of a time-dependent mobility, or alternatively, a distribution in

mobilities among different holes. This "anomalous transit-time dispersion" is a characteristic of numerous amorphous solids [35] in which transient photocurrent response cannot be predicted using simple drift-diffusion equations. For MOS devices, the transit time dispersion spreads out the time-dependent recovery in threshold voltage observed as holes leave the oxide (see Figure 1). The effect of holes transporting out of the oxide on $I_D - V_G$ measurements is illustrated in Figure 8. The variation in hole transport distances indicated in this figure illustrates the dispersive nature of hole transport.

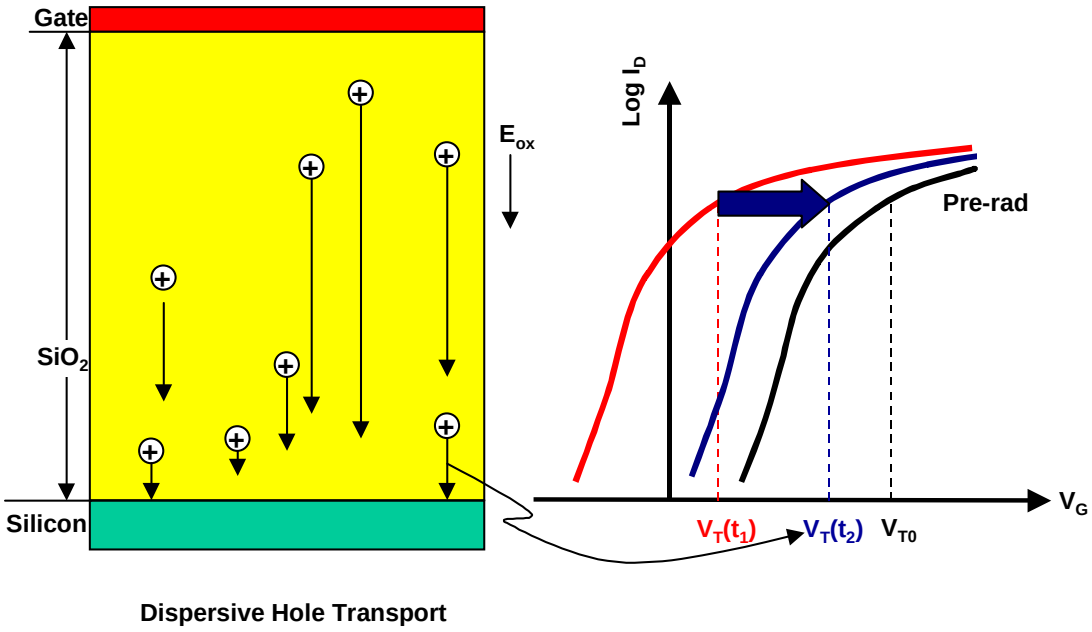

Figure 8: During the hole transport phase ($t_1 < t < t_2$), many holes escape the oxide, thus reducing the net positive charge density in the oxide and shifting $I_D - V_G$ curves positively along the gate voltage axis.

The dispersive nature of hole transport has been described in terms of a phonon-assisted tunneling process [18, 36] as well as by drift-diffusion transport that is repeatedly interrupted by trapping and detrapping from a broad distribution of states near the oxide valence band [18, 37, 38, 39]. Two distinct (but mathematically equivalent) quantitative methods have been applied to these physical models. The phonon-assisted tunneling process is addressed with Continuous Time Random Walk (CTRW) methods [36, 40] and the modified drift-diffusion model is addressed with Multiple Trapping-Detrapping (MTD) methods [37, 38, 39, 41, 42].

Phonon-Assisted Tunneling (Continuous Time Random Walk)

The phonon assisted tunneling process (also termed polaronic hopping) is illustrated schematically in Figure 9. Here, the wide dispersion in the macroscopic transit times of individual holes is attributed to a wide distribution in the amount of time a given hole pauses between discrete tunneling events. A likely microscopic origin of the wide distribution in pausing times is a statistical distribution of tunneling distances, associated with disorder in the SiO_2 network [18], specifically disorder that randomizes the distance between nonbonding-oxygen orbitals. It has been suggested that energy transfer to the SiO_2 network associated with the phonon-assisted tunneling process liberates protons from hydrogen-related defects in the oxide [43]. The significance of this for subsequent interface trap formation processes will be discussed later, however, it is not explicitly addressed in CTRW transport calculation methods.

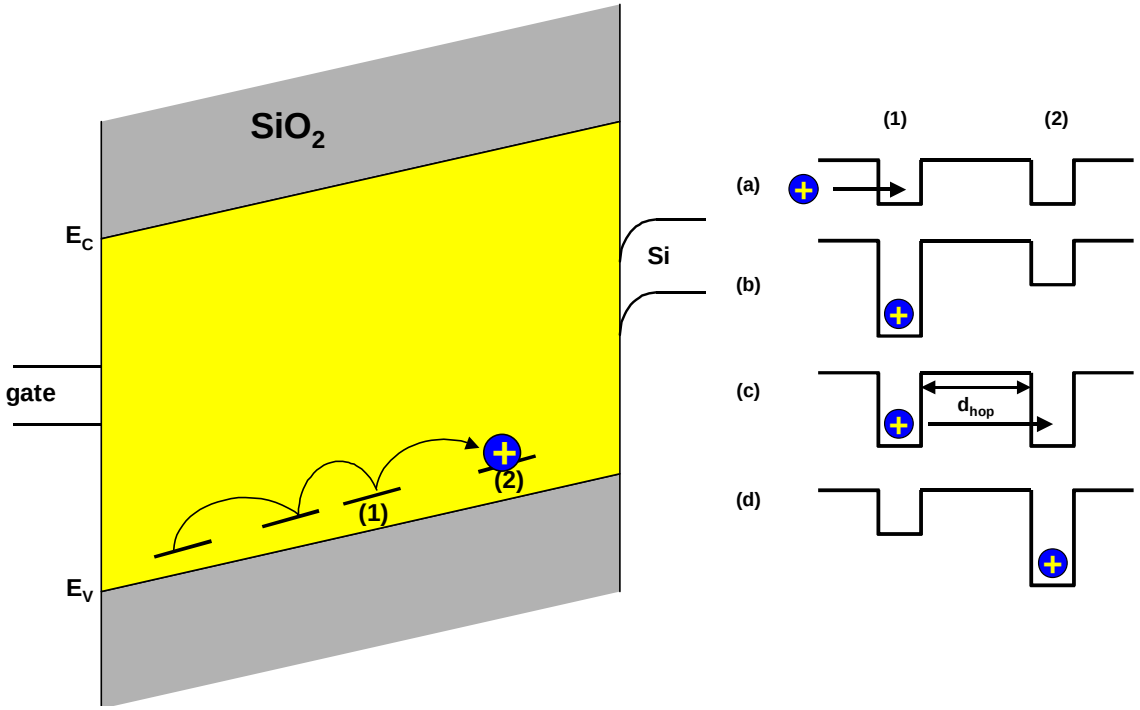

Figure 9: Illustration of polaronic hopping transport mechanism. (a) Initially sites (1) and (2) are both empty; (b) Upon capturing a hole, the energy of site (1) is lowered via lattice distortion, (c) after pausing for a time determined by a randomly varying tunneling distance, d_{hop}, the hole tunnels to site (2); (d) the hole becomes localized at site 2.

In the CTRW formalism, transport is viewed as a series of discrete displacement events, in which the time between successive displacement events is represented by a pausing time distri-

bution function, $\Psi(t)$. When $\Psi(t)$ is a slowly decaying function, there is a significant probability for long pauses between hops; this is the fundamental source of dispersive transport in CTRW. For holes in SiO_2, the pausing time distribution function has been found to have the form, $\Psi(t) \sim t^{-(1+\alpha)}$, where α is thought to be related to the density, N_D, and localization radius, R_D, of hopping sites according to $\alpha \sim (4\pi/3)N_D R_D^3$ [17, 35]. Typically, α assumes a value between 0.15 and 0.35 for holes in SiO_2 with lower values indicating greater dispersion.

The pausing time distribution function is used to obtain a Green's function, typically specified in one spatial dimension as P(x,t), which gives the probability distribution for a hole to arrive at position, x, at time, t, given that it was generated at x=0 at t=0. The transport calculation is carried out using this Green's function as follows [36]:

$$\rho(x,t) = \int_0^L dx' \rho_0(x') P(x,t;x') \tag{6}$$

where $\rho(x,t)$ is the hole concentration at position, x, and time, t and $\rho_0(x')$, the initial hole concentration, is assumed to exist immediately after a pulse of radiation. $P(x,t;x')$ is the probability distribution for a hole initially at position, x', to be found at position, x, at time, t. For holes starting at positions other than x=0, the calculations can be carried out assuming $P(x,t;x') \rightarrow P(x-x',t)$ by recognizing that the variable x represents the displacement rather than the absolute position of the hole. Rather involved mathematical procedures are required to obtain specific expressions for P(x,t) [36, 40]. Here, it is sufficient to state simply that the derivation, which depends on the pausing time distribution function, $\Psi(t)$ and the average displacement distance, involves considerable abstraction from the actual microscopic transport mechanism, i.e., derivations of P(x,t) are not typically provided based on actual tunneling calculations. Another important general observation regarding CTRW calculations is the lack of generality of Equation 6; specifically, CTRW calculations consider only one carrier (holes) and apply only to pulsed-irradiation conditions (charge generation is represented as an initial condition, $\rho_0(x')$). These limitations will be revisited later; we now turn to a transport model that is inherently compatible with a continuity equation approach to transport in SiO_2.

Multiple Trapping and Detrapping (MTD)

In contrast to CTRW, which views transport solely in terms of elemental displacements, the MTD approach explicitly identifies three separate components of transport, as illustrated in Figure 10 [37]. Here, the horizontal arrows in the valence band refer to transport governed by the usual coupled continuity and drift-diffusion equations with a well-defined mobility. Carrier motion is interrupted when they are trapped in a shallow "bandtail" state and then resumes when they are detrapped according to a characteristic emission time, τ, which is proportional to the trap energy relative to the valence band. In general, the bandtail states are characterized by a uniform spatial distribution and a continuous or quasi-continuous exponential distribution in energy as illustrated in Figure 10.

The mathematics of MTD is accomplished by coupling multiple trapping and detrapping equations to the carrier continuity equation. For holes the trapping rate is:

$$\sum_{i=1}^{N_{Tp}} -\left.\frac{dp}{dt}\right|_{[\mathrm{MTD}]}^{(i)} = \sum_{i=1}^{N_{Tp}} \left.\frac{dp_t}{dt}\right|_{[\mathrm{MTD}]}^{(i)} \tag{7}$$

$$= \sum_{i=1}^{N_{Tp}} \left\{ \sigma_{p,\mathrm{MTD}} v_{th,p} p \left[N_{T,p}^{(i)} - p_t^{(i)} \right] - \frac{p_t^{(i)}}{\tau_p^{(i)}} \right\} \tag{8}$$

The summation here results from the discretization of the bandtail state energy distribution into N_{Tp} distinct levels. $\sigma_{p,\mathrm{MTD}}^{(i)}$ is the (possibly field- and energy level-dependent) capture cross section for holes, $v_{th,p}$ is the hole thermal velocity, $N_{T,p}^{(i)}$ is the density of the i^{th} trap level, $p_t^{(i)}$ is the concentration of holes trapped in the i^{th} level, and the characteristic emission time, $\tau_p^{(i)}$, is given by:

$$\tau_p^{(i)} \sim \exp\left(\frac{E_{T,p}^{(i)}}{kT}\right) \tag{9}$$

As with CTRW, the MTD transport calculation method does explicitly address the possibility that transporting holes release hydrogen in the oxide. However, it is not unreasonable to suggest that hydrogenated defect sites may contribute some of the transport-mediating bandtail states and that capture and emission processes may be accompanied by the release of mobile hydrogen. This is speculative and not specifically addressed in the mathematics of MTD.

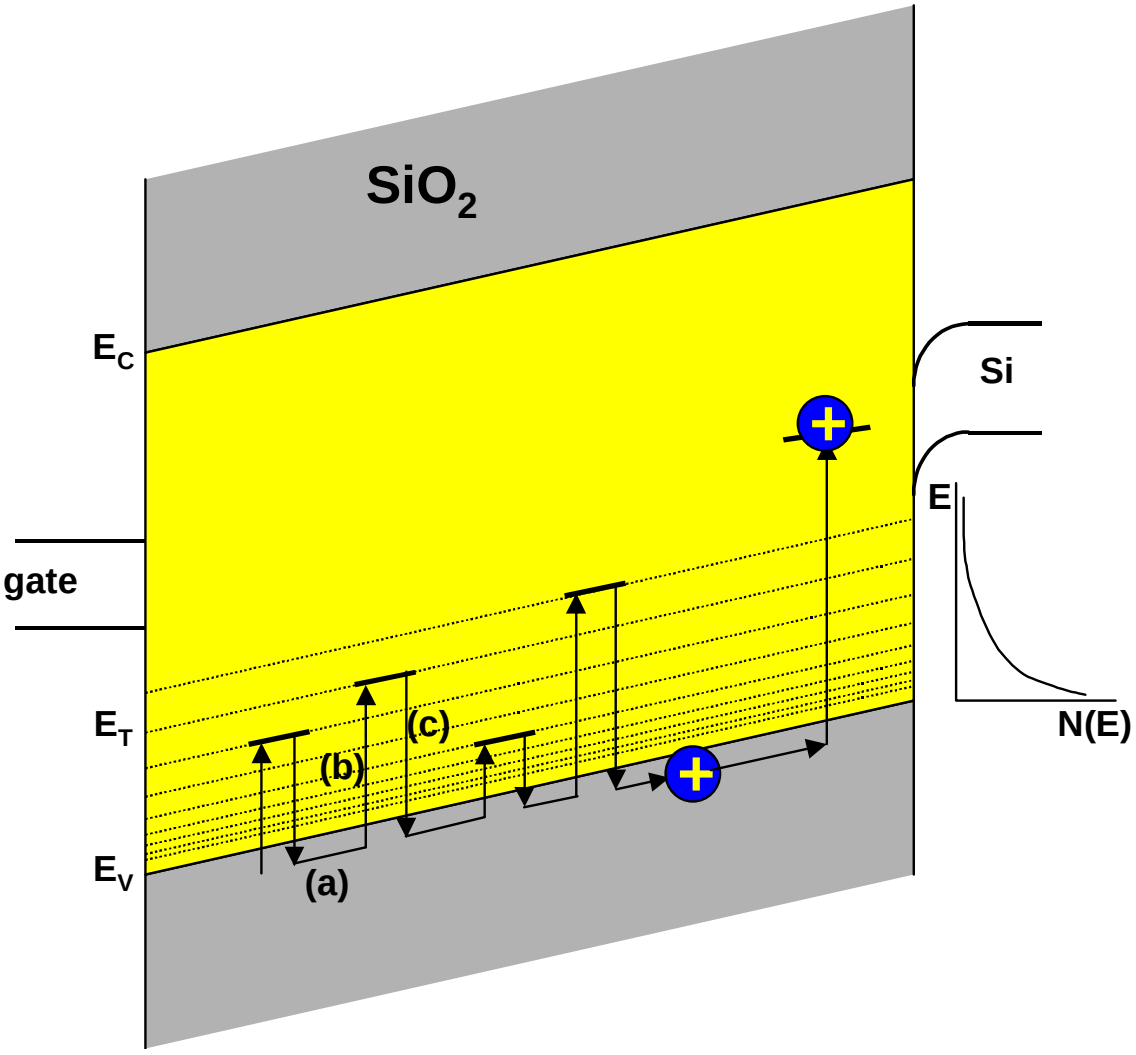

Figure 10: Illustration of 3 components of MTD theory of dispersive transport: (a) free translation in valence band states, (b) trapping into shallow state, and (c) detrapping into the valence band.

Equivalence Between MTD and CTRW

It has been mathematically demonstrated [41, 42] that an exponential density of states function of the form, $N(E) \sim \exp(-E/\beta)$, produces the same dispersive behavior as CTRW calculations employing the power law for $\Psi(t)$. Furthermore, the MTD disorder parameter, β, can be related to its CTRW counterpart, α, using $\beta = kT/\alpha$. Typically, CTRW methods have employed a temperature-independent α with considerable success [17, 18], however, in [37] MTD is found to provide better fits than CTRW to data that exhibit slight temperature dependence in the degree of dispersion. Additional discussion of the physical origins of temperature dependence in MTD theory can be found in [42]. The equivalence between both CTRW and MTD is revisited in Chapter IV in order to address the role of dispersive proton transport.

Prompt Hole Transport

The motion of holes in SiO_2 also appears to be governed by a very short period, on the order of 10^{-7} seconds, of prompt transport [17, 34]. This prompt transport stage accounts for approximately the first 10 nanometers of displacement and proceeds even at low temperatures with a mobility on the order of 10^{-7} $cm^2/V \cdot s$ (unlike the dispersive transport phase which is essentially halted at low temperature). Because it occurs on such a short time scale, prompt hole transport is difficult to characterize experimentally. It has been suggested that the microscopic mechanism for prompt transport is intrinsic polaronic hopping between nearest neighbor nonbonding oxygen orbitals and that the dispersive transport sets in after disorder, e.g. bandtail states or randomness in tunneling distances, begin to mediate the transport. In any case, the early time transport process is expected to be significant only in cases where the prompt displacement distance of 10 nm is a significant fraction of the oxide thickness.

Defect Formation Processes

The preceding sections of this chapter cover the basic mechanisms of and associated calculational methods for modeling carrier generation and transport in irradiated SiO_2. The key concept in the above discussion is the use of continuity equation methods for modeling carrier transport in SiO_2, including the dispersive nature of hole transport. A continuity equation-based description of

generation and transport of carriers is all that is necessary for modeling the radiation response of active semiconductor regions of irradiated devices. It is also sufficient for modeling the transient imbalances in mobile charge in device oxides. However, the long-lasting damage that uniquely characterizes the response of irradiated oxides requires a description of defect formation processes that are driven by carrier generation and transport. A recent review of the various microstructural models of defect formation is found in [44]. The specific defect formation processes that dominate radiation-induced parameter shift in many semiconductor devices are (1) hole trapping, (2) annealing and compensation of trapped holes, and (3) interface trap formation.

Hole Trapping

As holes transport through the oxide, some become trapped at defects in the oxide for extended periods of time instead of escaping. The accumulation of a stable positive charge distribution in the oxide is the reason for the lack of full recovery in V_T in Figure 1. The defect primarily responsible for hole trapping in many device oxides is the oxygen vacancy [44, 45, 46]. Hole trapping at oxygen vacancies, as illustrated in Figure 11, is to be distinguished from that postulated in the MTD model for transport; specifically, hole trapping at oxygen vacancies is accompanied by a specific structural relaxation and associated shift in the local electronic energy levels. The result is a stable (or at least long-lived relative to dispersive transport time scales), positively charged and paramagnetic defect known as the E' center. In addition, oxygen vacancies are often preferentially located near the substrate silicon-SiO_2 interface [45] whereas the transport-mediating trap levels are typically considered to be uniformly distributed in the oxide. The rate equations for hole trapping at oxygen vacancies are similar to those in the MTD description of dispersive transport, however, the stability of the E' center is appropriately represented mathematically using an infinite, or finite but large, thermal emission time constant, i.e., a deep level in the energy band.

Another type of hole trapping process has been suggested to involve hydrogen-related defects distributed somewhat more uniformly throughout the oxide than oxygen vacancies [47, 48, 49]. This type of hole trapping process has been cited as a mechanism for the release of mobile hydrogen in the oxide, however, the microstructural models for the defect itself and its interaction

with holes are not as confidently known as that of hole trapping at oxygen vacancies. In general, E′ centers dominate the electrically measurable effects of hole trapping because of their close proximity to the interface with silicon. Hole trapping at hydrogen-related defects assumes an important intermediate step in interface trap formation.

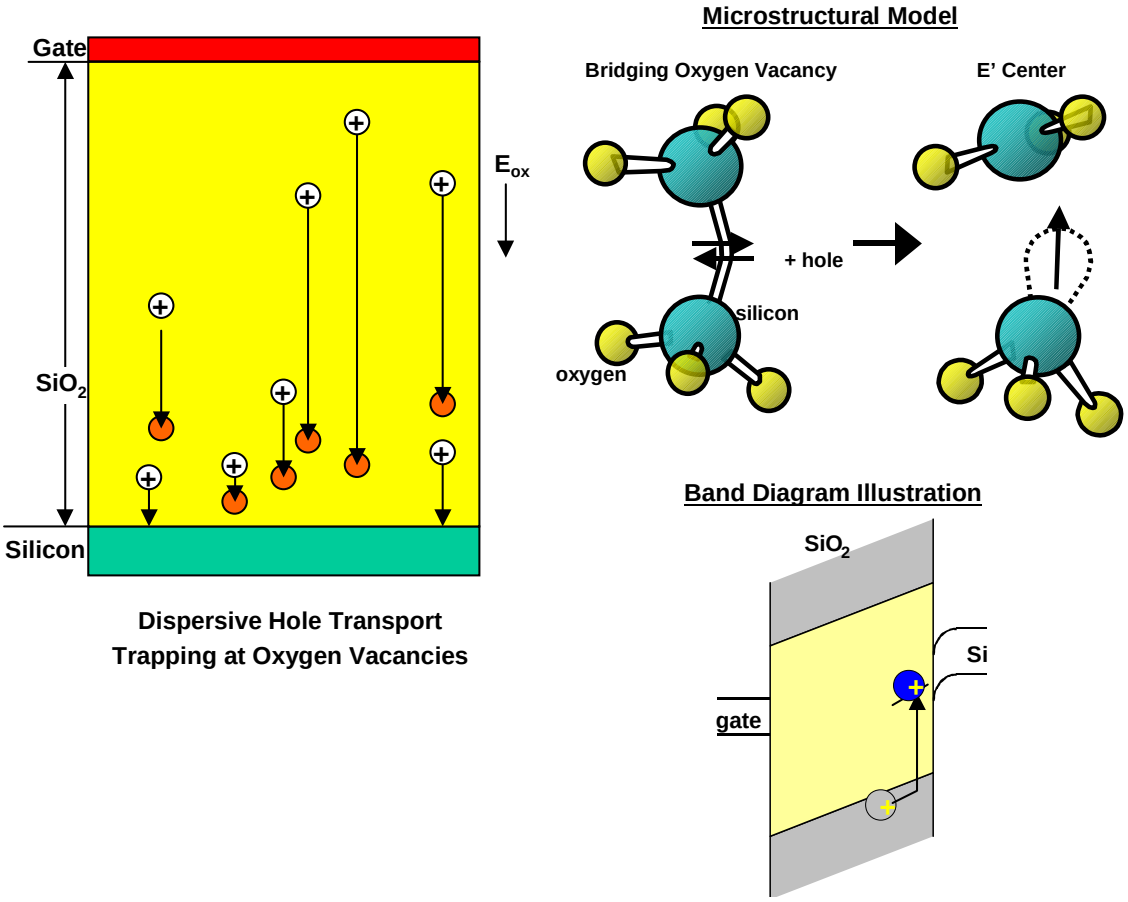

Figure 11: Microstructural model for dominant radiation-induced hole trapping process - hole trapping at oxygen vacancies to form E′ centers.

Compensation and Annealing of Trapped Holes

Over time, some trapped holes may become neutralized by capturing electrons [16, 50, 51, 52, 53, 54, 55, 56, 57]. Various sources of electrons in the oxide are possible. Conduction band electrons that are generated by incident radiation may become trapped by formerly trapped holes (in addition to recombining with a free hole or escaping the oxide) [21]. Electrons may

also be injected from nearby silicon interfaces, either through direct tunneling [52] or thermionic emission [53] (Figure 12). The latter mechanism is more likely to occur in aggressively scaled devices in which hot electron injection becomes more severe. It should be noted that although some true annealing may occur, the original oxygen vacancy structure may not always be recovered when an electron is captured by an E' center. Instead, the relaxed atomic structure may persist in a compensated, neutral charge state which can, in fact, lose the compensating electron and regain the positive charge state or trap an additional electron to become net negatively charged [50, 58].

The capture of electrons at E' centers can be modeled using trapping equations similar to those for holes in which the trapped hole term assumes the role of electron trap. It must be remembered, however, that recovery of the oxygen vacancy structure requires not just electronic interaction but also thermal energy in order to recover the unrelaxed atom positions. The thermal activation of trapped hole annealing can be modeled by including the emission term to the rate equation for hole trapping. The neutralization of E' centers via thermal and/or tunnel annealing accounts for the gradual threshold voltage recovery that occurs following the more rapid period of hole transport and trapping (see late time region of Figure 1).

Interface Trap Formation

The gradual threshold voltage recovery illustrated at late times in Figure 1 is also furthered by the formation of interface traps - dangling bond defects that produce energy levels which are spatially localized at the Si-SiO_2 interface and distributed in energy throughout the silicon band gap [59]. Because these energy levels are in direct electronic contact with the silicon they have different effects on transistor current-voltage characteristics than charge trapped in the oxide. They increase threshold voltage by capturing carriers as the silicon surface is swept from accumulation toward inversion. This can be viewed as robbing the inversion layer of mobile charge, and produces a stretchout in the subthreshold region of $I_D - V_G$ characteristics [60]. They also reduce carrier mobility in the inversion layer through Coulombic scattering [61, 62]. Finally, the energy levels associated with these dangling bonds serve to enhance surface recombination; this effect is maximized with the surface potential near midgap [63].

Models for interface trap formation fall in two basic categories: (1) trapped hole conversion

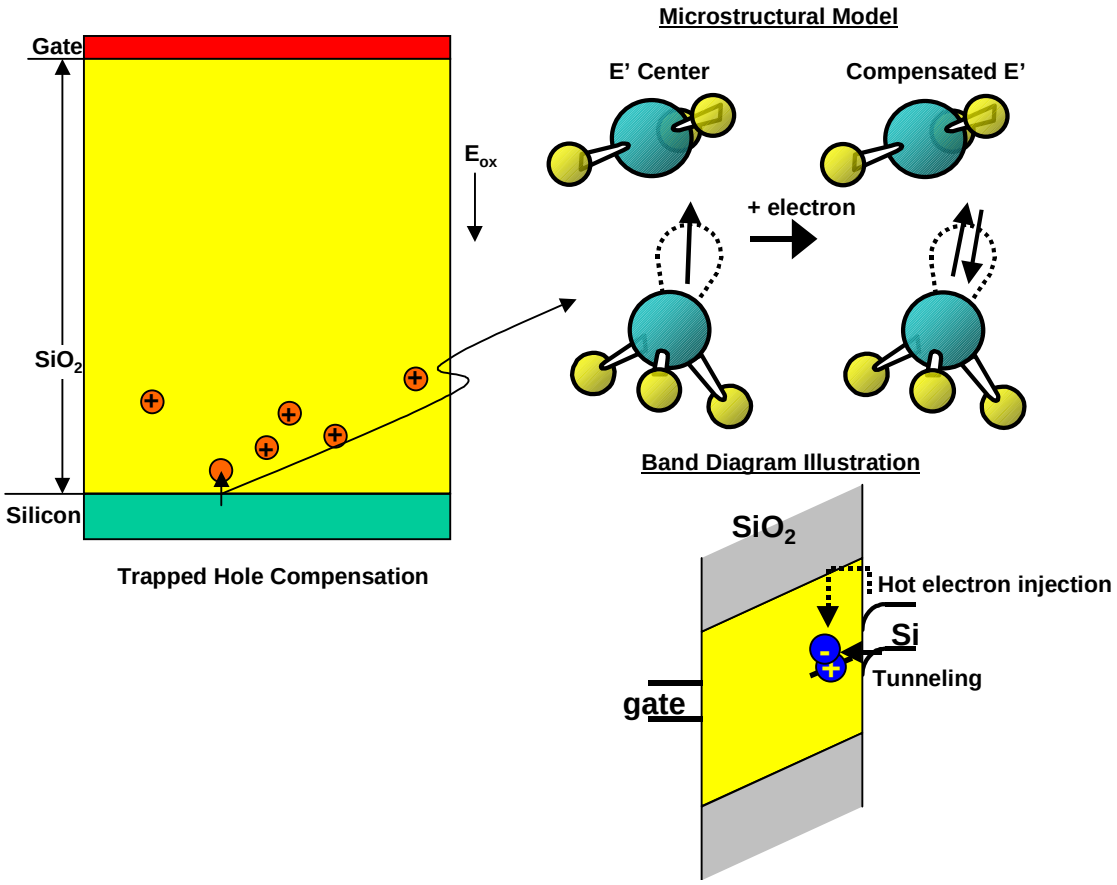

Figure 12: Trapped hole neutralization proceeds when electrons are captured by E′ centers. The result is not necessarily bond reformation but rather a compensated defect that can re-emit an electron or capture a second electron. As shown in this figure, electrons can be supplied after the initial radiation exposure by injection or tunneling from nearby interfaces with silicon.

models [64, 65, 66] and (2) hydrogen-mediated formation models [47, 48, 49, 67, 68, 69, 70, 71, 72, 73, 74, 75, 76]. In the trapped hole conversion models, interface traps are thought to be formed through strain-induced migration of trapped holes to the interface [66]. It has also been suggested that the energy lost as holes fall from the oxide to the silicon valence band may drive some sort of bond disruption at the interface [65]. Transporting and/or trapped hole-conversion processes are believed to account for a relatively small fraction of radiation-induced interface traps, on the order of 10 percent [76].

In hydrogen-mediated models, interface trap formation occurs through the reaction illustrated in Figure 13. It is postulated in this model that dangling bonds present after oxidation are passivated with hydrogen and rendered electrically inactive during subsequent anneals [77], e.g., post-metal annealing in forming gas. During radiation these bonds are depassivated by reacting with hydrogen that is liberated from hydrogen-related defects in the oxide. The result of this depassivation reaction is a paramagnetic defect at the interface known as the P_b center. Once depassivated, P_b centers influence threshold voltage, mobility, and surface recombination as discussed above. It should be noted that the reaction illustrated in 13 can also proceed in the reverse direction, i.e., atomic hydrogen can also react with depassivated P_b centers to tie up the dangling bond and remove the defect's electrical behavior as an interface trap.

Issues for Numerical Modeling

The preceding review of physical mechanisms provides a partial basis for planning a numerical approach to simulating radiation-induced degradation of semiconductor device oxides. A continuity-equation approach to modeling electron and hole transport in SiO_2 is introduced along with required descriptions of electron-hole pair generation and recombination, dispersive hole transport, and hole trapping and detrapping. Previous numerical modeling work has been identified which addresses these mechanisms, however, these efforts do not account for interface trap formation.

In order to formulate an approach to numerical simulation of interface trap formation, the description provided by Figure 13 requires further discussion. The two main problematic issues in describing radiation-induced interface trap formation are (1) the precise mechanisms by which

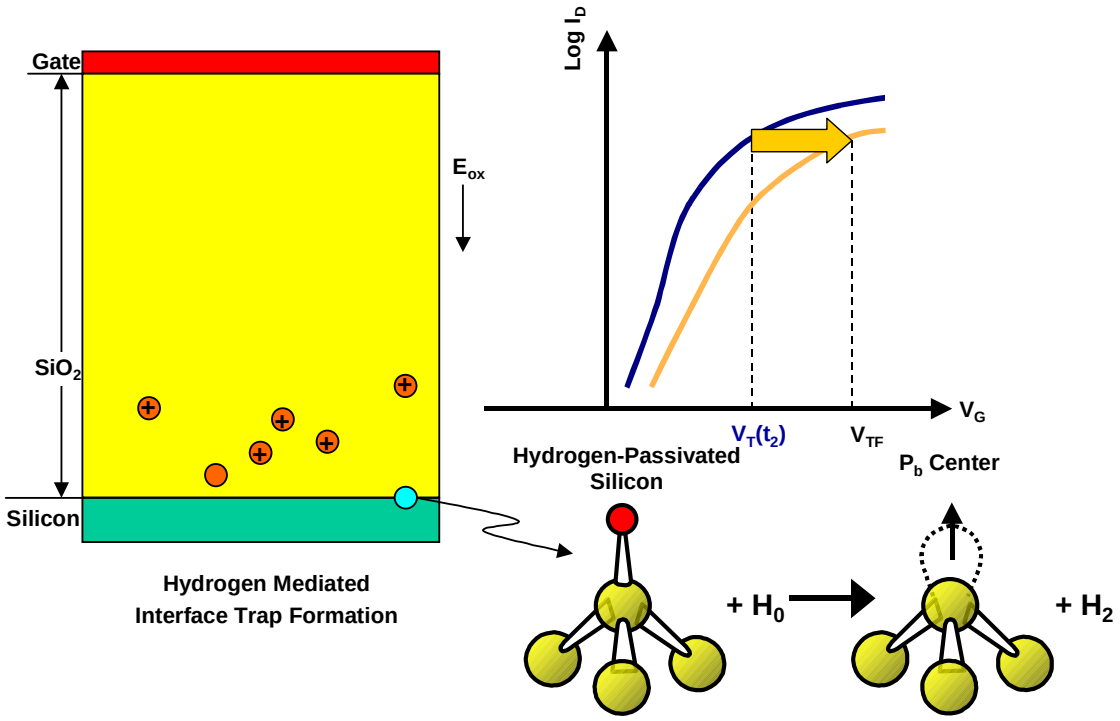

Figure 13: Microstructural model for formation of P_b interface trap defects and their effects on $I_D - V_G$ measurements.

hydrogen is released in the oxide and (2) the transport processes that govern how the liberated hydrogen is eventually supplied at the interface to participate in the depassivation reaction. Attention to these issues has been focused specifically on whether the hydrogen is released in the bulk as a neutral species, i.e., as H_o or whether it is released as a proton, H^+, and then converted to H_o by an electron from the silicon when it arrives at the Si-SiO_2 interface.

The current view on this subject, as reviewed in [67], is that both processes occur, with the contribution from protons accounting for the majority of the overall interface trap formation. The conclusion that protons dominate is based partially on the observation that much of the interface trap formation exhibits a bias-dependence that suggests the involvement of a positively charged rather than neutral species. Additionally, the long time-scale over which the (bias-dependent) interface trap formation occurs is consistent with a polaronic (dispersive) transport mechanism for protons in SiO_2 that is analogous to that of holes [69, 70, 78]. In these studies, the dispersive nature of proton transport is supported by the success of Continuous Time Random Walk theory in predicting the time-dependence of interface trap formation following pulsed irradiation. However, as evident from the above discussion for holes, CTRW theory involves mathematical methods that are not compatible with (continuity equation-based) numerical device simulation. Furthermore, despite the emerging consensus that both H_o and proton transport to the interface drives interface trap formation, and that proton transport often dominates the overall response, a single unified model for how ionizing radiation acts to liberate H_o and H^+ in bulk regions of device oxides has not yet been universally accepted. These two issues, proton transport and hydrogen release chemistry constitute the primary scientific challenges faced in the numerical approach presented in this dissertation. Chapter III provides a focused discussion of the hydrogen-release chemistry. The result of this discussion is a proton generation rate that is coupled to hole trapping at hydrogen-related defects in the SiO_2. The issue of dispersive proton transport is revisited in the beginning of Chapter IV before presenting the complete mathematical model.

CHAPTER III

HYDROGEN CHEMISTRY

Modeling Approach and Justification

The previous chapter identifies two types of interface trap formation models: (1) trapped hole conversion and (2) hydrogen-mediated formation. The present work considers hydrogen-mediated interface trap formation, more specifically that associated with proton transport. This chapter considers the mechanisms by which protons are released in the oxide during radiation exposure. We begin the discussion with a brief review of the information available in the literature.

Hole Transport-Induced Proton Release

The model for proton release proposed by McLean [43], postulates that localized energy transfer associated with hole transport in the vicinity of an initially charge-neutral hydrogenated defect disrupts the hydrogen bond. It is postulated in this model that the positive charge of the hole is transferred to the hydrogen, liberating it from its bonding site in the form of a proton. This energy-deposition model is supported by several observations that interface-trap formation increases with increasing electric fields for metal gate capacitors [79, 80, 81, 82]. Specifically, increasing the electric field increases the energy holes transfer to the lattice as they transport. This direct process of proton release may be expressed as:

$$p + DH \rightarrow D_o + H^+ \qquad \text{(R1)}$$

In later work on devices with polysilicon gates, interface trap formation was observed to follow an $E^{-1/2}$ dependence, which conflicts with the hole transport-induced model for proton release and instead, points to a proton release mechanism that is enhanced at *lower* fields [49, 83]. This observation has inspired the several modifications to the original McLean model. These are, in general, slightly more complicated in the sense that they postulate an intermediate role of H_o in a multiple-step process involving electron-hole pair recombination or exciton motion, hole transport

and/or trapping, and in some cases the formation and cracking of molecular hydrogen. We now review the "H_o release" models.

H_o Release and Conversion to H^+

Roughly three different explanations have been given to explain observations that interface trap formation is greater at lower electric fields during irradiation. One of these, proposed by Saks and Brown in [78] states that the energy released during electron-hole pair recombination results in the production of H_o which subsequently reacts with a hole to form H^+. In this model, the higher recombination probability for low electric field provides the explanation for increased interface trap formation at low field.

A slightly different explanation given by Griscom [67] states that neutral excitons (bound electron-hole pairs) move randomly throughout the oxide and eventually recombine at a hydrogen defect causing the release of H_o. Like electron-hole pair recombination, the stability of excitons is expected to be enhanced at low electric fields. Since the eventual H_o release mechanism is recombination at a hydrogen defect, the exciton model may be interpreted as a modification to the geminate recombination model for H_o release which considers the possibility that the electron-hole pair moves before recombining. A more distinguishing characteristic of the model proposed by Griscom is the suggestion that H_o is converted to H^+ upon interaction with *self-trapped holes* (STH). This aspect of the model is based largely on the results of experiments in which irradiation was performed at low temperature (4 K) in which virtually all interface trap formation is suppressed. The relative contributions of H_o transport and H^+ transport to the interface are then selectively observed by observing interface trap formation as the samples are warmed to room temperature. Up to about 120 K, a small bias-dependent increase in interface trap density is observed and attributed to H_o production via exciton recombination at hydrogen defects very near the Si-SiO_2 interface. Upon warming to above 200 K, the simultaneous reduction in H_o and STH and subsequent bias-dependent formation of interface traps suggest that H_o interacts with STH to form protons which, under positive applied bias, then drift to the interface to create interface traps.

Another class of models which is consistent with a $E^{-1/2}$ dependence of interface trap

formation) states that hydrogen release is initiated by hole *trapping* [48, 49]. In the hole-trapping/hydrogen transport model proposed in [49], it is argued that the $E^{-1/2}$ field-dependence of interface trap formation is a consequence of the field-dependence characteristic of hole-trapping capture cross section. In this work, however, specifics are not given as to the possible intermediate role of H_o production in the eventual release of H^+.

These specifics are however, quite well-developed in the model proposed by Mrstik and Rendell [48] which describes a three-step process beginning with the capture of radiation-generated holes, p, by existing hydrogen-related defect sites, DH (e.g., SiOH), resulting in a trapped positive charge, D^+, and the release of atomic hydrogen, H_o.

$$p + DH \rightarrow H_o + D^+ \tag{R2}$$

The critical experimental result in this work is the observation that interface traps are formed when a device is subjected to a room temperature, hydrogen anneal *after* radiation exposure, and that the number these new interface traps is roughly equal to the number that were created *during* the radiation exposure. This observation suggests that for each interface trap generated during radiation, some defect must remain in the oxide that results in the formation of another interface trap during post-irradiation exposure in H_2. This leads the authors to propose that instead of being immediately converted to H^+, the H_o first dimerizes to form H_2:

$$H_o + H_o \rightarrow H_2 \tag{R3}$$

The H_2 is subsequently "cracked" at one of the positively charged sites of hole trapping, D^+, resulting in the recovery of the original neutral hydrogen defect, DH, and the formation of a proton.

$$H_2 + D^+ \rightarrow DH + H^+ \tag{R4}$$

This proton then drifts under an applied positive bias to create one radiation-induced interface trap. The key feature of this model is that for every proton released (i.e., interface trap formed) one cracking site, D^+, remains behind in the oxide. These residual D^+ sites are available to crack the H_2 supplied during post-irradiation H_2 annealing, releasing protons which then drift to the interface and create more interface traps. The number of additional interface traps created during

the H_2 anneal will equal the number of cracking sites (and therefore interface traps) produced during the preceding irradiation. This is a key experimental result that cannot be reconciled with models in which there is a one-to-one correspondence between hole trapping and proton release.

It is stated in [48] that these reactions completely specify the bulk proton release process. However, as mentioned in the previous chapter, hole trapping at (intrinsic) oxygen vacancies, OV,

$$p + OV \rightarrow E' \tag{R5}$$

is typically the primary determinant of electrically measurable shift due to trapped oxide charge. This is a consequence of the close proximity of OV sites to the Si-SiO_2 interface (compared with D^+ centers which are thought to be more uniformly distributed in the bulk [70] and are, therefore, less influential electrostatically [48]. In contrast to the conclusions in [48], there have been reports that H_2 cracking at E′ centers [84] plays a primary role in interface-trap formation [72]. In [72] H_o as well as H^+ are considered possible products of the cracking reaction:

$$H_2 + E' \rightarrow E'H + H^+ \quad \text{or} \quad H_2 + E' \rightarrow E'H + H_o \tag{R6}$$

The specific reaction pathway linking carrier generation, transport, and/or trapping to H_2 production are not clearly specified in [72]. However, it is reasonable to imagine that H_2 supplied by reactions (R2) and (R3) could drive cracking (R5) as well as (R6). Since E′ centers are known to be located preferentially near the Si-SiO_2 interface, reaction (R6) provides a possible physical explanation for observations of enhanced near-interfacial proton generation in previous work [70]. It is also worth noting that despite the conclusions in [48], the role of E′ centers in cracking is acknowledged in later work [85, 86].

Overall, the model described by reactions (R2-R6) provides a complete description of many experimental results. Specifically, it accounts for the dominant role of proton transport in determining the time-dependence of interface traps formation. It also accounts for the field dependence in the release of protons (Given the conclusions in [49] that the different field-dependence observed in some metal gate structures may be due to different spatial distributions of hydrogen release rather than a unique hydrogen release mechanism, this model may also be appropriate for oxides with metal gates, i.e., parasitic field oxide structures). Finally, these equations also account for the interface trap build-up during post-irradiation exposure in H_2. There are, however,

several reports of interface trap build-up after very long times which are addressed in a slightly more complicated model involving water molecules [73, 74]. No specific attempt is made in the present work to incorporate these models, however, the present approach may, in principle, be extended to include them.

Interfacial Reactions

As discussed in the previous chapter, models for interface trap formation typically state that protons transporting to the interface are converted to H_o by a substrate electron and then participate either in interface trap formation via the depassivation reaction:

$$SiH + H_o \rightarrow Si^* + H_2 \tag{R7}$$

or interface trap passivation via the reaction:

$$Si^* + H_o \rightarrow SiH \tag{R8}$$

where Si^* is the P_b interface trap defect.

Rate Equations/Simplifying Assumptions

The model reported here applies first-order kinetics for the proton release mechanisms described by reactions R2, R3 and R4. The resulting rate equation for reaction R2 is:

$$\left.\frac{d[H_o]}{dt}\right|_{R2} = \left.\frac{d[D^+]}{dt}\right|_{R2} = -\left.\frac{d[DH]}{dt}\right|_{R2} = -\left.\frac{dp}{dt}\right|_{R2} \tag{10}$$

$$= \sigma_{p,DH} v_{th,p} p[DH] \tag{11}$$

where $\sigma_{p,DH}$ is the hole trapping cross section of the DH defect, $v_{th,p}$ is the hole thermal velocity, and [DH] is the volume density of DH defects. Here, $|_{R2}$ means "due to reaction R2". Similarly, we obtain,

$$\left.\frac{d[H_2]}{dt}\right|_{R3} = -\frac{1}{2}\left.\frac{d[H_0]}{dt}\right|_{R3} \tag{12}$$

for R3 and

$$\left.\frac{d[DH]}{dt}\right|_{R4} = \left.\frac{d[H^+]}{dt}\right|_{R4} = -\left.\frac{d[D^+]}{dt}\right|_{R4} = -\left.\frac{d[H_2]}{dt}\right|_{R4} \tag{13}$$

for R4.

At this point we identify a total of four transporting species (holes, H_o, H_2, and H^+) involved in interface trap formation. The present work applies two fundamental assumptions to simplify the problem. First, we assume that the H_o released when holes are trapped at DH sites is "promptly and locally" converted to H_2. This assumption is expressed as:

$$\left.\frac{d[H_o]}{dt}\right|_{R2} = -\left.\frac{d[H_o]}{dt}\right|_{R3} \tag{14}$$

Combining 10, 12, and 14 allows us to write

$$\left.\frac{d[H_2]}{dt}\right|_{R3} = \frac{1}{2}\left(\sigma_{p,DH} v_{th,p} p[DH]\right) \tag{15}$$

Similarly, we assume that the H_2 produced in the dimerization reaction, which is now represented in 15, is promptly and locally cracked at D^+ sites. This is expressed as:

$$\left.\frac{d[H_2]}{dt}\right|_{R3} = -\left.\frac{d[H_2]}{dt}\right|_{R4} = \frac{1}{2}\left(\sigma_{p,DH} v_{th,p} p[DH]\right) \tag{16}$$

Finally, 16 can be used in Eq. 13 to relate proton generation directly to hole capture at DH sites:

$$\left.\frac{d[H^+]}{dt}\right|_{R4} = \frac{1}{2}\sigma_{p,DH} v_{th} p[DH] \tag{17}$$

Our definition of "prompt and local" dimerization and cracking states that they occur rapidly compared to the time scale for D^+ creation and H^+ transport, as well as relatively near their points of origin. This allows us to absorb H_o and H_2 transport into the proton release kinetics. In effect, we replace reactions (R2), (R3), and (R4) with a single net reaction:

$$2p + 2DH \rightarrow D^+ + DH + H^+ \tag{R9}$$

Note that H_2 cracking at E′ centers (R6) is not accommodated in this set of assumptions. The H_2 in reaction (R6) is typically viewed as being supplied by other reactions in the bulk of the oxide; treating this requires an explicit transport model for H_2. In our approach, spatially nonuniform

proton release originates from the spatial distribution in DH density. We do, however, preserve the role of E′ centers in charge trapping using the following rate equation for reaction (R5).

$$\frac{d[E']}{dt} = -\frac{dp}{dt}\bigg|_{[OV]} = \sigma_{p,OV} v_{th,p} p([OV] - [E']) \tag{18}$$

Finally, we assume first-order kinetics for reactions (R7) and (R8). Using the proton current density, J_{H^+}, at the interface to represent proton arrival at passivated (SiH) and depassivated (Si^*) interface sites, we calculate the net rate of depassivation as:

$$\frac{d[Si^*]}{dt}\bigg|_{net} = (k_1[SiH] - k_2[Si^*])\frac{J_{H^+}}{q} \tag{19}$$

where k_1 and k_2 are the reaction rate constants for depassivation and passivation, respectively.

Our application of reactions R2, R3, and R4 is specifically designed to obtain a proton generation rate for use in a proton transport model. At first, this may seem at odds with the analysis in [48], in which the time-dependence of interface-trap formation during post-irradiation exposure in H_2 was examined using a tarnishing reaction. It is expected that H_2 diffusion is the rate-limiting process during H_2 annealing because it is introduced at the oxide boundaries and must transport throughout the oxide in order to encounter all the cracking sites. However, during radiation the H_2 is inherently produced in the vicinity of cracking sites. Indeed, since the proton release kinetics proposed in [48] are stated to be valid during radiation exposure as well as during H_2 annealing, we are led to an interesting test of our approach. Specifically, with an appropriate transport model coupled to the proton release kinetics, we should be able to predict the results of pulsed-radiation/switched bias experiments using a single transient simulation. This simulation study, in fact, functions as a key validation of the model and is presented in Chapter V. First, however, we assemble the information presented in this and the previous chapters into a complete mathematical model.

CHAPTER IV

MATHEMATICAL MODEL

Past Radiation-Effects Modeling Efforts

Numerical device simulation permits charge transport in active semiconductor device regions to be studied in considerable detail. Consequently, device simulation has long been recognized as a useful tool for transient radiation-effects analysis (of semiconductor response to ionizing radiation). Device simulation methods for analyzing total ionizing dose effects are comparatively less developed due to added complexity associated with the dispersive nature of hole transport in SiO_2 and also long-term defect formation processes. There have been numerous numerical simulation studies of charge transport in SiO_2 which have used either nondispersive [27, 28, 29, 30, 31, 32, 33] or dispersive models [35, 36, 37, 38] for holes. Some of these have addressed specific device parameter-shift problems [30, 31, 32, 33] and radiation-response optimization [32]. However, the models used in these studies have been based exclusively on electron and hole transport. These are of little use in studying radiation-induced interface trap formation, which is known to involve the transport of several forms of hydrogen.

As mentioned in Chapter II, previous discussions of hydrogen-mediated interface-trap formation have focused largely on qualitative descriptions of hydrogen reaction sequences. In general, these reactions describe the release of some form of hydrogen, protons (H^+), H_2, H_o, due to the transport and/or trapping of holes, with proton drift cited as the rate-limiting factor in many cases of radiation-induced interface trap formation. However, these qualitative models for hydrogen release and transport have been applied in only a few numerical studies. Approaches based on bimolecular reaction theory provide some information on the kinetics of interface trap formation [73, 74]. However, in this type of approach, transport models are not provided for the involved hydrogen species. This prevents the tracking of spatial variation in the bulk as well as interfacial defect populations. Proton transport modeling using Continuous Time Random Walk (CTRW) theory [36] has been applied to pulsed-radiation/switched-bias experiments with success [70, 75]. However, the mathematics of this approach is not easily generalizable for ar-

bitrary time-varying biases [75], dose-rate, etc. Furthermore, CTRW methods for interface trap modeling are driven by assumed initial proton profiles rather than a unified model linking proton release kinetics to carrier generation, transport and trapping. In general, previous interface trap formation models have not been cast in a form suitable for device simulation. The inability to model interface trap formation self-consistently along with charge trapping constitutes a serious impediment to device simulation methods for total dose response optimization.

Numerical Approach for Simulating Hole Trapping and Interface Trap Formation

In Chapter II, the basic physics and corresponding calculational methods required for a continuity equation-based approach to transport and trapping in SiO_2 were described, with particular attention devoted to three issues that have not been coherently addressed in much of the previous work in the area: (1) the distinction between initial recombination and recombination between free electrons and holes; (2) the dispersive behavior of hole transport and the two main quantitative approaches for modeling this behavior; (3) the lack of sufficient clarity in previous models for numerical modeling of interface trap formation, specifically regarding bulk hydrogen release processes. Chapter III focuses specifically on this latter point, arriving at a rate equation that describes hole-trapping-induced proton release in bulk regions of the SiO_2.

In the present chapter, the basic calculational methods cited in Chapter II as well as the proton generation rate derived in Chapter III are used to specify a system of continuity equations for three carriers - electrons, holes, and protons. As in previous (two-carrier) transport models, radiation-induced electron-hole pair generation-recombination processes enter the electron and hole continuity equations as a net generation rate term accounting for geminate recombination. The present model also provides a proton generation rate which was derived in Chapter III from a set of rate equations describing hydrogen reaction chemistry in the bulk regions of SiO_2. In particular, the role of hole trapping in hydrogen release serves to couple the hole and proton continuity equations. Transport of all three carriers is based on standard drift-diffusion equations. However, our approach also provides dispersive transport models for holes as well as protons based on the theory of multiple trapping and detrapping (MTD) processes. The development of the proton generation rate and the use of this generation rate in a proton continuity equation

along with the MTD methods for proton transport are the primary novel achievements in the present work. Since the application of MTD methods for hole and especially proton transport represents a departure from previous work which uses CTRW methods, a brief justification of the MTD methods for both holes and protons is provided before assembling the complete model.

CTRW versus MTD

The similarity between the polaronic hopping model for hole transport and the concept of "elemental displacement" makes CTRW an intuitively sensible choice for modeling hole transport. It has also been argued that the particular temperature dependence expected for polaronic hopping is consistent with CTRW predictions, specifically the observation that α is essentially independent of temperature. However, several calculational aspects of CTRW present fundamental barriers to application in more general irradiation scenarios. For example, it is not clear how CTRW methods can be made to accommodate conditions of continuous generation rate. Specifically, the introduction of new charge at additional times, $t > 0$, would require a cumbersome discretization scheme in which Equation 6 must be evaluated separately for successive delta function approximations to newly added increments of charge. More problems arise in the case of spatially and/or time-varying electric fields. In this case, the expression for P(x,t) itself varies with time and position through the parameter μ. However, the CTRW method expects a single P(x,t) to apply for a given transport calculation. Once again, one is forced to consider impractical and cumbersome discretization schemes in which individual CTRW calculations must be separately applied to small increments in position and time. Indeed, it should be emphasized that applications of CTRW have focused virtually exclusively on pulsed-irradiation conditions in which the electric field is assumed to be constant.

One attempt to apply CTRW under varying electric field is found in a study of proton transport under switched bias conditions [75]. Specifically, CTRW is applied to obtain the proton profile after a long enough period of negative bias that some protons are lost at the gate. This result was then used as the initial condition for a second CTRW calculation for transport under positive bias. This method overestimates the rate of transport in the positive bias phase because the dispersion during the preceding negative bias step is lost. This study demonstrates a basic difficulty with

handling time varying electric fields using CTRW theory.

The MTD approach to dispersive transport possesses far greater compatibility with device simulation compared with previous CTRW methods for proton transport. Most importantly, a self-consistent, coupled model for proton, hole and electron transport is straightforward using continuity equations. However, the treatment of multiple carrier types is not well-developed in CTRW. It must be admitted, however, that the values as well as physical interpretation of the parameters of the proton MTD equations are not well-known. Nevertheless, the computational advantages and generality of MTD methods are not achieved at the expense of physical interpretation. In fact, there have been prior suggestions that, like holes, protons transport via polaronic hopping. Although polaronic hopping is typically associated more closely with the "elemental displacement" concept of CTRW, such an interpretation is, if appropriate, inherently preserved and recoverable through the equivalence between MTD to CTRW that is formally established by Noolandi in [41] and Schmidlin in [42].

The Complete Model

Poisson's equation

In irradiated oxides, Poisson's equation is appropriately expressed as:

$$\nabla^2\psi = -\frac{q}{\varepsilon_{ox}}\left(p - n + [H^+] + [D^+] + [E'] + \sum_{i=1}^{N_{Tp}} p_t^{(i)} + \sum_{i=1}^{N_{TH^+}} H_t^{+(i)}\right) \tag{20}$$

in order to account for the electrostatic effects of mobile charge in the oxide (n, p, H^+), holes trapped at OV and DH sites (E' and D^+), and holes and protons trapped in shallow transport-mediating states (p_t and H_t^+) as prescribed by the MTD transport model.

Continuity Equations

Transport of free electrons, holes, and protons is modeled using a coupled set of three continuity equations.

$$\frac{\partial n}{\partial t} = \frac{1}{q}\nabla\cdot\mathbf{J_n} + G_{ehp}(E) - \alpha np \tag{21}$$

$$\frac{\partial p}{\partial t} = -\frac{1}{q}\nabla \cdot \mathbf{J_p} + G_{ehp}(E) - \alpha np - \left.\frac{\partial p}{\partial t}\right|_{[OV]} - \left.\frac{\partial p}{\partial t}\right|_{[DH]} - \sum_{i=1}^{N_{Tp}} \left.\frac{\partial p}{\partial t}\right|_{[MTD]}^{(i)} \tag{22}$$

$$\frac{\partial [H^+]}{\partial t} = -\frac{1}{q}\nabla \cdot \mathbf{J_{H^+}} + \left.\frac{\partial [H^+]}{\partial t}\right|_{R4} - \sum_{i=1}^{N_{TH^+}} \left.\frac{\partial [H^+]}{\partial t}\right|_{[MTD]}^{(i)} \tag{23}$$

Drift-Diffusion Equations

The flux terms, $\mathbf{J_n}$, $\mathbf{J_p}$, and $\mathbf{J_{H^+}}$, are each obtained from standard drift-diffusion equations in which the Einstein relation between mobility and diffusivity is applied.

$$\mathbf{J_n} = qn\mu_n \mathbf{E} + qD_n \nabla n \tag{24}$$

$$\mathbf{J_p} = qp\mu_p \mathbf{E} - qD_p \nabla p \tag{25}$$

$$\mathbf{J_{H^+}} = q[H^+]\mu_{H^+} \mathbf{E} - qD_{H^+} \nabla [H^+] \tag{26}$$

Net Electron-Hole Pair Generation Rate

The radiation-induced electron-hole pair generation appears in the electron and hole continuity equations as a field-dependent net generation rate, $G_{ehp}(E)$. This quantity is obtained by scaling the product of the dose-rate, $\dot{D}$ rad(SiO_2)/s, and generation factor, g_o=7.6×10^{12} ehp/rad(SiO_2), by a field-dependent fractional yield, Y(E), which accounts for loss of electron-hole pairs through geminate (initial) recombination.

Free Electron and Hole Recombination

Following the approach used to describe recombination in ion-induced charge tracks, recombination between free electrons and holes is modeled using the αnp term used in [24] where α is given by $\alpha = q(\mu_n + \mu_p)/\varepsilon\varepsilon_0$ [25, 26]. Under conditions in which the instantaneous densities of electrons and holes are not simultaneously very high, this term may be neglected without introducing significant error. Such is the case for low dose-rate exposures in which space-charge effects do not prevent electrons from escaping the oxide. This is, in fact, assumed in the simulation studies reported in the results chapters that follow.

Hole Trapping at OV sites

The rate equation describing hole trapping at oxygen vacancies is:

$$\frac{d[E']}{dt} = -\frac{dp}{dt}\bigg|_{[OV]} = \sigma_{p,OV} v_{th,p} p([OV] - [E']) \tag{27}$$

Here we are assuming that once a hole is trapped at an oxygen vacancy it is stable, i.e., no terms are provided for describing thermal emission or compensation by electrons. This type of charge exchange associated with E′ centers has been addressed before, however, the emphasis in this dissertation is to demonstrate the novel features of the improved model, specifically, hydrogen-mediated interface trap formation.

Hole Trapping at DH sites

The net rate of hole trapping at DH sites is obtained by considering reactions (R2) as well as (R4):

$$\frac{d[D^+]}{dt}\bigg|_{R2} + \frac{d[D^+]}{dt}\bigg|_{R4} = \frac{1}{2}(\sigma_{p,DH} v_{th,p} p[DH]) \tag{28}$$

Proton Generation Rate

As developed in Chapter III (Equation 17), the proton generation rate is given by:

$$\frac{d[H^+]}{dt}\bigg|_{R4} = \frac{1}{2}\sigma_{p,DH} v_{th,p} p[DH] \tag{29}$$

MTD Equations

The MTD equation for holes (given previously in Chapter II) is:

$$\begin{aligned}\sum_{i=1}^{N_{Tp}} \frac{dp}{dt}\bigg|_{[MTD]}^{(i)} &= \sum_{i=1}^{N_{Tp}} \frac{dp_t}{dt}\bigg|_{[MTD]}^{(i)} \\ &= \sum_{i=1}^{N_{Tp}} \left\{ \sigma_{p,MTD} v_{th,p} p \left[N_{T,p}^{(i)} - p_t^{(i)} \right] - \frac{p_t^{(i)}}{\tau_p^{(i)}} \right\}\end{aligned} \tag{30}$$

The analogous expression for protons is obtained by replacing "p" with "H^+".

Implementation

An important consequence of the use of MTD methods for dispersive transport is a mathematical similarity between our description of carrier transport in SiO_2 and previous descriptions of transport in amorphous and poly-crystalline silicon. Recognizing this, we have adapted the technique described by Colalongo *et al.* for transient simulation of thin film transistors [87]. Specifically, the locality of the MTD equations permits a complete description of dispersive transport (as well as trapping at OV and DH sites) without increasing the number of equations with respect to the purely drift-diffusion case. The resulting system of equations 20-23 is numerically solved using a globally-convergent variant of the Newton-Raphson method [88]. The set of linear equations resulting from finite-difference discretization is solved using the conjugate-gradient-squared (CGS) method with incomplete LU (ILU) decomposition for preconditioning [89]. The time-step size was adaptively calculated using the TR/BDF scheme [90].

Overview of Simulation Studies

The model presented in this chapter achieves unprecedented completeness in the mathematical description of the radiation response of SiO_2. Consequently, an extensive range of practical applications of the model can be imagined, too extensive to be covered in the course of this dissertation. The specific simulation studies presented here are chosen with two goals in mind.

The first goal emphasizes the novel technical accomplishments represented in the model for hydrogen-mediated interface trap formation. This goal is addressed in Chapter V, which presents a one-dimensional simulation study patterned after previous "Pulsed Irradiation/Switched Bias Simulation" experiments. This results of this study validate the main scientific aspects of the present work, i.e., the proton release kinetics and MTD approach to dispersive transport. This study was performed using a stand-alone program written in C++.

The second goal reflects the motivation for this work that was summarized in the introduction, specifically, the advancement of Technology Computer Aided Design (TCAD) approaches to radiation-response optimization. This goal is addressed in Chapters VI and VII, which both report the results of two-dimensional process simulation and device simulation in which only hole trapping is accounted for and dispersive transport is neglected. This is achieved by imple-

menting a simplified set of equations (omitting the proton continuity and MTD equations) in a commercial TCAD environment. The model used in these studies is scientifically similar to that used in numerous previous studies. However, the integration with process simulation permits the demonstration of novel engineering applications of physically based models for radiation response. Specifically, Chapter VI clarifies an important radiation-induced leakage current problem in Mesa-isolated SOI technology and Chapter VII demonstrates the more general concept of applying radiation-response modeling in the "computational split lot" approach to process optimization.

CHAPTER V

PULSED RADIATION/SWITCHED BIAS STUDY

Simulation Description/Experimental Motivation

This chapter reports the results of a series of transient simulations of a 1 kRad(SiO_2) pulse of radiation delivered to an MOS capacitor structure with t_{ox}=35 nm. The pulse has Gaussian time dependence with standard deviation, σ=1.0 ms and mean, μ=2.0 ms. Two applied bias conditions were studied: in one case a bias of +7 V was maintained throughout the entire simulation (10^6 seconds). In the other case, the bias was held at -7 V for 10 ms, switched to +7 V in 1 ms, and then held constant for the remainder of the 10^6 seconds. We adopt the labeling conventions "+2 MV/cm" and "-2/+2 MV/cm" for these two bias conditions. This simulation study is patterned after the experimental work described in [70], in which CTRW calculations were performed with assumed initial proton profiles in order to analyze the time-dependence of interface trap formation. The mathematical model presented in the previous chapter offers an alternative approach for simulating the pulsed-radiation/switched bias experiment which is inherently more general than previous CTRW methods.

Mathematical Model and Parameters

The equations used in the simulation study are as presented in Chapter IV with one exception: the αnp recombination is neglected based on the assumption that the dose-rate and total-dose used in the simulation are sufficiently low that pure geminate recombination dominates the overall response. For conditions in which carrier densities are extremely high this mechanism must be included. The remaining information is summarized in Table 1. Note that results reported in this paper have been obtained without MTD enabled for holes. This choice was made because the triangular shape of the initial proton profiles that have been inferred in previous work appears to be consistent with proton release occurring during the prompt, nondispersive period of transport [17]. This view is reasonable since the distance covered by this transport phase, $\sim$ 10 nm, is a significant fraction of the 35 nm oxide. In general, differences in proton release associated with holes

transporting dispersively and nondispersively have not been resolved in the literature and require further study. For protons we have performed dispersive as well as nondispersive simulations.

Table 1: Values of key model parameters used in pulsed-radiation/switched bias simulation

Parameter	**Value**	**Units**
$\sigma_{p,DH}$	1×10^{-15}	cm^2
$v_{th,p}$	1×10^{7}	cm/s
$[DH]_0$	1×10^{15}	cm^{-3}
$[SiH]_0$	1×10^{12}	cm^{-2}
$\sigma_{H^+,MTD}$	1×10^{-15}	cm^2
N_{TV,H^+}	1×10^{18}	cm^{-3}
β_{H^+}	0.075	eV
N_{V,H^+}	1×10^{19}	cm^{-3}
E_{T,H^+}	0.01 to 2.50	eV
N_{T,H^+}	50	N/A
μ_n	20	cm^2/Vs
μ_p	1×10^{-5}	cm^2/Vs
μ_{H^+}	4.6×10^{-7} (MTD and no MTD) 10^{-8}, 10^{-12}, 10^{-18} (no MTD)	cm^2/Vs

Whether proton release occurs uniformly throughout the oxide, only at the interfaces, or a combination of the two cases has received some attention in the literature [49, 70]. Although the model introduced in this dissertation is well-suited for studying different DH distributions, the results reported here are exclusively for a uniform DH density equal to 10^{17} cm^{-3}. It should be recognized that enhanced interfacial proton generation may be achieved with a uniform distribution of DH sites if cracking at E' centers is occurring. This issue should be explored since contributions from both hydrogen-related and intrinsic defects may provide an explanation for the process dependence in the distributions of initial proton profiles inferred from switched bias experiments.

Results and Discussion

Figure 14 shows the proton profiles at t=10 ms for each bias condition. These results are obtained with the proton MTD equations enabled and proton mobility, $\mu_{H^+}=4.6\times10^{-7}$. Using the same proton mobility without MTD equations results in complete loss of protons well before 10 ms.

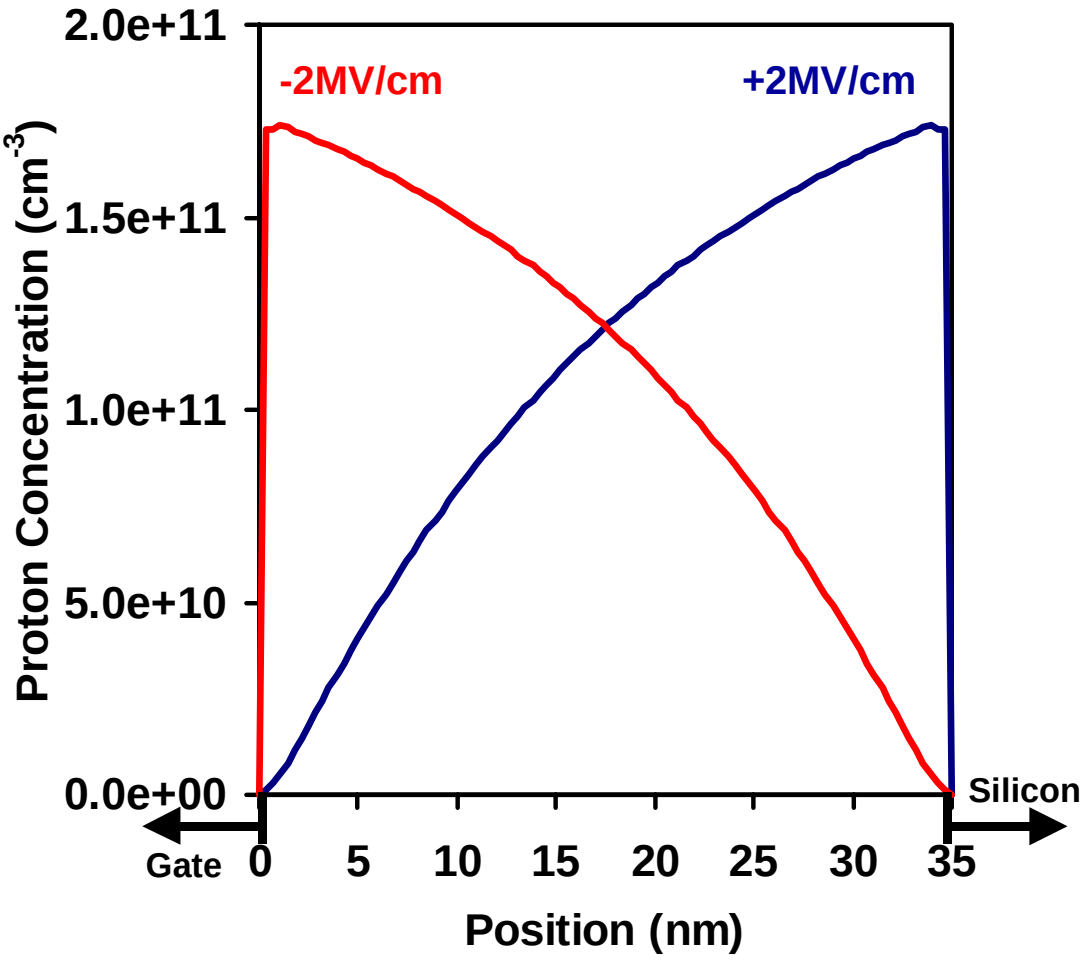

Figure 14: Proton profiles at 10 ms for positive and negative bias during the pulsed irradiation. Results are only shown for dispersive proton transport calculations because the corresponding drift diffusion simulation results in virtually complete proton loss by 10 ms.

Figures 15 and 16 display the proton concentration at the Si-SiO_2 interface as a function of time for the +2 MV/cm case and the -2/+2 MV/cm case, respectively. Figure 15 provides results for both dispersive and nondispersive proton transport; here the nondispersive model results in

almost no delay between the end of the radiation pulse and completion of the proton transport. The dispersive model, however, produces an initial delay in the proton arrival at the interface followed by a gradual decay over many decades in time. Results for the nondispersive model do not appear in Figure 16 because, under negative bias, all the protons exit the oxide at the gate-SiO_2 interface. Integration of $H^+(t)$ in Figures 15 and 16 reveals only 5% proton loss for the dispersive calculation of the -2/+2 MV/cm bias case, resulting in similar saturation values of interface trap density for the two cases.

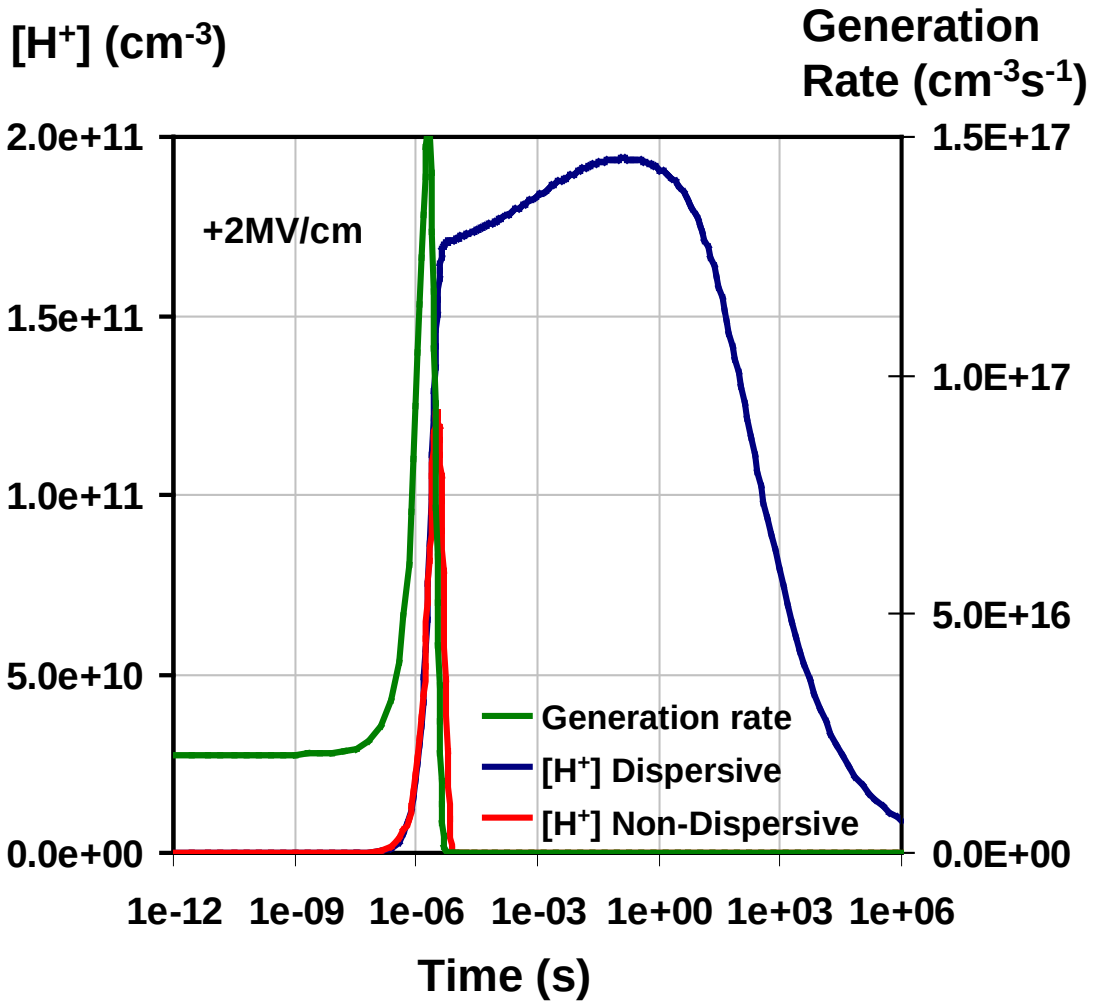

Figure 15: Proton concentration at the Si-SiO_2 interface as a function of time for the +2 MV/cm bias case. Non-dispersive proton transport calculations vastly overestimate the rate of proton arrival at the interface.

The time-dependence of interface trap formation is determined by the flux of protons arriving

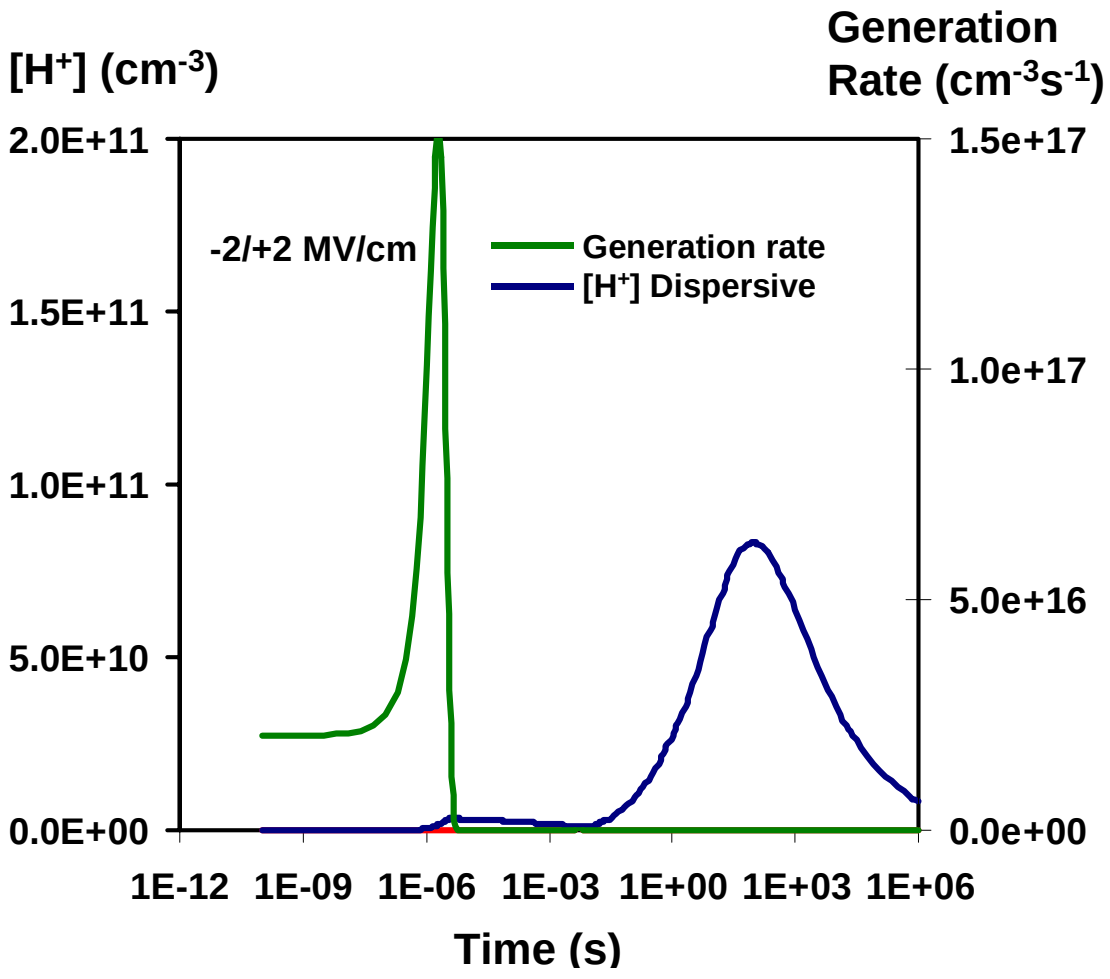

Figure 16: Proton concentration at the Si-SiO_2 interface as a function of time for the -2/+2 MV/cm bias case.

at the Si-SiO_2 interface (See Equation 19). Figure 17 shows the normalized interface trap concentration as a function of time resulting from nondispersive calculations (MTD disabled) along with experimental data taken from [70]. Simulation results for each bias condition and three different proton mobilities are shown here. In the case of the highest mobility ($\mu = 10^{-8}\text{cm}^2/\text{Vs}$), the results for the -2/+2 MV/cm bias condition are absent. The reason for this appears in the earlier explanation of Figure 16, i.e., complete proton loss occurs during the negative bias period so interface trap formation does not occur after the bias is switched. Results for the two lower mobilities qualitatively exhibit the delay in the formation time when the bias is initially negative and then switched positive (recall that for this case more protons are released farther from the Si-SiO_2 interface). However, regardless of mobility, the nondispersive calculations are unable to predict the gradual interface trap formation over many decades in time.

Figure 18 shows results for dispersive proton transport calculations (MTD enabled). Here, we see that results for each bias condition are predicted well by the continuity-equation-based approach to modeling interface trap formation. Note that we obtain a satisfactory prediction without any form of enhanced proton generation near the interfaces. More thorough testing of the spatial distribution in proton release should, however, be pursued through spatially varying DH distributions and also H_2 cracking at E' centers.

Conclusions

The problem of representing the microscopic transport behavior of SiO_2 in a macroscopic numerical model is a difficult one, precisely because absolute certainty with regard to the microscopic physics is not yet available. This issue is particularly evident in the rather anomalous transport properties observed in the oxide layers of protonic memory structures [91]. Although the microscopic mechanisms underlying the properties of these (as well as conventionally-processed oxides) have not yet been completely resolved, the present numerical model can assist in the exploration of candidate models as they are developed. For example, protons in protonic memory structures are observed to transport faster and less dispersively than in conventional oxides; it may be useful to consider this behavior in the context of MTD equations using a smaller β and higher mobility (and the corresponding CTRW interpretation). Furthermore, proton trapping

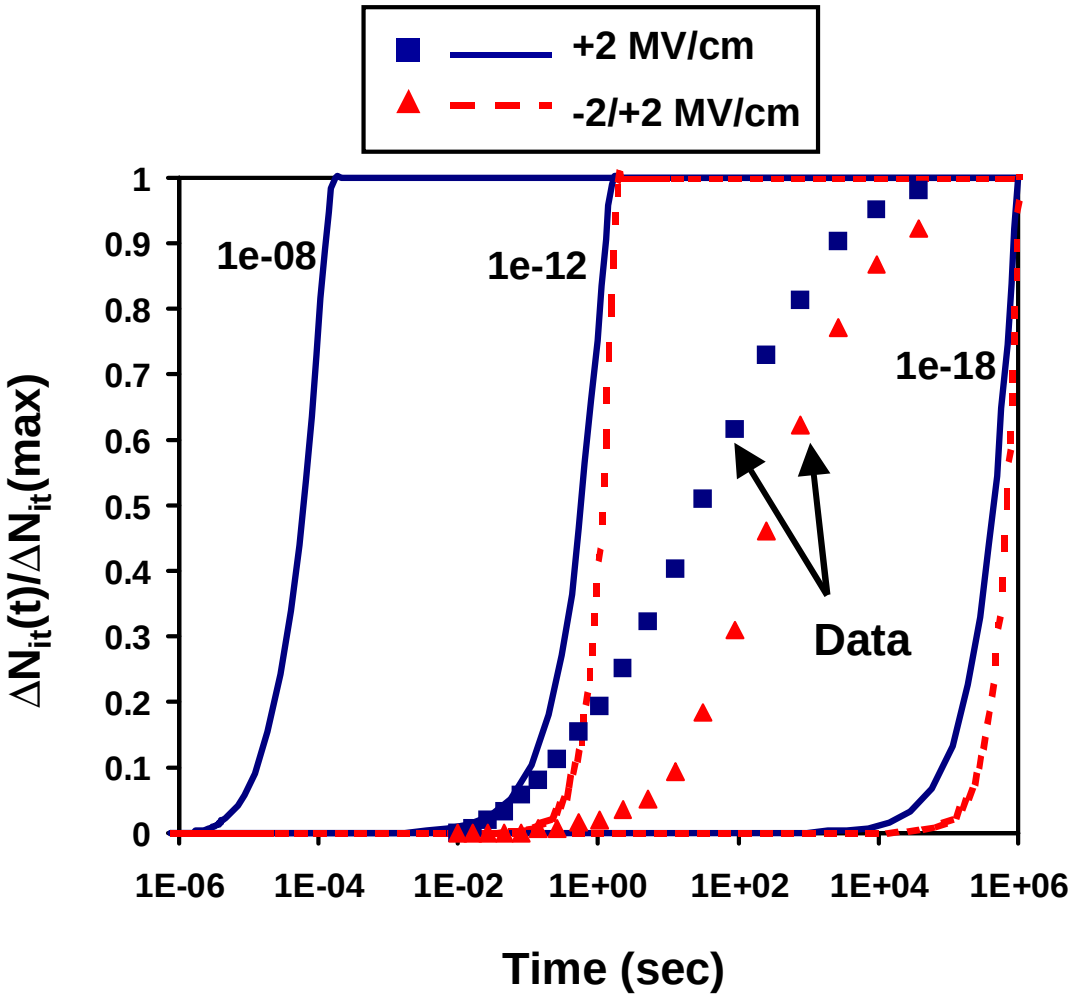

Figure 17: Normalized interface trap buildup vs. time using nondispersive transport for protons. The poor fit to data regardless of mobility value indicates that dispersive transport is essential for modeling time-dependent interface trap formation. Data for -2/+2 MV/cm is absent for the case of $\mu = 10^{-8}\text{cm}^2/\text{V}\cdot\text{s}$ because with this mobility value the protons are completely lost at the gate side before the bias is switched.

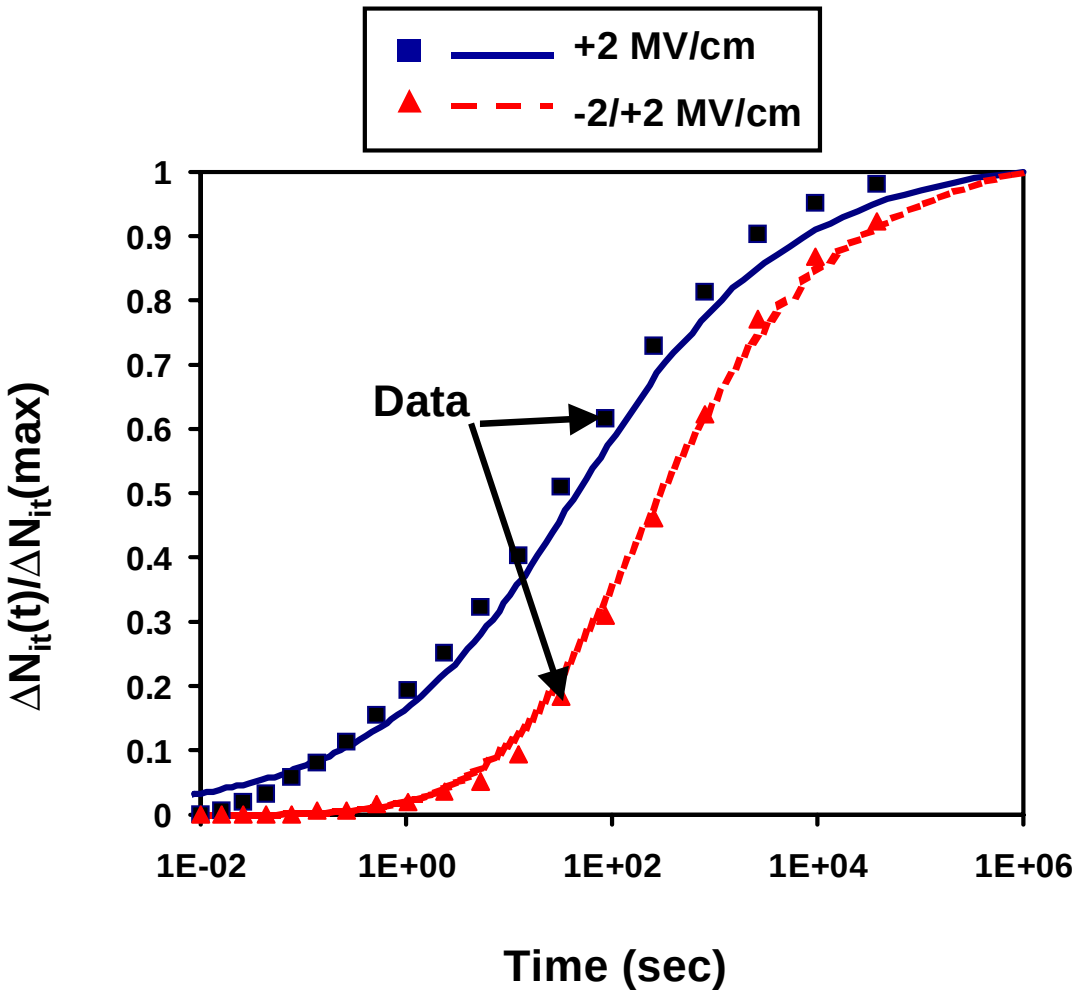

Figure 18: Normalized interface trap buildup vs. time using nondispersive transport for protons. The simulation parameters are calibrated to the $+2$ MV/cm data; simulations of the -2/$+2$ MV/cm exposure condition using these same parameters provide a good fit to the corresponding measured data.

and confinement effects can be represented with additional trapping terms in proton continuity and modified boundary conditions, respectively. In addition to unresolved issues regarding the role of hydrogen in silicon dioxide, the model described in this dissertation does not address the (trapped hole-conversion) process thought to be responsible for the prompt component of interface trap formation which, in some studies, has been observed to contribute significantly to the overall radiation response [92]. Nevertheless, the three-continuity equation approach described in this dissertation accomplishes an important first step in numerical approaches to modeling both charge trapping and interface trap formation in irradiated MOS structures.

CHAPTER VI

SOI BACK-CHANNEL LEAKAGE STUDY

Overview

Isolation-related leakage is emerging as the principal total dose issue in advanced semiconductor technology due to aggressive scaling of typical gate oxides and device geometries. This chapter presents experimental results of enhanced radiation-induced backchannel leakage in a mesa-isolated SOI device architecture as well as simulation results which clarify the origin of this enhancement. Specifically, using two-dimensional process and device simulation equipped with the model for hole trapping at oxygen vacancies (Equation 27 on Page 42), the cause of this is identified to be enhanced hole trapping in the buried oxide near the island edge. Simulations suggest that body ties placed at the edge of the island can suppress the leakage associated with the enhanced hole trapping if they are made sufficiently wide. Simplified current calculations provide quantitative estimates of radiation-induced leakage as a function of radiation absorbed dose and body tie width. Finally, potential performance and manufacturing impacts of controlling enhanced back-channel leakage in mesa devices using wider body ties at the island edge are discussed.

Background

A simple isolation method in SOI technology is to build devices in separate islands of silicon, or mesas, using anisotropic etching [93]. However, as shown in Figure 19 (top), a parasitic drain-to-source leakage path exists along the vertical edge, or sidewall, of the island [94]. A leakage path also exists on the bottom surface of the island. This backside leakage is normally small due to the high threshold voltage associated with the thick buried oxide. The edge leakage path can be suppressed by creating narrow p-type body-tied-to-source (BTS) tabs in the source side of the device at the edges of the island (Figure 19 (bottom)). Normally, BTS tabs are used in partially depleted SOI devices to suppress floating body effects [95], however, when they are placed at the edge of the island they also serve to block parasitic leakage by separating the source region

from the parasitic channel associated with the vertical edge of the island. Note that this blocking action occurs on the front and back surfaces of the island over the width of the BTS, thereby reducing the effective device width.

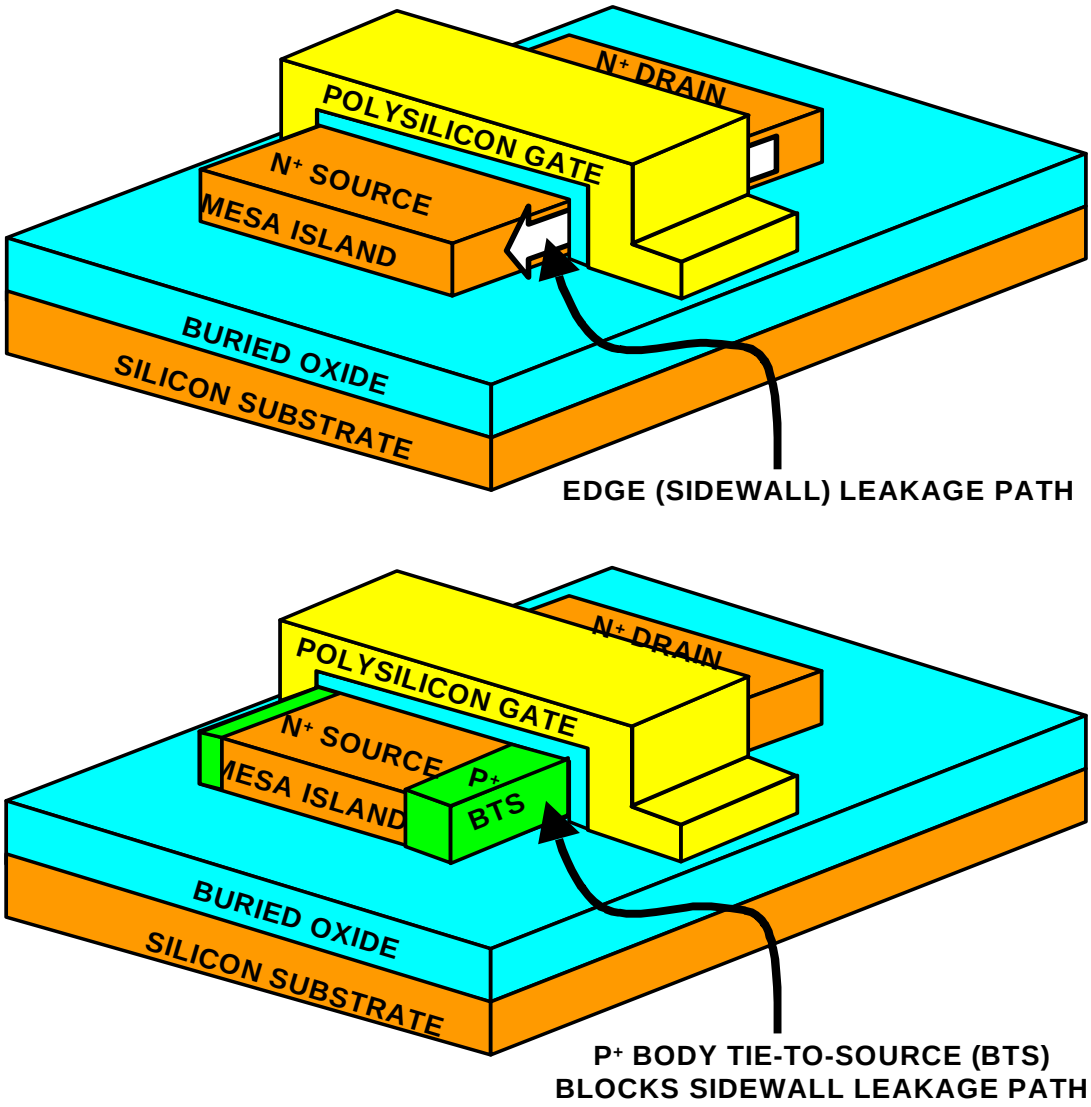

Figure 19: Basic structure of SOI nMOSFET built using mesa isolation. (top) White arrow shows parasitic leakage path along the vertical edge of the mesa. (bottom) Body-tied-to-source tabs are placed at the edge of the mesa to suppress the parasitic edge leakage path.

Another important feature of the mesa device architecture is that the polysilicon gate runs down the vertical edge of the island to the top surface of the buried oxide (BOX). This results in high electric fields in the BOX near the island edge (along the length of the device) when the

gate is biased at a high voltage.

This chapter presents an analysis showing that enhanced hole trapping due to this high field region explains enhanced back-channel leakage observed in an SOI nMOSFET irradiated with V_G=5.0 V and $V_S = V_D = V_B$=0.0 V. We then consider the ability of BTS tabs located at the edge of the island to block some or all of the enhanced near-edge region of back-channel leakage that results from the enhanced hole trapping. Specifically, using simplified leakage current calculations, estimates of back-channel leakage are obtained as a function of total dose exposure and BTS width.

Experimental

The n-channel SOI nMOSFETs used in this study were fabricated at the SPAWAR facility [96] using mesa isolation methods on SIMOX wafers with buried oxide thickness of 400 nm and silicon film thickness of 220 nm. The highest temperature during fabrication was a 1320°C anneal in 99.5% Argon and 0.5% Oxygen that occurs as part of the SIMOX wafer processing. The gate oxide thickness for these devices was 15 nm.

Two test structures were used to study edge effects in total dose response: a closed geometry nMOSFET with L=0.8 μm and W=200 μm and a set of 40 L=0.8 μm and W=5 μm devices built in separate islands and connected in parallel (giving the same effective active region dimensions as the closed geometry device and a total of 80 parasitic edge leakage paths).

BTS tabs with a width of 0.8 μm were used to provide body contact in both test structures. The BTS tabs were created by exposing regions of the source side of the nMOS device to the pMOS source/drain implantation steps. This results in narrow tabs of p-type silicon that are self-aligned to the gate and penetrate the full depth of the island to the BOX. These p-type tabs are shorted to the n-type region of the source during contact formation, providing a grounded contact to the body. In the multiple edge devices the BTS tabs were placed at the edges of the island to suppress sidewall leakage. The existence of sidewall leakage in devices without BTS tabs at the edge was confirmed using test structures without BTS tabs that displayed the characteristic two slopes in subthreshold characteristics [97].

The edgeless and multiple-edge structures were irradiated using a Co^{60} source to a total dose

of 1 Mrad(SiO_2) at a dose-rate of 256 rad(SiO_2)/s with their gates biased at +5 V and other terminals grounded. Figure 20 shows pre- and post-irradiation characteristics of the multiple-edge and edgeless devices. The pre-irradiation characteristics of each test structure are identical, indicating that the BTS tabs are effective in preventing edge leakage. However, there is a large enhancement in the post-irradiation subthreshold leakage current in multiple-edge devices. The gate-bias independence of this leakage and the negligible shift in frontside threshold voltage indicates this current is flowing along the backside. The much smaller backside leakage in edgeless devices suggests the leakage enhancement in multiple-edge devices is related to the island edge. The remainder of this chapter describes the use of numerical simulation to identify the underlying cause of the enhanced leakage in multiple edge devices, specifically, an edge-related enhancement in the buried oxide hole trapping.

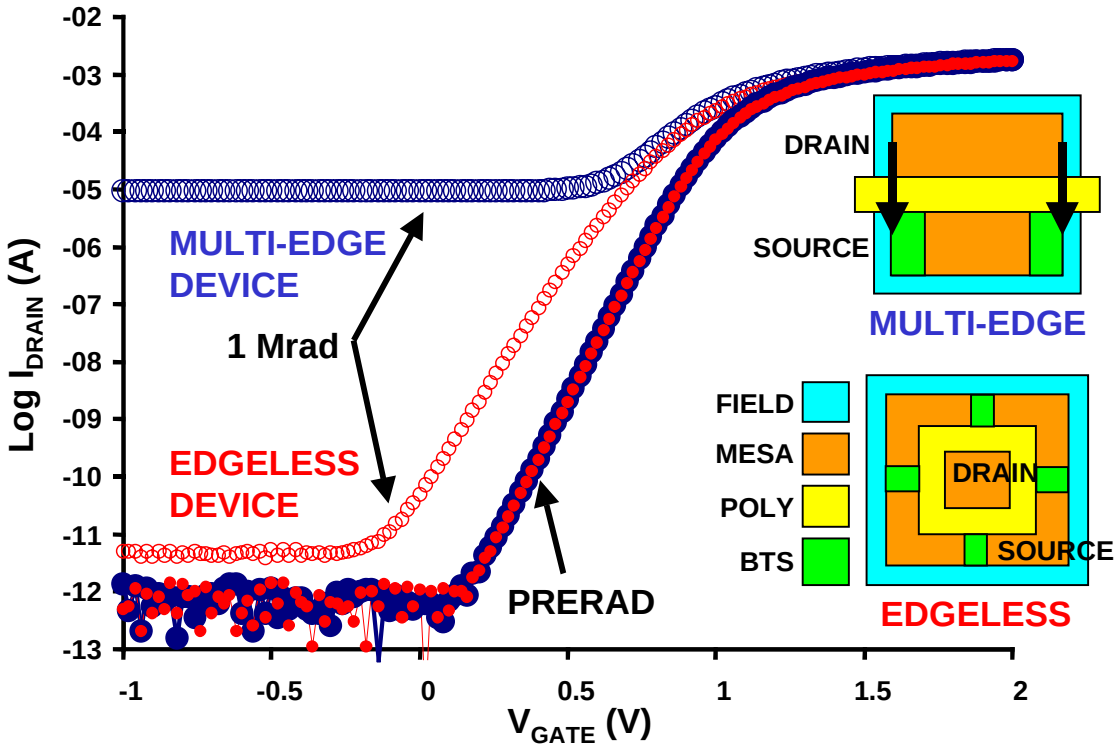

Figure 20: Pre- and post-irradiation $I_D - V_G$ characteristics showing that edge effects are absent in pre-rad characteristics but back-channel leakage is significantly enhanced in irradiated multiple edge devices.

Simulation

As stated at the end of Chapter IV, the goal of this simulation study is to demonstrate a successful engineering solution to a practical radiation-effects problem using Technology Computer Aided Design practices. For this reason, a brief discussion is provided of the overall role of TCAD in process optimization followed by a description of the hole trapping model and parameters used for this simulation study.

Standard TCAD

Typical TCAD environments integrate the activities of process and device simulation, device model parameter extraction, and circuit simulation, into the framework illustrated in Figure 21 [98, 99]. Process simulation uses models for implantation, diffusion, etc. to predict the structures generated by specific sequences of processing steps. Device simulation uses complete structures along with carrier transport models to predict current vs. voltage (IV) characteristics of devices as well as experimentally inaccessible internal features such as potential and charge distributions. Simulated IV characteristics are used in the same way as experimental data to parameterize compact device models used in circuit simulation tools such as SPICE. However, additional physical insight gained from internal information provides a basis for process/device optimization beyond that possible with experimental data alone.

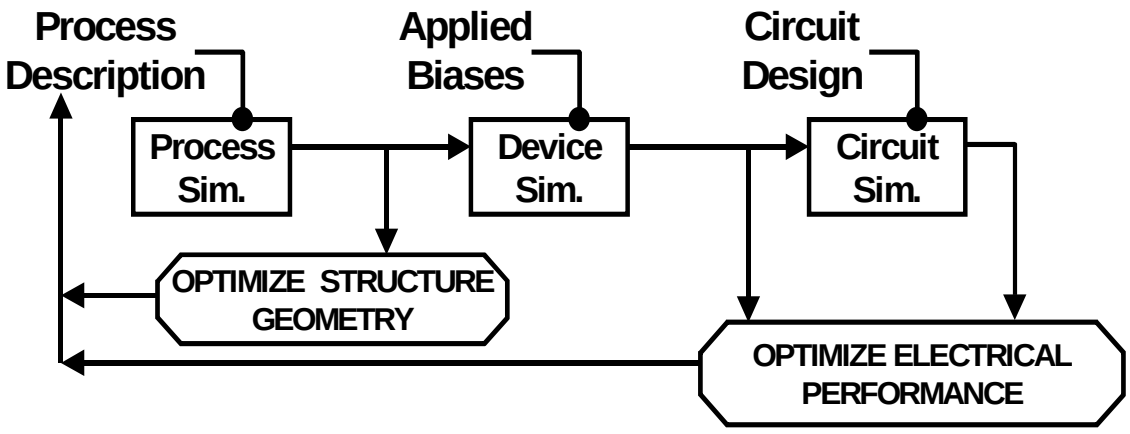

Figure 21: Simulation path illustrating the integrated hierarchy of process, device and circuit simulation provided by standard TCAD tools.

TCAD-Based Hole Trapping Simulation

The total dose simulations described in the following section were performed using an integrated simulation capability for hole trapping implemented in a commercial TCAD tool. As indicated in Figure 22, each level of the TCAD hierarchy has a role in predicting radiation response. The SOI study described in this paper uses the ATHENA process simulator and the ATLAS device simulator equipped with the model for radiation-induced hole trapping at oxygen vacancies described earlier.

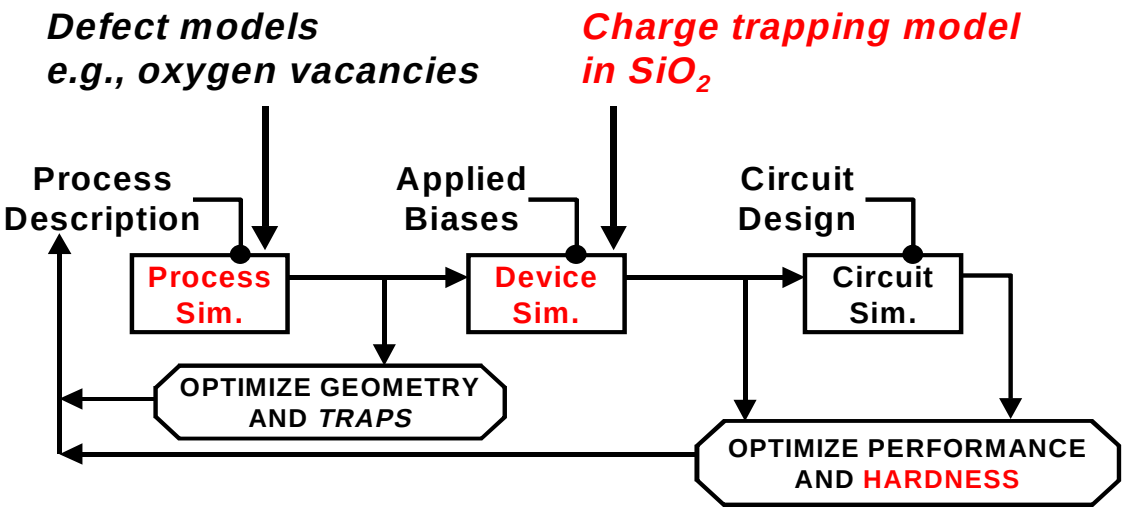

Figure 22: Simulation path illustrating the application of TCAD tools for simulating (total dose) radiation response.

Standard device simulators provide the basic carrier transport models necessary for studying transient phenomena in semiconductor devices. Although the high carrier densities and concentration gradients in ion-induced charge tracks violate certain assumptions in these models [4], commercial device simulators have proven valuable for studying single-event effects [5, 6]. Dose-rate studies have also been performed using numerical device simulation [10].

Device-level total dose simulation requires models for carrier generation, recombination, transport and trapping in insulator regions. Various models for these processes have been implemented in stand-alone numerical device simulators described in [28, 29, 30, 38, 39]. In general, similar approaches have been used to model carrier transport in SiO_2, i.e., coupled continuity and drift-diffusion equations. Radiation-induced electron-hole pair creation appears in the continuity

equations as a field-dependent net generation rate accounting for geminate recombination [100]. Effective mobilities are used in the drift-diffusion equations to account for the different time scales for electron and hole transport. Although this approach neglects the dispersive nature of hole transport in SiO_2, the comparison given in [38] of drift-diffusion calculations with those obtained using the dispersive multiple-trapping model indicate that for typical total dose exposure conditions at room temperature, the simpler drift-diffusion model is adequate.

Various SiO_2 charge accumulation mechanisms are included in these simulators: hole and electron trapping, thermal emission of trapped holes and electrons, and trapped hole compensation. Tunnel annealing of holes is a mechanism that has not been included in these device simulators, but is known to contribute to radiation-induced parameter shift, i.e., recovery in threshold voltage after pulsed irradiation. Quantitative studies [52, 54] of tunneling effects have, however, provided equations which may, in principle, be useful in a 2D device simulator.

Recently, the implementation [31] and application [32] of a two-dimensional hole trapping model in the ATLAS device simulator [99] were reported. This model applies the system of coupled differential equations for electrons and holes in the oxide regions of device structures provided either by the ATHENA process simulator or the device editing tool, DEVEDIT [99].

Following previous approaches [29, 30], carrier transport in SiO_2 is approximated with standard drift-diffusion equations using effective mobilities for electrons, μ_n=20 cm^2/Vs and holes, μ_p=10^{-5} cm^2/Vs. Generation-recombination processes are accounted for with the net generation term in the carrier continuity equations that accounts for geminate recombination. The accumulation of trapped holes is modeled using first order trapping theory with the spatial distribution of trap density defined by the user. The effects of trapped holes and mobile carriers on the electric field distribution are contained in Poisson's equation.

It is worth noting a few differences between the hole trapping simulations described here and those described in [28, 29, 30, 38]. The model used in the present simulations does not include thermal emission of trapped holes, trapped hole compensation, or electron trapping effects. These effects are known to be significant in a number of oxides and exposure conditions [57]. Low dose-rate effects in bipolar transistors, for example, require detrapping and/or compensation terms for the charge buildup process. The absence of electron trapping in these SOI simulations prevents quantitative agreement with experimental data at high total dose levels (as discussed in the next

section). Furthermore, the present simulations do not include dispersive transport of holes. In cases where dose-rate changes rapidly with time or when temperature varies significantly during exposure, the MTD equations for must be added to the model. Finally, the absence of the interface trap formation model in these simulations is justified by the dominance of hole trapping that was observed in the experimental data.

Hole Trapping Simulation Results

In order to analyze the edge-related enhancement in back channel leakage, 2D process simulation was performed for a widthwise slice through the center of the channel at the edge of the island (Figure 23). The resulting structure was then used in the hole trapping simulations. Since the source and drain are both grounded during irradiation, the hole trapping is expected to be relatively uniform along the channel length dimension, justifying the use of a single 2D cross section in the hole trapping calculation.

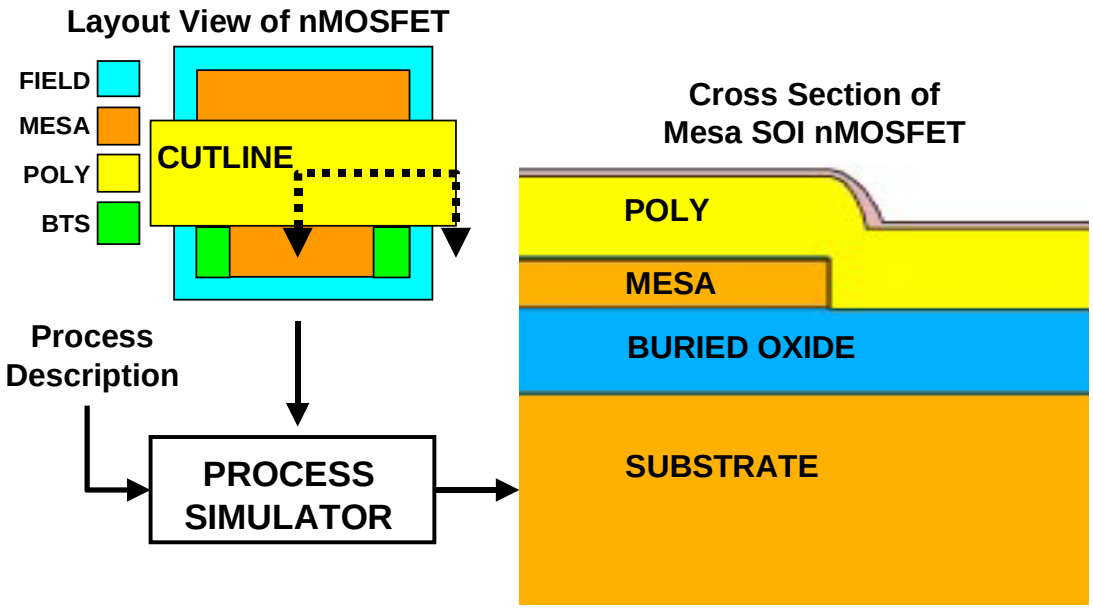

Figure 23: Schematic showing the cutline location for the structure used in simulation of the SOI nMOS transistor.

The radiation effects simulations reported here were performed using the Leray model for geminate recombination [100], a capture cross section for holes, σ_p=1.25 $\times$ 10^{-13} cm^2 and a

uniform density of hole traps, $N_{Tp}(x,y)=2\times10^{18}$ cm^{-3}. These values provide a reasonable fit to the experimental data shown later and are consistent with values found in the literature [21, 101]. In particular, the hole trap density agrees with the prediction of the model in [101] for a 1320°C SIMOX anneal (to within the factor of 2 accuracy expected for electron spin resonance measurements). To mimic experimental exposure conditions, the polysilicon gate region was biased at 5 V in the hole trapping simulations. Hole trapping is enabled only in the buried oxide since our focus is the back-channel leakage (and the results of Figure 20 suggest that hole trapping in the sidewall and front gate oxide is negligible).

Figure 24 shows the simulated trapped hole density, p_t, in the buried oxide after 400 krad(SiO_2). These results reveal an enhancement in the hole trapping in the buried oxide close to the island edge (circled region in Figure 24). The 2D solutions reveal the origin of this to be enhanced electron-hole pair yield, and thus net generation rate, associated with high electric fields in the oxide where the sidewall portion of the polysilicon gate meets the top surface of the BOX (Figure 25). The enhanced generation rate along with the drift-diffusion transport model results in enhanced hole current density, and therefore, hole trapping in a small region of the BOX near the island edge.

The enhanced near-edge BOX hole trapping produces a corresponding enhancement in the backside inversion near the island edge. At low radiation doses, the BTS is wide enough to suppress the leakage along this near-edge region of enhanced inversion in the same way it blocks the edge leakage. However, as the device is subjected to higher doses, the width of the region of enhanced charge trapping (and hence backside inversion) exceeds the width of the BTS (Figure 26). At this point, significant leakage currents can flow on the back surface of the silicon island near the BTS.

Simplified Leakage Current Calculations

Although 3D device simulation is available, for simplicity we calculated the leakage current by analyzing the 2D electron density distributions obtained using a gate bias of -1 V and a drain bias of 0.1 Vin the structures obtained for various dose levels. At any given point, x, along the back interface, the charge due to electrons in the inversion layer, $Q_n(x)$, can be calculated by

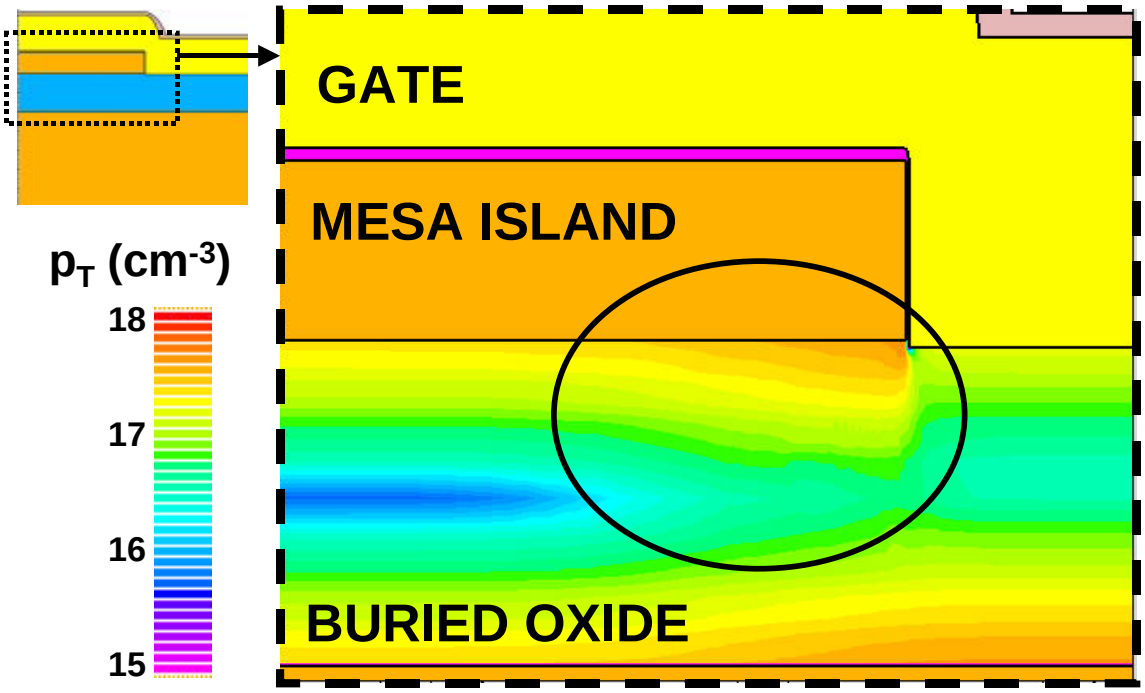

Figure 24: Simulations reveal enhanced trapped hole density, p_t, in the buried oxide near the island edge.

integrating the electron concentration along a vertical line from the back to the front interface of the island. The leakage current along a thin strip of width Δx at x was approximated using [102]:

$$\Delta I(x) = \mu_n \left(\frac{\Delta x}{L} \right) Q_n(x) V_D \tag{31}$$

Here, μ_n is the electron mobility (650 cm^2/Vs), L is the channel length (0.8 μm), and V_D is the drain bias (0.1 V). Finally, the total leakage current for a given width of the BTS tabs was calculated by adding the contributions, ΔI(x), over the region of the back interface which is not covered by the tabs:

$$I_{\text{LEAK}}|_{V_G=-1,V_D=0.1} = \sum_{W_{BTS}}^{W-W_{BTS}} \Delta I(x) \tag{32}$$

Two main assumptions are used here. First, the method in [102] assumes the gradual channel approximation is valid. Although this may introduce some error in a device with L=0.8 μm, the uniformity in trapping along the channel length dimension expected for ON state irradiation as well as the low drain bias that is used in the calculation makes the gradual channel approximation reasonable for obtaining estimates. Second, we assume that the BTS tab is completely effective

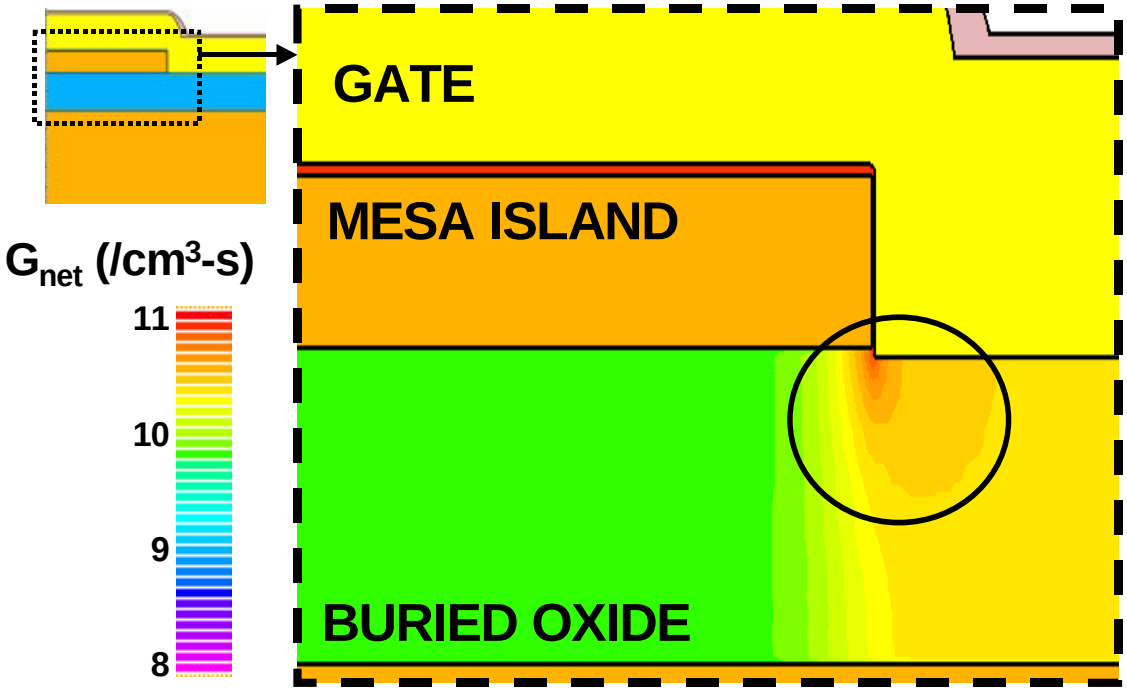

Figure 25: The underlying cause of the enhanced hole trapping is seen to be a local region of higher net generation rate associated with the high electric fields in the buried oxide near the edge of the island.

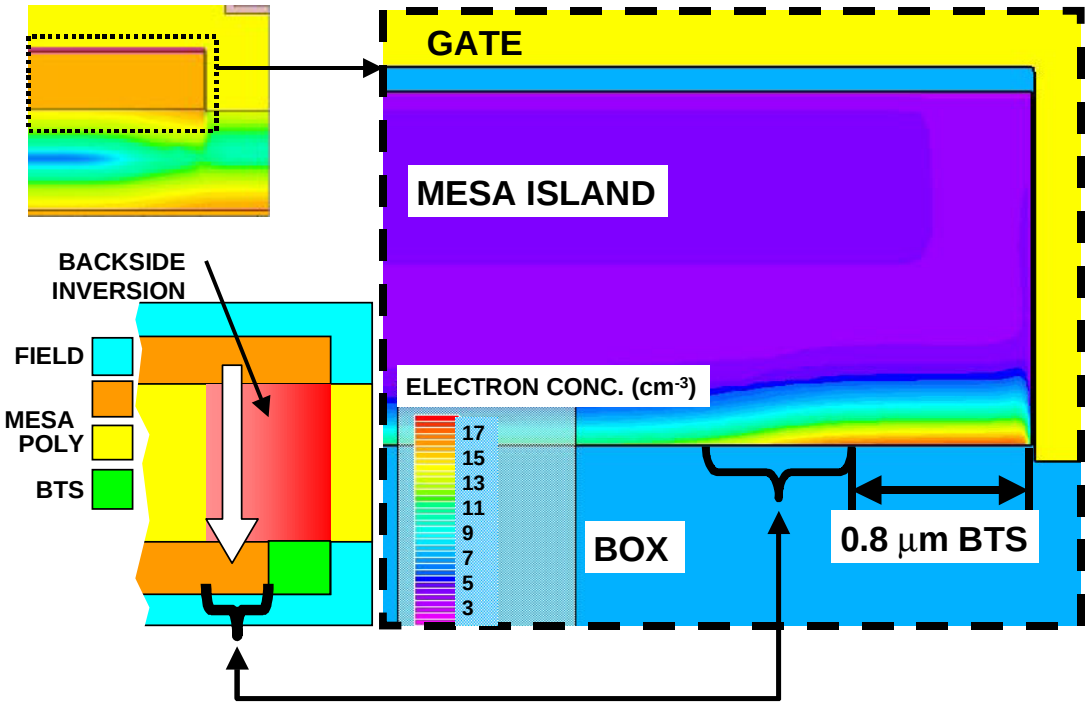

Figure 26: Region of enhanced electron concentration eventually extends beyond the BTS width forming a direct backside leakage path from drain to source.

in blocking leakage throughout its drawn width. In reality, the effectiveness of the BTS will attenuate over a finite distance due to straggle in the BTS doping and 3D features of the leakage current path.

Figure 27 compares simplified calculations with experimental leakage current results as a function of total dose for a BTS width of 0.8 μm. The apparent deviation of the simulations from experimental data at low dose is due to the detection limits of the experimental current measurements. However, the deviation at high dose (greater than 400 krad(SiO_2)) is due to the absence of electron trapping in these simulations. Specifically, the saturation of leakage at high dose seen experimentally is consistent with the significant role for electron trapping that has been observed in SIMOX buried oxides [94]. In the simulations, the compensating effects of electron trapping are absent, causing the leakage current to be overestimated at high doses.

The results of simple hole trapping calculations can be viewed as providing a worst case estimate for leakage current degradation; this is a useful observation under conditions where the buried oxide electron trap density may not be well controlled. The good agreement between

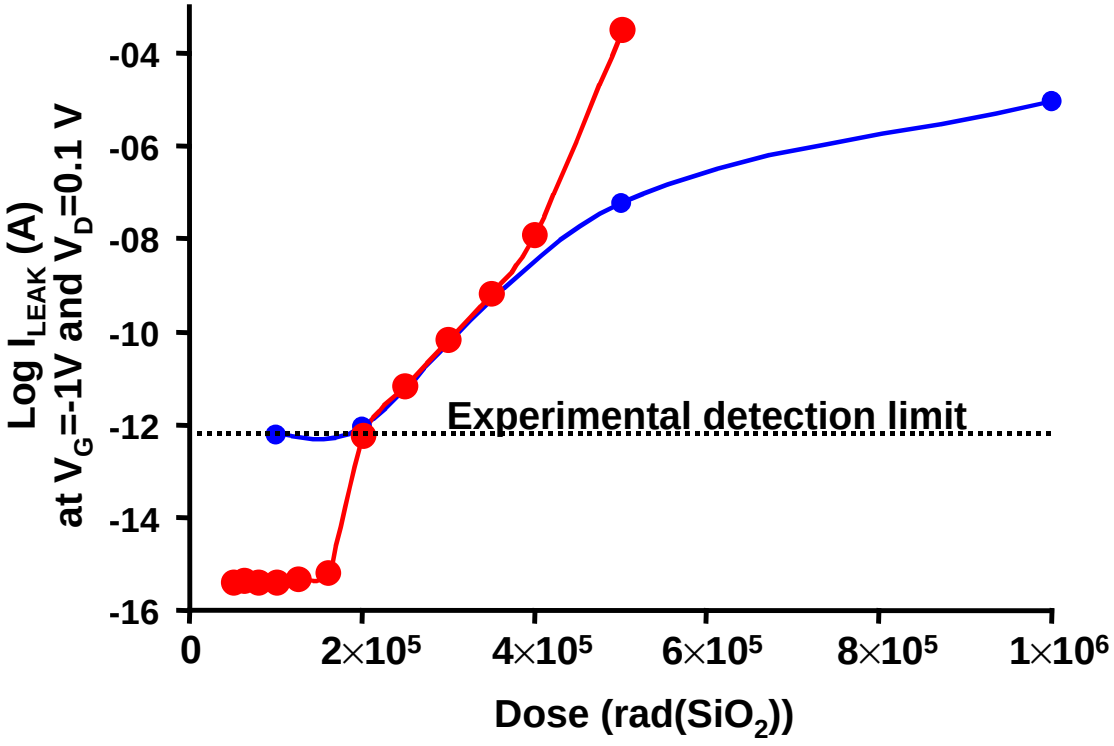

Figure 27: Simulated and experimental leakage currents at $V_G = -1$ V and $V_D = 0.1$ V as a function of dose for a BTS width of 0.8 μm.

experimental and simulated leakage for low doses indicates that the hole trapping simulations are providing the essential features of the radiation response, in particular, the role of the BTS in suppressing backchannel leakage near the island edge. Specifically, we note that the sharp increase in leakage at 200 krad(SiO_2) occurs when the region of enhanced hole trapping begins to extend beyond the width of the BTS.

Hardness/Performance/Manufacturing Analysis

These simulation results suggest a fundamental relationship exists between BTS width and total dose hardness of mesa isolation technology. The leakage currents at V_G=-1 V and V_D=0.1 V obtained using the technique described in the previous section have been plotted as a function of the BTS width for various total dose exposures in Figure 28.

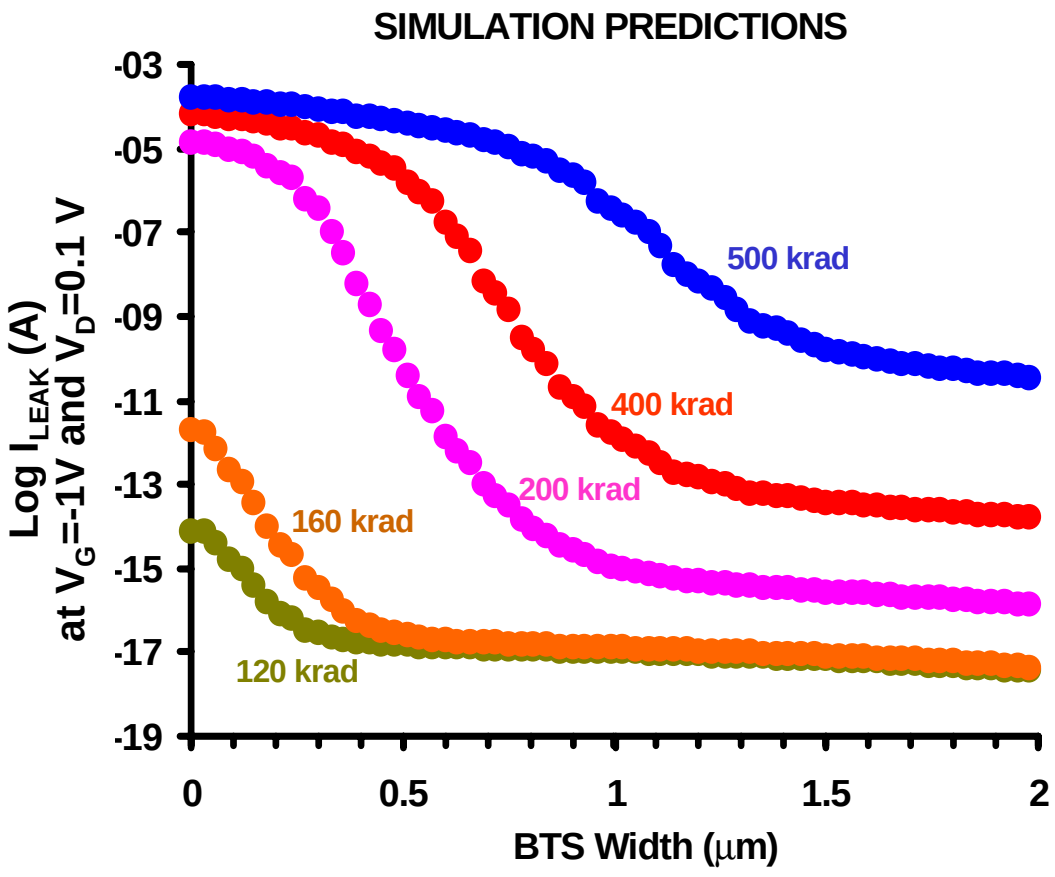

Figure 28: Leakage current vs. BTS width at various doses.

Test structures with varying BTS width have been designed to systematically test these predictions; however, our conclusion that BTS tabs act to block near-edge back-channel leakage is qualitatively supported by comparatively larger enhanced leakage (data not shown) observed in devices without BTS tabs, i.e., $W_{BTS} \rightarrow 0$. It should be remembered that the high dose region of this analysis represents the worst case condition where electron trapping is absent. The 500 krad(SiO_2) curve of Figure 28 indicates that even in such a worst case scenario, increasing the BTS width is expected to have a considerable effect at high dose levels.

The increase in total dose hardness with BTS width is plotted in Figure 29. Here, hardness is defined as the dose at which the leakage exceeds 1 nA. Since the experimental and simulation results match reasonably well for this level of degradation (see Figure 27), this analysis may be regarded as relatively insensitive to the absence of electron trapping in the total dose simulations. This observation is valid for the range of BTS widths, since the source and drain are grounded during exposure and likely to contribute only minor edge effects (justifying the use of hole trapping simulations in a 2D widthwise plane in the active region).

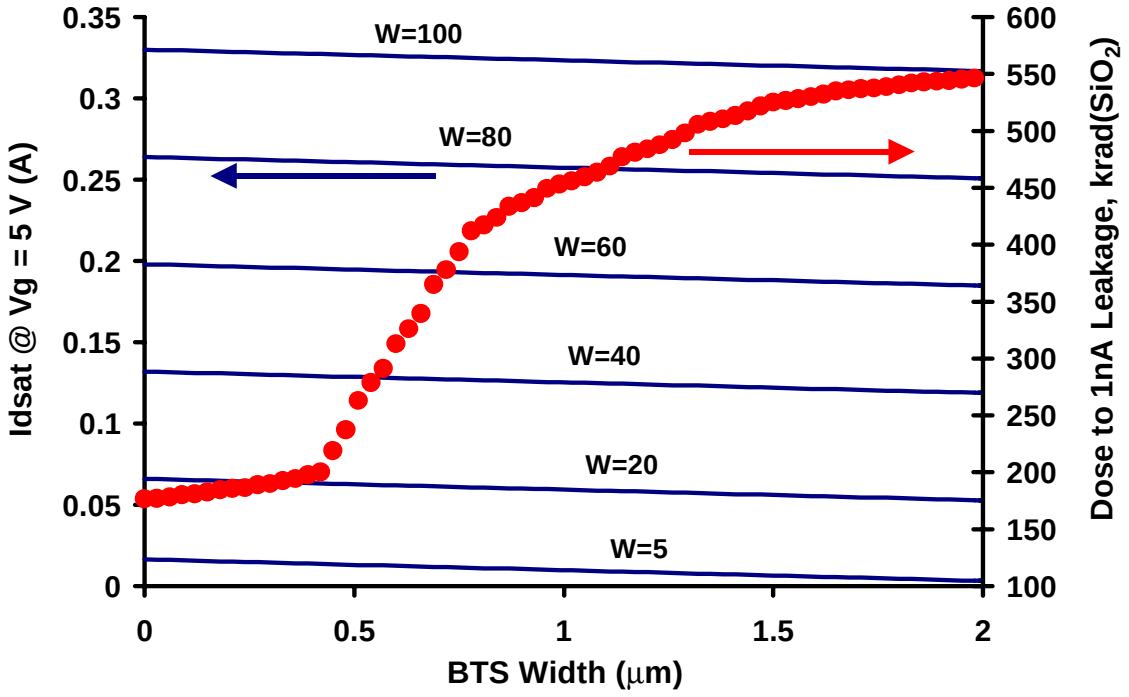

Figure 29: Hardness (circles) and I_{dsat} (lines) versus BTS width.

Figure 29 also shows the saturation drain current (I_{dsat} at V_G=5.0V) versus W_{BTS} curves obtained by considering the reduction in effective device width that accompanies the BTS width increase. Specifically, the I_{dsat} at V_G=5.0 V curves are calculated using:

$$I_{dsat} = \frac{1}{2}\mu_n C_{ox}\frac{W - W_{BTS}}{L}(V_G - V_t)^2 \tag{33}$$

with six different values of W ranging from 5 μm to 100 μm. Here, C_{ox} is the oxide capacitance per unit area, V_G is the gate bias (5V), and V_t is the threshold voltage (0.8 V). The information presented in Figure 29 can be used to identify layout parameters, W and W_{BTS}, that simultaneously meet a given set of hardness and I_{dsat} criteria. As seen from Figure 29, an increase in the BTS width results in increased hardness levels but also lowers the saturation drain current at any given device width W. However, higher hardness requirements can be met without lowering I_{dsat} by using larger drawn widths in order to compensate for the increased BTS widths. Although the trends in Figure 29 are not qualitatively surprising, they illustrate the important task of deriving quantitative estimates of simultaneous hardness and performance criteria using an integrated design tool.

The analysis of Figure 29 also raises an important manufacturing issue. Specifically, increasing the drawn device width in order to achieve a higher hardness level without lowering I_{dsat} implies an increase in the total die area. This results in fewer die per wafer and therefore, higher production costs for a given number of integrated circuits (ICs).

Conclusions

In this study, numerical process and device simulations have been used to clarify an important SOI hardening issue. Specifically, the underlying cause of enhanced back channel leakage is found to be enhanced hole trapping in the buried oxide near the island edge. The simulations suggest that sufficiently wide BTS tabs located at the edges of the islands will suppress this leakage enhancement. Finally, quantitative estimates are provided for the relationship between BTS width and realistic hardness and performance criteria.

CHAPTER VII

LOCOS FIELD IMPLANT SPLIT-LOT STUDY

Overview

The dependence of total-dose-induced parasitic leakage currents on field oxide implant parameters has been simulated using the same Technology Computer Aided Design framework described in the previous chapter. In this study, computational split lots are performed by systematically varying the dose and energy of the field oxide implant in a LOCOS isolation process simulation. Trapped charge distributions as a function of total-dose exposure are obtained for each of the resulting structures using two-dimensional simulation of hole trapping. Leakage current simulations performed for each structure at increasing exposure levels yield results consistent with typical experimental observations. Optimal implant parameters are suggested by the response surface generated from simulation data and hypothetical hardness, performance, and manufacturing constraints. This study demonstrates the application of sophisticated Technology Computer Aided Design practices for optimization of radiation-hardened semiconductor fabrication processes.

Background

Hole trapping in silicon dioxide is a primary underlying cause of circuit failure due to long-term ionizing radiation exposure. Holes trapped in oxide regions increase the electron concentration at nearby silicon surfaces, leading to degraded electrical behavior of both MOS and bipolar semiconductor devices. For example, trapped holes in gate and bird's beak oxide regions reduce threshold voltage and increase subthreshold and edge leakage current in nMOSFETs. Holes trapped in thick isolation oxides degrade gain in bipolar devices and increase leakage current between adjacent nMOSFETs. Models for radiation-induced hole trapping have been integrated in a simulation framework that leverages sophisticated Technology Computer Aided Design (TCAD) tools. Here, we report the application of this tool to examine the total-dose response of a bulk silicon MOS technology employing partially recessed LOCOS isolation. The specific structure

examined is the parasitic n-channel transistor formed where drain regions of adjacent nMOSFETs are separated by field oxide (Figure 30).

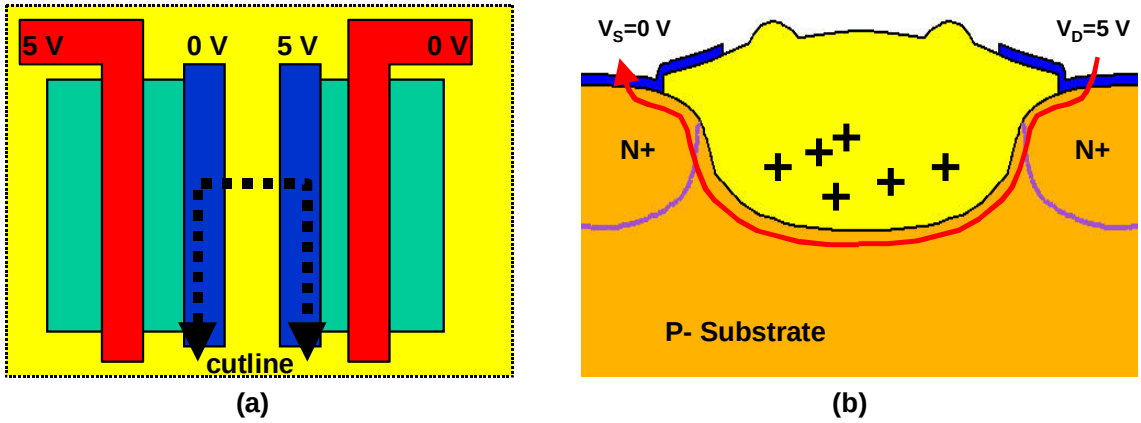

Figure 30: (a) Simplified layout view of two adjacent nMOSFETs. The cutline specifies the position of the parasitic transistor whose cross section, shown in (b), illustrates the leakage path formed when trapped holes invert the silicon surface.

Since isolation oxides are normally very thick, these parasitic transistors have high threshold voltages and are non-conducting. However, in a total-dose environment, trapped holes can invert the underlying p-type silicon, forming inter-device leakage paths that degrade circuit performance [103]. This leakage can be controlled using a p-type implant prior to oxidation to increase the parasitic nMOSFET threshold voltage. However, such measures may be constrained by other performance parameters (e.g., junction breakdown voltage) and/or manufacturing issues (e.g., implant cost). Experimentally determining the optimal energy and dose of the implant in light of such tradeoffs between desired hardness and performance and manufacturing criteria is a costly process requiring fully processed test structures from multiple lots and radiation testing. Here we demonstrate a more efficient, simulation-based approach to optimizing field implant parameters.

Computational Split Lots and Prerad Leakage Currents

Process simulations with different combinations of dose and energy of a boron field implant were used to generate 25 parasitic nMOSFET structures. Figure 31(a) illustrates the implant into a shallow trench formed by reactive ion etching through an oxide/nitride/photoresist stack. The lot splits were simulated with combinations of five doses: 1×10^{11}, 5×10^{11}, 1×10^{12}, 5×10^{12},

1×10^{13} cm^{-2}; and five energies: 30, 50, 70, 90 and 110 keV. Figure 31(b) shows the boron doping in the LOCOS structure after selective oxidation of the trench, gate oxidation, nMOS threshold tailor, and source/drain processing.

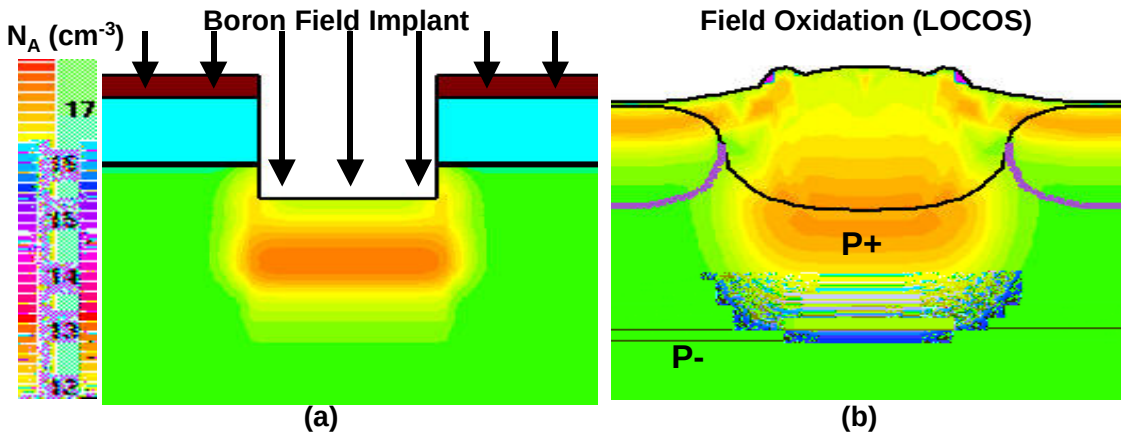

Figure 31: (a) Boron concentration immediately after field implant and (b) Boron concentration in LOCOS structure after complete processing.

After simulating contact formation and metalization, pre-irradiation leakage current simulations were performed by ramping V_D positive with V_S and V_B grounded. Figure 32 displays leakage current simulation results for 4 different structures and illustrates the definition of V_{FAIL}, a performance parameter defined as the value of V_D that produces 1pA/μm width leakage. There are two mechanisms that determine the value of this parameter. The first is punchthrough current due to drain-induced barrier lowering between the source and drain of the parasitic nMOSFET [104]. The field implant limits this leakage by reducing the depletion region spreading at high V_D. However, the second mechanism, breakdown of the reverse-biased substrate/drain junction, places practical limits on the field implant parameters. Specifically, when the dose and energy of the field implant produce sufficiently high p-type doping near the n-type regions, junction breakdown-induced leakage acts to reduce V_{FAIL}. This effect is visible in Figure 32 where the increase in implant dose eventually produces a decrease in the leakage failure voltage from 33 to 25 V. V_{FAIL} also depends on energy through variations in the subsurface position of the peak of the as-implanted profile; the final acceptor doping under the LOCOS region depends on how much of the tail of the implant is consumed during oxidation (as well as boron segregation and diffusion). The energy dependence is visible in the contour plot of Figure 33.

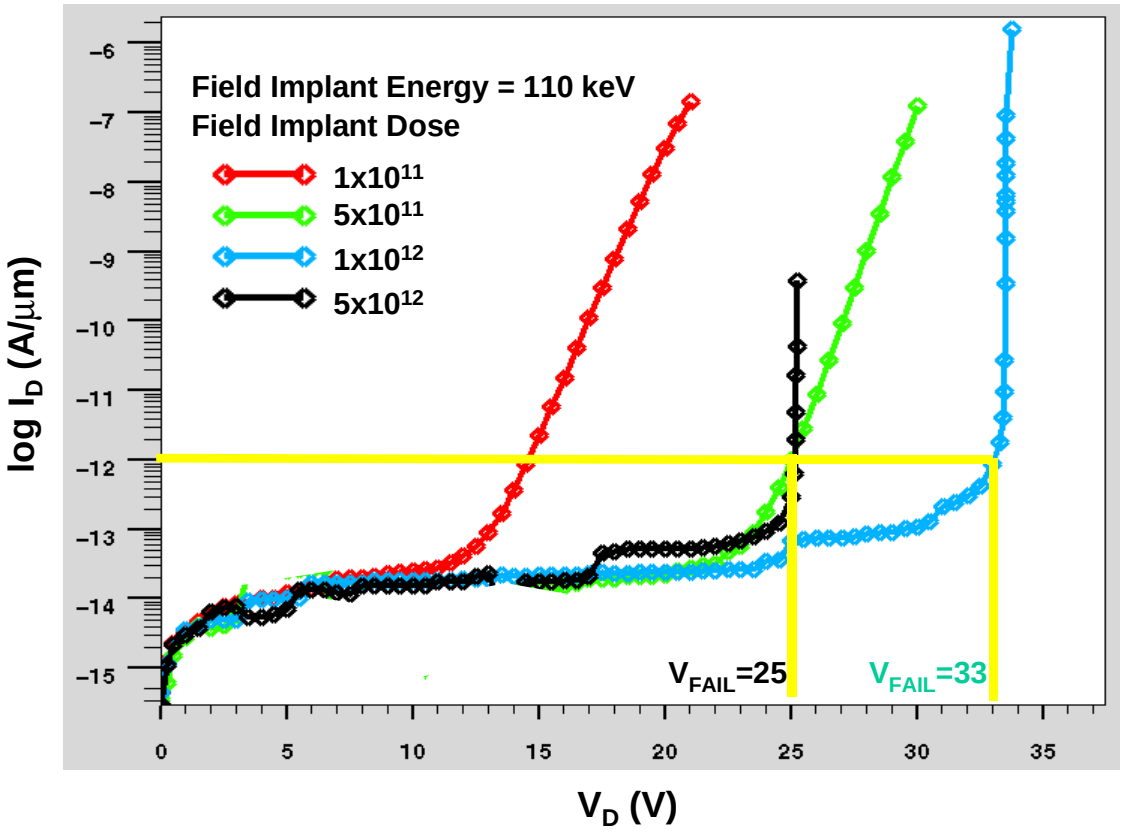

Figure 32: Sample pre-irradiation leakage current simulation results illustrating the definition of V_{FAIL} as the value of V_D that produces 1pA/μm leakage. Increasing implant dose increases V_{FAIL} by preventing source/drain punchthrough until the point at which junction breakdown dominates the leakage.

The contour plot shown in Figure 33 summarizes V_{FAIL} for all 25 structures. For low doses and energies, V_{FAIL} increases with increasing dose and energy due to punchthrough prevention. However, in the upper right region of the contour plot, junction breakdown begins to dominate and further increases in dose and/or energy conspire to reduce V_{FAIL}. Nevertheless, all of the chosen dose/energy combinations provide a reasonable leakage current margin for a 5 V technology, implying that significant statistical variation in dose and energy of the field implant may be tolerated in a commercial technology. We will, however, demonstrate shortly how this variation poses a severe threat to total dose hardness.

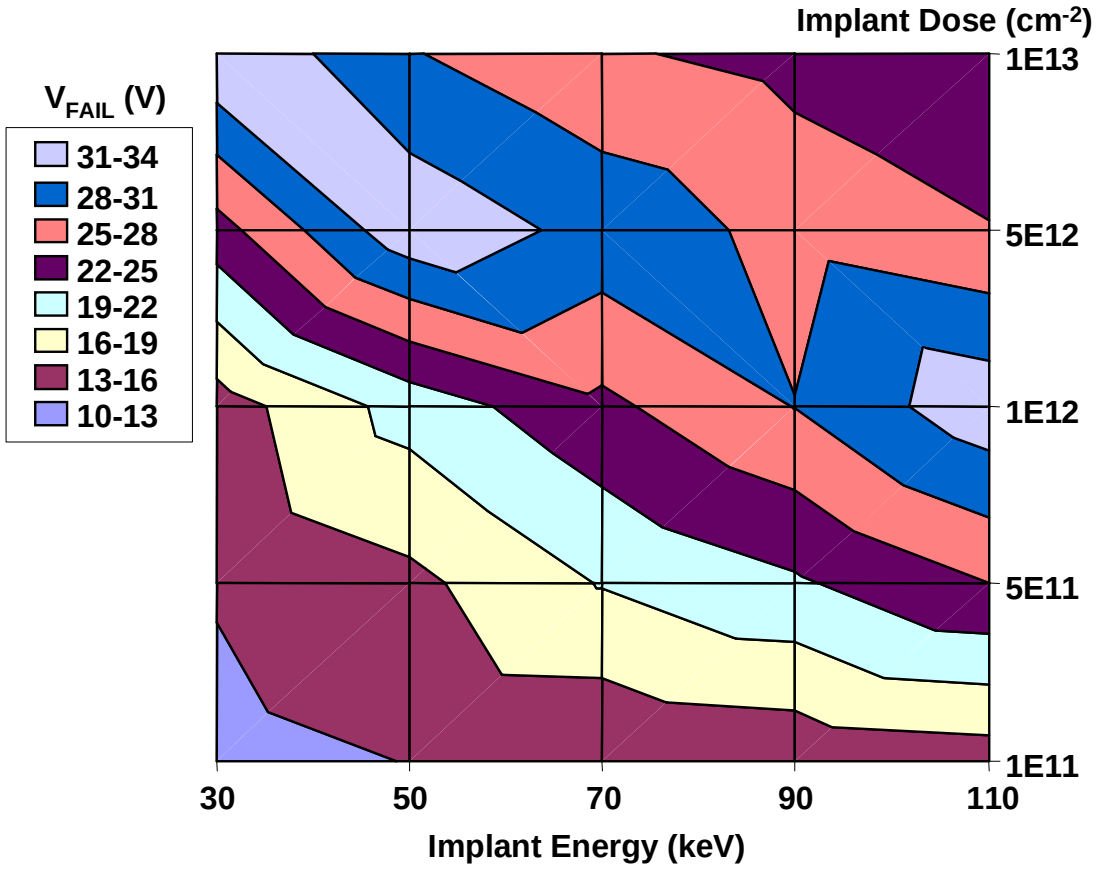

Figure 33: Contour plot of V_{FAIL} versus implant dose and energy. The non-monotonic trend of V_{FAIL} with dose and energy arises from the tradeoff between reduced barrier lowering and increased junction breakdown due to increased acceptor doping.

Simulated Radiation Exposure

Two-dimensional simulation of a 60 kRad(SiO_2) exposure at a constant dose-rate of 0.1 Rad(SiO_2)/s is performed with V_D=5.0 V and $V_S = V_B = 0.0$ V. This study provides results obtained by assuming a spatially uniform density of hole traps, $N_T = 6 \times 10^{16}$ cm^{-3}, in the LOCOS isolation. Additional studies should be performed with more accurate descriptions accounting for process-dependent thermal history, mechanical stress, and increased oxygen vacancy density near the Si-SiO_2 interface. Unique insight is provided by the internal information provided by this two-dimensional simulation. Specifically, this study reveals a typically unappreciated dependence of hole trapping on the field implant parameters: although the bias conditions are identical for all 25 devices, they have different trapped hole distributions after the same total-dose. Figure 34 illustrates this for two devices after 5 kRad(SiO_2). The trapped holes in device (1) are distributed differently than in device (2).

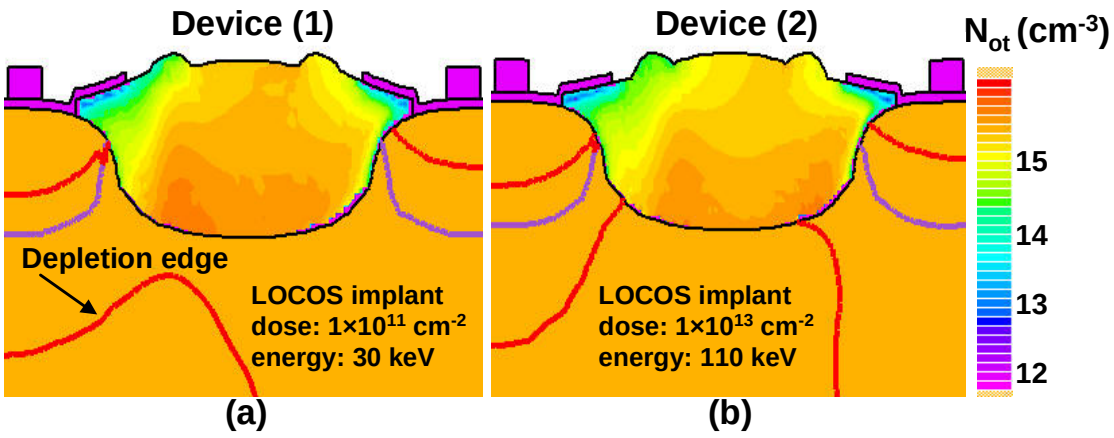

Figure 34: Spatial distribution of trapped holes depends on the field implant parameters.

The explanation for this effect is, as suggested by the different depletion edges, related to different electric field distributions. Figure 35 shows the electric field distributions in the same devices at the beginning of radiation exposure, and their respective doping profiles.

The electric fields in device (1) are visibly lower than in those in device (2) due to increased depletion region spreading associated with low doping density. This results in different hole trapping behavior through the field-dependence in models for geminate recombination and hole transport (field-dependent hole capture cross section is an option in our model, however, it was not

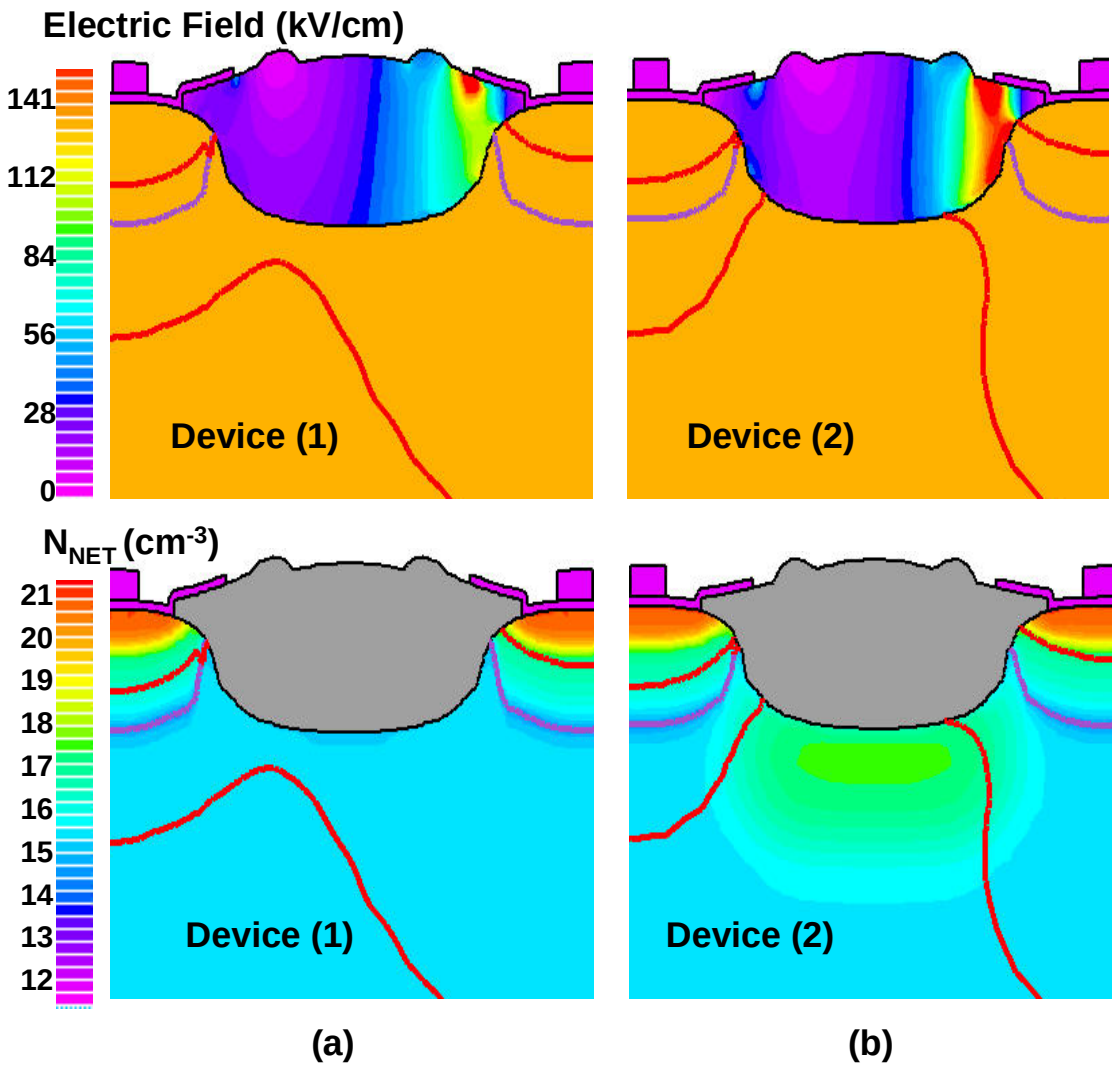

Figure 35: Electric field and net doping distributions in (a) Device (1) and (b) Device (2) reveal the effects of doping on electric field distribution to be root cause of the different spatial distributions of trapped holes seen in devices processed with different field implant parameters.

applied in the present simulations). For these structures, the small differences in the distribution of trapped holes play a negligible role in determining the dependence of post-irradiation leakage on field doping. As long as the trapped hole distributions are not significantly different, the direct influence of doping profile in preventing trapped hole-induced inversion dominates the trend of hardness versus field implant parameters. To observe the overall dependence of hardness on field implant parameters we have applied a definition of total dose failure to post-irradiation leakage currents.

Total Dose Induced Parasitic Leakage Current

After performing hole trapping simulations, leakage current simulations were performed to obtain the post-irradiation response of all 25 structures. Figure 36 displays simulation results for a device "processed" with field implant dose = 10^{12} cm^{-2} and energy = 90 keV. Figure 36 also illustrates the application of a failure definition to extract total dose hardness from the simulated data. Failure is defined as leakage in excess of 1 pA/μm width when the parasitic transistor is biased with V_D=5.0 V and the other terminals grounded. This corresponds to the circuit condition in which two adjacent transistors store opposite bits. According to this definition, the device represented in Figure 36 fails at 28 kRad. Note that the 22 kRad curve narrowly escapes the failure criterion, indicating that leakage current simulations at intermediate doses may be desirable. This analysis was performed for all 25 devices to obtain total dose-hardness as a function of field implant parameters.

Total Dose Hardness Contour Map

The dependence of total dose hardness on field implant parameters is summarized in the contour plot shown in Figure 37.

The increase in hardness as implant dose and energy are increased is due to the increase in parasitic threshold voltage as the surface acceptor doping increases. The dependence of surface doping on the field implant parameters has been described earlier. However, unlike the V_{FAIL} parameter, the total dose hardness exhibits an entirely monotonic dependence on implant dose and energy. This is due to the fact that post-irradiation leakage failure is due to barrier lowering caused

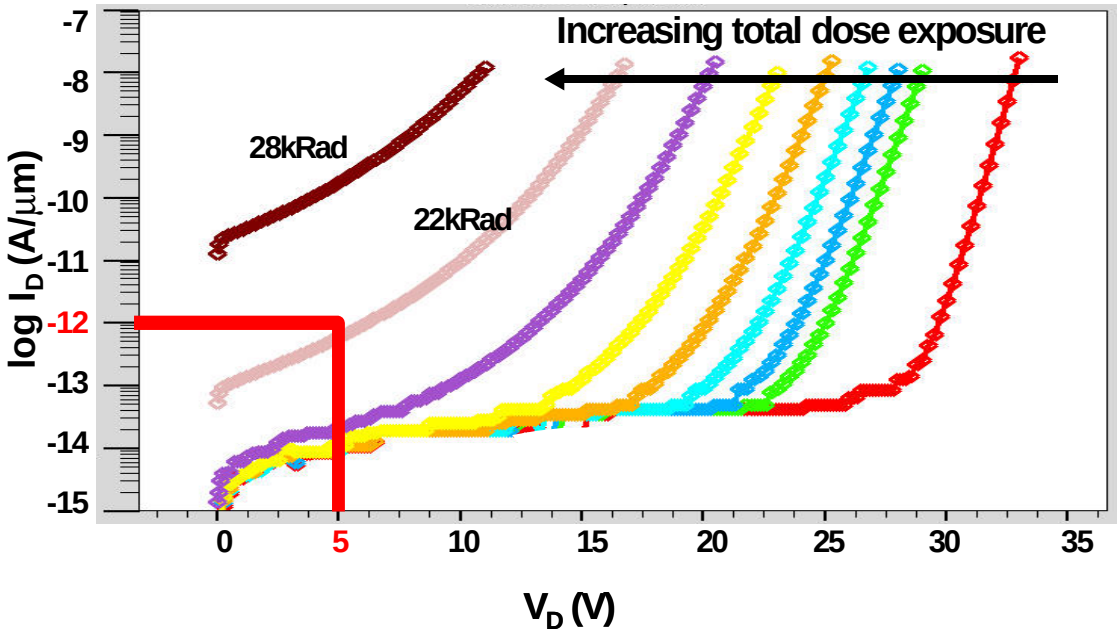

Figure 36: Leakage current as a function of total dose exposure for LOCOS structure processed with field implant dose = 10^{12} cm^{-2} and energy = 90 keV. This structure meets the total dose failure criterion of 1pA/μm leakage at V_D=5 V at an exposure level of 28 kRad(SiO_2).

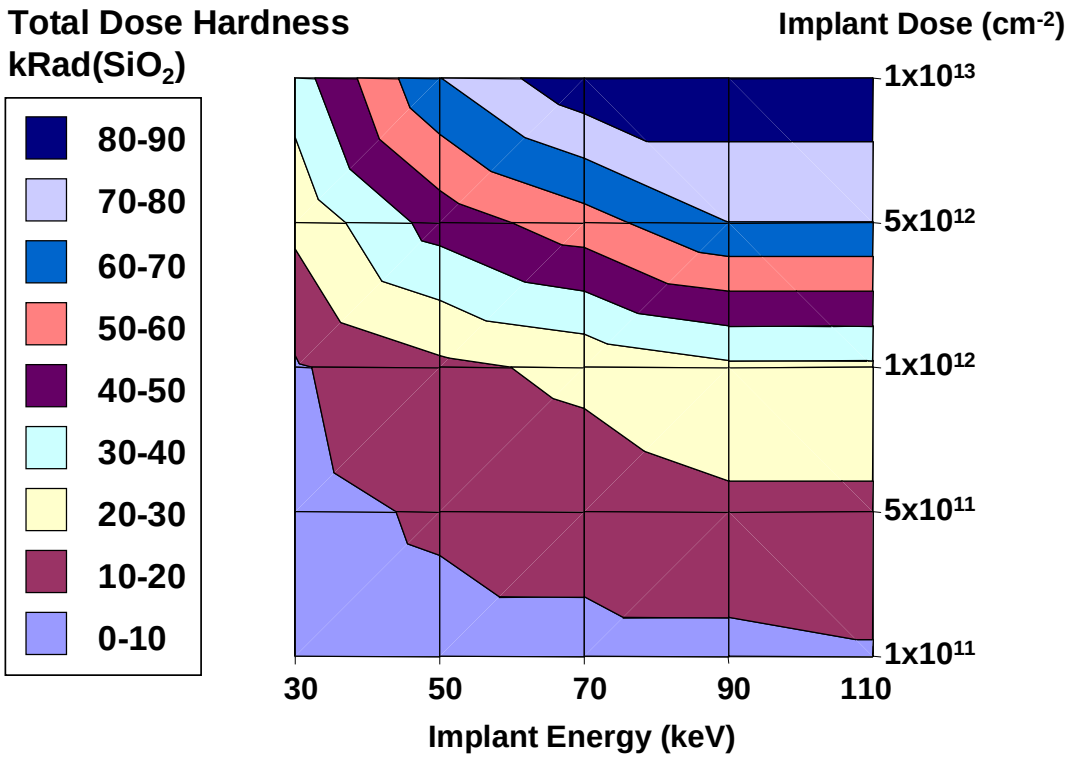

Figure 37: Contour map summarizing the dependence of total-dose hardness on field implant parameters.

by the holes trapped in the gate rather than junction breakdown (For higher energies than reported here, a non-monotonic dependence on energy may appear because the Si-SiO_2 interface remains in the tail region of the profile after oxidation). The discussion so far has identified the surface doping as a key parameter determining the behavior of the LOCOS parasitic nMOSFET. Although the TCAD analysis package allows detailed visualization of the surface doping, as well as other relevant quantities, e.g., potential and carrier distributions, the data is presented here in a format that emphasizes the dependence on process parameters. This illustrates the ability of TCAD tools enhanced with radiation-effects models to contain the effects of numerous, coupled, 2D phenomena into easily visualized relationships between hardness and actual equipment settings. This ability is the foundation for adapting formal TCAD principles to reducing the empiricism in developing, optimizing, and maintaining radiation hardened technology. The following section illustrates the use of contour maps to identify adjustments to a commercial fabrication technology that simultaneously satisfy hardness, performance, and manufacturing constraints.

Illustration of Process Optimization Using Contour Maps

Figure 37 displays a wide range in total dose response as implant parameters are varied. This demonstrates a commonly cited reason for large variations in the hardness of commercial technology. Since the pre-irradiation leakage current simulations suggest that any of the dose/energy combinations result in low initial leakage, significant variation in the field implant parameters is tolerable in a commercial application of this technology. Therefore, for the purpose of illustration, we assume a 5 V commercial process which uses a field implant with dose $= 3 \times 10^{11}$ cm^{-2} and energy $= 40$ keV (Figure 38). These parameters provide a satisfactory margin against leakage induced by small amounts of processing-induced positive charge. However, they provide a hardness of less than 10 kRad according to Figure 37. If we suppose a minimum hardness requirement of 60 kRad, the dose/energy combinations covered by the black region in Figure 38 are no longer available and the field implant parameters must be moved to the upper right portion of the contour map. Using Figure 33, one determines that raising the dose and energy of the implant to satisfy the hardness requirement produces a device in which junction breakdown begins to dominate the leakage current. However, for the hypothetical technology we have assumed, this

actually results in a net increase in V_{FAIL}.

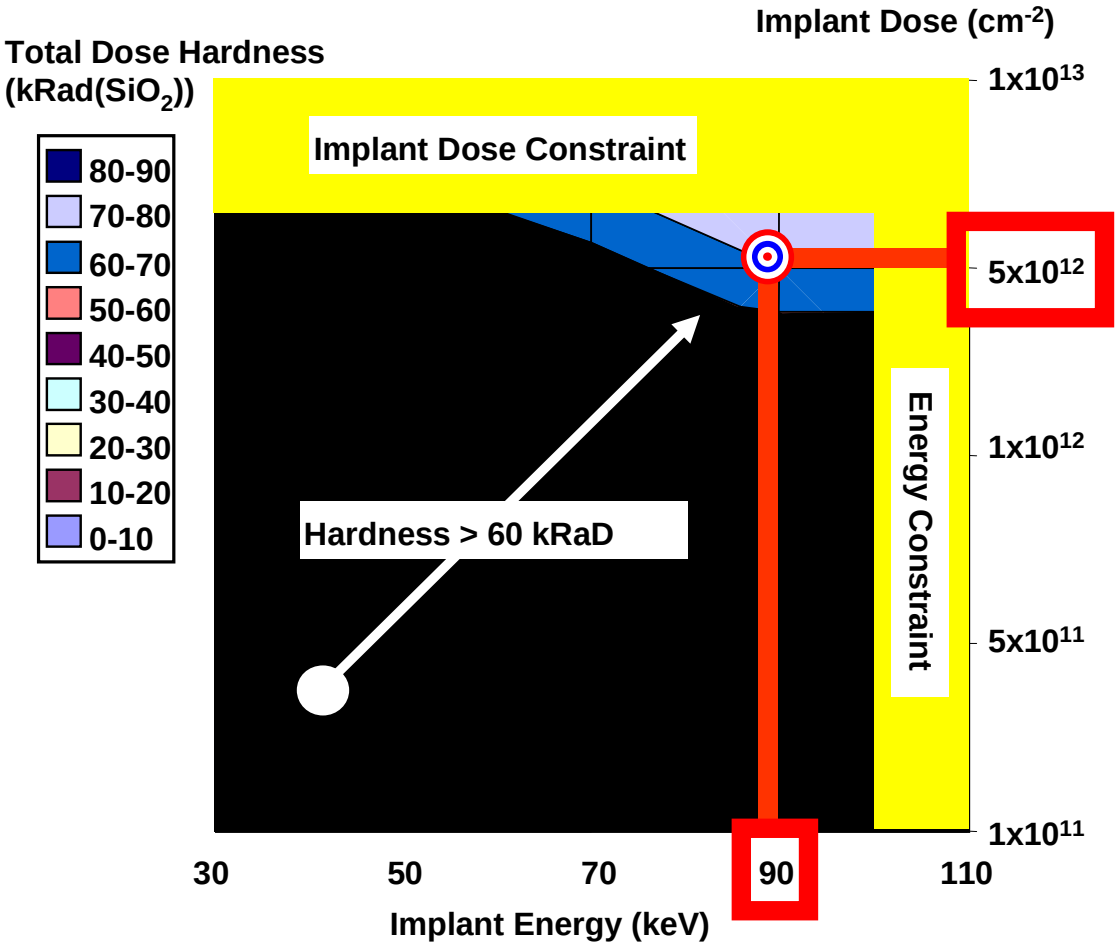

Figure 38: Total dose hardness contour map with disallowed regions determined by hardness and implant dose and energy constraints. Initial parameters for a commercial technology, indicated by the white circle, of dose $= 3 \times 10^{11}$ cm^{-2} and energy $= 40$ keV are assumed for illustration. The final "centered" values of field implant and dose are enclosed in squares.

Manufacturing constraints may also limit the choice of field implant parameters. For example, although the higher doses in this example do not pose a threat to the performance parameter V_{FAIL}, it is possible for throughput constraints of a commercial fabrication line to limit the time, and consequently the dose, of the field implant. Constraints may also be placed on the energy of the implant by masking limitations. As implant energy is increased, the photoresist/nitride stack may become ineffective in preventing boron from penetrating to active regions of the wafer. Increasing the thickness of masking regions can have undesirable effects on bird's beak shape or be impractical from the standpoint of lithography. These considerations are illustrated

in Figure 38 using the yellow areas of disallowed dose/energy combinations. The final step in applying the contour map is to choose values of field implant dose and energy lying in the center of the remaining available area. Therefore, the field implant parameters that simultaneously satisfy our hypothetical hardness, performance, and manufacturing constraints are found to be: dose $= 5 \times 10^{12}$ cm^{-2} and energy $= 90$ keV.

Conclusion

The total-dose response of a parasitic nMOSFET associated with LOCOS isolation has been examined using a Radiation-Hardened Technology Computer Aided Design tool consisting of two-dimensional process, device, and hole trapping simulation. Although quantitative comparisons to a given technology require tool calibration, the overall agreement between simulation results and typical experimental observations of radiation-induced leakage constitutes successful demonstration of the chosen model set. This study demonstrates, through a plausible generic example, the ability of physically based simulation to provide understanding of the influence of process variables on detailed internal degradation mechanisms as well as overall hardness criteria. Finally, this study demonstrates the use of simulated split-lot data to identify processing parameters that simultaneously satisfy potentially competing hardness, performance, and manufacturing constraints.

CHAPTER VIII

FUTURE WORK, SUMMARY AND CONCLUSIONS

Future Work

The carrier transport-based modeling methods described here have significant potential to improve the applicability of device simulation practices in radiation-hardened technology development. However, the simulation studies reported here exercise only a small range of this potential and several areas of future work should be mentioned. In particular, the proton release kinetics should be explored in more detail.

In the study presented in Chapter V, the initial negative period of the switched bias condition (-2/+2 MV/cm) is purposely kept short enough that very few protons are lost at the gate-SiO_2 interface. This results in a different time-dependence of interface trap formation but similar saturation values for the switched and constant bias conditions. Although the good match to experimental data demonstrated in this study provides a convincing validation of the model, more rigorous testing of the model is necessary.

One aspect of the interface-trap formation model deserving further study is the spatial distribution of proton release. The spatial distribution of proton release can be investigated using modified pulsed-radiation/switched bias experiments in which duration of the initial -2 MV/cm period is selectively varied in order to adjust the amount of time protons are lost at the gate-SiO_2 interface before switching positive [75]. By observing the variation in the time-dependence and saturation value of interface trap density after the bias is switched, inferences can be made regarding the spatial distribution of initial proton profile. Attempts have been made to analyze these proton loss experiments using two successive CTRW calculations. In these calculations, an assumed proton profile is used to calculate the proton distribution in the oxide after the initial negative bias stage in which protons are lost at the gate interface. This proton distribution is then used as the initial proton profile in a second CTRW calculation for the positive bias stage. Unfortunately, the "memory" of the initial negative bias transport stage is not preserved in the subsequent positive bias transport calculation and, therefore, the rate of proton transport

is overestimated in the second stage calculation. However, since the memory of dispersive transport is inherently preserved by MTD methods (in the instantaneous concentrations of protons trapped in transport-mediating bandtail states), the proton loss experiment presents no difficulty to the model presented here. Furthermore, the present model relies on the rate-equation for hole-trapping-induced proton release rather than assumed proton profiles. Therefore, the spatial distribution in the "initial proton profile" can be investigated directly at the level of the spatial distribution in the underlying physical parameters, i.e., spatially varying DH distributions and/or capture cross sections of the DH defect for holes.

In addition to varying the parameters of the present model, additional physical mechanisms should also be acknowledged as possible origins of spatial variation in the proton release. Although the simulations reported here do not include H_2 cracking at E' centers, it should be noted that, despite the conclusions in [48], compelling evidence exists for room temperature reactions between E' centers and H_2 [72, 84]. A logical extension to the set of mechanisms included in the present implementation is to add an additional source of proton generation due to cracking at E' centers. One approach to adding this mechanism to the present model is simply to remove the assumption that H_2 is promptly cracked at D^+ sites. Instead, the rate equation for dimerization (Equation 12 on Page 34) must be used as a generation term in a fourth continuity equation for molecular hydrogen. Here, the H_2 flux density can be modeled using a simple diffusion equation and an explicit rate equation must be specified for the interaction between E' centers and diffusing H_2 (Reaction R6).

Summary and Conclusions

The radiation-effects modeling approach described in this dissertation merges two fundamental concepts that have historically received separate emphasis in two different experiments. The first is the hydrogen release chemistry underlying interface trap formation that has been studied in post-irradiation hydrogen annealing studies. The second is the dispersive proton transport that has been identified as the rate limiting factor in interface trap formation during pulsed-radiation/switched bias experiments. The approach presented here applies standard continuity and drift-diffusion equations in a model which integrates the proton release and dispersive trans-

port processes with radiation-induced generation, transport, and trapping of holes. Furthermore, the parameters of the equations are predominantly physical in nature, i.e., related to fundamental geometric and microstructural structure properties of the device oxide. This model has been validated in a simulation study of previous pulsed-radiation/switched bias experiments. Two additional simulation studies using a two-dimensional implementation of a simpler hole trapping model are reported that demonstrate the application of Technology Computer Aided Design practices for analyzing technologically relevant radiation-response optimization problems.

REFERENCES

[1] W. Dutton, B. Troyanovsky, Yu Zhiping, E. C. Kan, K. Wang, Chen Tao, T. Amborg, and J. H. Wuorinen, "TCAD for Analog Circuit Applications: Virtual Devices and Instruments," in *Digest of Technical Papers, 42nd International Solid-State Circuits Conference*, 8-10 Feb. 1996, p. 78. 2

[2] J.-C. Lu, W. C. Holton, J. S. Fenner, S. C. Williams, K. W. Kim, A. H. Hartford, D. Chen, K. Roze, and M. A. Littlejohn, "A New Device Design Methodology for Manufacturability," *IEEE Transactions on Electron Devices*, vol. 45, pp. 634, 1998. 2

[3] D. S. Boning and P. K. Mozumder, "DOE/Opt: A System for Design of Experiments, Response Surface Modeling, and Optimization Using Process and Device Simulation," *IEEE Transactions on Semiconductor Manufacturing*, vol. 7, pp. 233, 1994. 2

[4] P. E. Dodd, F. W. Sexton, and P. S. Winokur, "Three-Dimensional Simulation of Charge Collection and Multiple-Bit Upset in Si Devices," *IEEE Transactions on Nuclear Science*, vol. 41, pp. 2005, 1994. 2, 59

[5] P. E. Dodd, M. R. Shaneyfelt, and F. W. Sexton, "Charge Collection and SEU from Angled Ion Strikes," *IEEE Transactions on Nuclear Science*, vol. 44, pp. 2256, 1997. 2, 59

[6] C. Detcheverry, C. Dachs, E. Lorfevre, C. Sudre, G. Bruguier, J. M. Palau, J. Gasiot, and R. Ecoffet, "SEU Critical Charge and Sensitive Area in a Submicron CMOS Technology," *IEEE Transactions on Nuclear Science*, vol. 44, pp. 2266, 1997. 2, 59

[7] Lloyd Massengill, "SEU Modeling and Prediction Techniques," NSREC Short Course, December 1993. 2

[8] Lloyd W. Massengill and Sherra E. Diehl-Nagle, "Transient Radiation Upset Simulations of CMOS Memory Circuits," *IEEE Transactions on Nuclear Science*, vol. 31, pp. 1337, 1984. 2

[9] L. W. Massengill, S. E. Diehl-Nagle, and T. F. Wrobel, "Analysis of Transient Radiation Upset in a 2K SRAM," *IEEE Transactions on Nuclear Science*, vol. 32, pp. 4026, 1985. 2

[10] A. N. Ishaque, J. W. Howard, M. Becker, and R. C. Block, "Photocurrent Modeling at High Dose Rates," *IEEE Transactions on Nuclear Science*, vol. 36, pp. 2092, 1989. 2, 59

[11] P. S. Winokur and Jr. H. E. Boesch, "Annealing of MOS Capacitors with Implications for Test Procedures to Determine Radiation Hardness," *IEEE Transactions on Nuclear Science*, vol. 28, pp. 4058, 1981. 5

[12] T. P. Ma and P. V. Dressendorder, Ed., *Ionizing Radiation Effects in MOS Devices and Circuits*, chapter 8, John Wiley and Sons, 1989. 6

[13] G. A. Ausman and F. B. McLean, "Electron-Hole Pair Creation Energy in SiO_2," *Applied Physics Letters*, vol. 26, pp. 173, 1975. 8

[14] L. Onsager, "Initial Recombination of Ions," *Physical Review*, vol. 54, pp. 554, 1938. 8

[15] G. A. Ausman, "Field Dependence of Geminate Recombination in a Dielectric Medium," Tech. Rep. 2097, Harry Diamond Laboratories, Adelphi, MD, 1986. 8

[16] H. E. Boesch Jr. and J. M. McGarrity, "Charge Yield and Dose Effects in MOS Capacitors at 80K," *IEEE Transactions on Nuclear Science*, vol. 23, pp. 1520, 1976. 8, 24

[17] T. P. Ma and P. V. Dressendorder, Ed., *Ionizing Radiation Effects in MOS Devices and Circuits*, chapter 3, John Wiley and Sons, 1989. 8, 8, 11, 11, 11, 11, 19, 22, 22, 45

[18] H. E. Boesch Jr., F. B. McLean, J. M. McGarrity, and G. A. Ausman Jr., "Hole Transport and Charge Relaxation in Irradiated SiO_2 MOS Capacitors," *IEEE Transactions on Nuclear Science*, vol. 22, pp. 2163, 1975. 11, 17, 17, 18, 22

[19] R. C. Hughes, "Charge-Carrier Transport Phenomena in Amorphous SiO_2: Direct Measurement of Drift Mobility and Lifetime," *Physical Review Letters*, vol. 30, pp. 1333, 1973. 11, 11

[20] R. C. Hughes, E. P. EerNisse, and H. J. Stein, "Hole Transport in MOS Oxides," *IEEE Transactions on Nuclear Science*, vol. 22, pp. 2227, 1975. 11

[21] H. E. Boesch Jr., F. B. McLean, J. M. Benedetto, and J. M. McGarrity, "Saturation of Threshold Voltage Shift in MOSFETs at High Total Dose," *IEEE Transactions on Nuclear Science*, vol. 33, pp. 1191, 1986. 14, 24, 62

[22] G. Jaffe, "Zur Theorie der Ionisation in Kolonnen," *Ann. Phys. (Leipzig)*, vol. 42, pp. 303, 1913. 14, 14, 15

[23] H. A. Kramers, "On a Modification of Jaffe's Theory of Column-Ionization," *Physica*, vol. 18, pp. 665, 1952. 14, 14, 15

[24] T. R. Oldham and J. M. McGarrity, "Ionization of SiO_2 by Heavy Charged Particles," *IEEE Transactions on Nuclear Science*, vol. 28, pp. 3975, 1981. 14, 14, 14, 15, 41

[25] M. P. Langevin, "L'Ionization des Gaz," *Ann. Chim. Phys.*, vol. 28, pp. 289, 1903. 15, 41

[26] M. P. Langevin, "Recombinaison et Mobilities des Ions Dans Les Gas," *Ann. Chim. Phys.*, vol. 28, pp. 433, 1903. 15, 41

[27] R. Sokel and R. C. Hughes, "Numerical Analysis of Transient Photoconductivity in Insulators," *Journal of Applied Physics*, vol. 53, pp. 7414, 1982. 15, 16, 37

[28] V. Vasudevan and J. Vasi, "A Numerical Simulation of Hole and Electron Trapping Due to Radiation in Silicon Dioxide," *Journal of Applied Physics*, vol. 70, pp. 4490, 1991. 15, 16, 37, 59, 60

[29] V. Vasudevan and J. Vasi, "A Two-Dimensional Numerical Simulation of Oxide Charge Buildup in MOS Transistors Due to Radiation," *IEEE Transactions on Electron Devices*, vol. 41, pp. 3, 1994. 15, 16, 37, 59, 60, 60

[30] C. Brisset, V. Ferlet-Cavrois, O. Mosseau, J. L. Leray, R. Escoffier, and A. Michez, "Two-Dimensional Simulation of Total-Dose Effects on NMOSFET With Lateral Parasitic Transistor," *IEEE Transactions on Nuclear Science*, vol. 43, pp. 2651, 1996. 15, 16, 37, 37, 59, 60, 60

[31] R. Milanowski, M. Pagey, L. Massengill, R. Schrimpf, C. Nicklaw, R. Graves, H. Barnaby, K. Galloway, and J. Johann, "Radiation-Hardened Semiconductor Technology Computer Aided Design," in *1998 Digest of Papers, Government Microcircuit Applications Conference*, Mar. 1998, vol. XXIII, p. 573. 15, 16, 37, 37, 60

[32] R. Milanowski, L. Massengill, R. Schrimpf, M. Pagey, and C. Nicklaw, "Computational Split-Lot Study of the Effect of Implant Parameters on Total-Dose-Induced Leakage," in *1998 Digest of Papers, Government Microcircuit Applications Conference*, Mar. 1998, vol. XXIII, p. 582. 15, 16, 37, 37, 37, 60

[33] R. J. Milanowski, M. P. Pagey, L. W. Massengill, R. D. Schrimpf, M. E. Wood, B. W. Offord, R. J. Graves, K. F. Galloway, C. J. Nicklaw, and E. P. Kelley, "TCAD-Assisted Analysis Of Back-Channel Leakage In Irradiated Mesa SOI nMOSFETs," *IEEE Transactions on Nuclear Science*, vol. 45, pp. 2593, 1998. 15, 16, 37, 37

[34] R. C. Hughes, "Time-Resolved Hole Transport in a-SiO_2," *Physical Review B*, vol. 15, pp. 2012, 1976. 16, 22

[35] H. Scher and E. W. Montroll, "Anomalous Transit-Time Dispersion in Amorphous Solids," *Physical Review B*, vol. 12, pp. 2455, 1975. 16, 16, 17, 19, 37

[36] F. B. McLean and G. A. Ausman Jr., "Simple Approximate Solutions to Continuous-Time Random-Walk Transport," *Physical Review B*, vol. 15, pp. 1052, 1977. 17, 17, 19, 19, 37, 37

[37] O. L. Curtis Jr. and J. R. Srour, "The Multiple-Trapping Model and Hole Transport in SiO_2," *Journal of Applied Physics*, vol. 48, pp. 3819, 1977. 17, 17, 20, 22, 37

[38] V. Vasudevan and J. Vasi, "A Simulation of the Multiple Trapping Model for Continuous Time Random Walk Transport," *Journal of Applied Physics*, vol. 74, pp. 3224, 1993. 17, 17, 37, 59, 60, 60

[39] Claude Cirba, *Simulation Numerique du Piegeage et du Depiegeage dans les Oxydes de Composants MOS*, Ph.D. thesis, Academie de Montpellier, 1996. 17, 17, 59

[40] E. W. Montroll and G. H. Weiss, "Random Walks on Lattices. II," *Journal of Mathematical Physics*, vol. 6, pp. 167, 1965. 17, 19

[41] J. Noolandi, "Equivalence of Multiple-Trapping Model and Time Dependent Random Walk," *Physical Review B*, vol. 16, pp. 4474, 1977. 17, 22, 40

[42] F. W. Schmidlin, "Theory of Trap-Controlled Transient Photoconduction," *Physical Review B*, vol. 16, pp. 2362, 1977. 17, 22, 22, 40

[43] F. B. McLean, "A Framework For Understanding Radiation-Induced Interface States in SiO_2 MOS Structures," *IEEE Transactions on Nuclear Science*, vol. 27, pp. 1651, 1980. 18, 30

[44] J. F. Conley Jr. and P. M. Lenahan, "A Review of Electron Spin Resonance Spectroscopy of Defects in Thin Film SiO_2 on Si," in *The Physics and Chemistry of* SiO_2 *and the Si-*SiO_2 *Interface - 3*, H. Z. Massoud, E. H. Poindexter, and C. R. Helms, Eds., vol. 96-1, p. 214. The Electrochemical Society, Pennington, NJ, 1996. 23, 23

[45] P. M. Lenahan and P. V. Dressendorfer, "Hole Traps and Trivalent Silicon Centers in Metal/Oxide/Silicon Devices," *Journal of Applied Physics*, vol. 55, pp. 3495, 1984. 23, 23

[46] L. Lipkin, L. Rowan, A. Reisman, and C. K. Williams, "Correlation of Fixed Positive Charge and E'_γ Centers as Measured via Electron Injection and Electron Paramagnetic Resonance," *Journal of Electrochemical Society*, vol. 138, pp. 2050, 1991. 23

[47] J. R. Schwank, D. M. Fleetwood, P. S. Winokur, P. V. Dressendorfer, D. C. Turpin, and D. T. Sanders, "The Role of Hydrogen in Radiation-Induced Defect Formation in Polysilicon Gate MOS Devices," *IEEE Transactions on Nuclear Science*, vol. 34, pp. 1152, 1987. 23, 27

[48] B. J. Mrstik and R. W. Rendell, "Si-SiO_2 Interface State Generation During X-Ray Irradiation and During Post-Irradiation Exposure to a Hydrogen Ambient," *IEEE Transactions on Nuclear Science*, vol. 38, pp. 1101, 1991. 23, 27, 32, 32, 33, 33, 33, 33, 36, 36, 84

[49] M. R. Shaneyfelt, J. R. Schwank, D. M. Fleetwood, P. S. Winokur, K. L. Hughes, and F. W. Sexton, "Field Dependence of Interface-Trap Buildup in Polysilicon and Metal Gate MOS Devices," *IEEE Transactions on Nuclear Science*, vol. 37, pp. 1632, 1990. 23, 27, 30, 32, 32, 33, 46

[50] A. J. Lelis and T. R. Oldham, "The Nature of the Trapped Hole Annealing Process," *IEEE Transactions on Nuclear Science*, vol. 36, pp. 1808, 1989. 24, 25

[51] R. C. Hughes and C. H. Seager, "Hole Trapping, Recombination and Space Charge in Irradiated Sandia Oxides," *IEEE Transactions on Nuclear Science*, vol. 30, pp. 4049, 1983. 24

[52] S. Manzini and A. Modelli, "Tunneling Discharge of Trapped Holes in Silicon Dioxide," in *Insulating Films on Semiconductors*, J. F. Verveij and D. R. Woltjer, Eds., p. 112. Elsevier Science Publishers B. V., North-Holland, 1983. 24, 25, 60

[53] S. C. Witczak, S. L. Kosier, R. D. Schrimpf, and K. F. Galloway, "Synergetic Effects of Radiation Stress and Hot-Carrier Stress on the Current Gain on NPN Bipolar Junction Transistors," *IEEE Transactions on Nuclear Science*, vol. 41, pp. 2412, 1994. 24, 25

[54] P. J. McWhorter, S. L. Miller, and W. M. Miller, "Modeling the Anneal of Radiation-Induced Trapped Holes in a Varying Thermal Environment," *IEEE Transactions on Nuclear Science*, vol. 37, pp. 1682, 1990. 24, 60

[55] F. B. McLean, "A Direct Tunneling Model of Charge Transfer at the Insulator-Semiconductor Interface in MIS Devices," Tech. Rep. HDL-TR-1765, U. S. Government, Oct. 1976. 24

[56] T. R. Oldham, A. J. Lelis, and F. B. McLean, "Spatial Dependence of Trapped Holes Determined from Tunneling Analysis and Measured Annealing," *IEEE Transactions on Nuclear Science*, vol. 33, pp. 1203, 1986. 24

[57] D. M. Fleetwood, L. C. Riewe, and J. R. Schwank, "Radiation Effects at Low Electric Fields in Thermal, SIMOX, and Bipolar-Base Oxides," *IEEE Transactions on Nuclear Science*, vol. 43, pp. 2537, 1996. 24, 60

[58] R. J. Milanowski, M. P. Pagey, A. I. Matta, L. W. Massengill, B. L. Bhuva, and S. E. Kerns, "Combined Effect of X-Irradiation and Forming Gas Anneal on the Hot-Carrier Response of MOS Oxides," *IEEE Transactions on Nuclear Science*, vol. 40, pp. 1360, 1993. 25

[59] Edward H. Poindexter, "MOS Interface States : Overview and Physiochemical Perspective," *Semiconductor Science and Technology*, vol. 4, pp. 961, 1989. 25

[60] P. J. McWhorter and P. S. Winokur, "Simple Technique for Separating the Effects of Interface Traps and Trapped-Oxide Charge in Metal-Oxide-Semiconductor Transistors," *Applied Physics Letters*, vol. 48, pp. 133, 1986. 25

[61] F. W. Sexton and J. R. Schwank, "Correlation of Radiation Effects in Transistors and Integrated Circuits," *IEEE Transactions on Nuclear Science*, vol. 32, pp. 3975, 1985. 25

[62] K. F. Galloway, C. L. Wilson, and L. C. Witte, "Charge-Sheet Model Fitting to Extract Radiation-Induced Oxide and Interface Charge," *IEEE Transactions on Nuclear Science*, vol. 32, pp. 4461, 1985. 25

[63] A. R. Hart, J. B. Smyth Jr., V. A. J. van Lint, D. P. Snowden, and R. E. Leadon, "Hardness Assurance Considerations for Long Term Ionizing Radiation Effects on Bipolar Structures," *IEEE Transactions on Nuclear Science*, vol. 25, pp. 1502, 1978. 25

[64] S. K. Lai, "Two-Carrier Nature of Interface-State Generation in Hole Trapping and Radiation Damage," *Applied Physics Letters*, vol. 39, pp. 58, 1981. 27

[65] S. K. Lai, "Interface Trap Generation in Silicon Dioxide when Electrons are Captured by Trapped Holes," *Journal of Applied Physics*, vol. 54, pp. 2540, 1983. 27, 27

[66] F. J. Grunthaner, P. J. Grunthaner, and J. Maserjian, "Radiation-Induced Defects in SiO_2 as Determined with XPS," *IEEE Transactions on Nuclear Science*, vol. 29, pp. 1462, 1982. 27, 27

[67] D. L. Griscom, "Hydrogen Model for Radiation-Induced Interface States in SiO_2-on-Si Structures: A Review of the Evidence," *Journal of Electronic Materials*, vol. 21, pp. 763, 1992. 27, 29, 31

[68] Nelson S. Saks and Dennis B. Brown, "The Role of Hydrogen in Interface Trap Creation by Radiation in MOS Devices–A Review," in *Proceedings of the* 2nd *Symposium on the Physics and Chemistry of* SiO_2 *and the Si–*SiO_2 *Interface, St. Louis, MO*, C. R. Helms and B. E. Deal, Eds. May 18–21 1992, Plenum Press. 27

[69] N. S. Saks and R. W. Rendell, "The Time-Dependence of Post-Irradiation Interface Trap Build-Up in Deuterium-Annealed Oxides," *IEEE Transactions on Nuclear Science*, vol. 39, pp. 2220, 1992. 27, 29

[70] D. B. Brown and N. S. Saks, "Initial Hydrogen-Ion Profiles During Interface Trap Formation in MOS Devices," *IEEE Transactions on Nuclear Science*, vol. 39, pp. 2236, 1992. 27, 29, 33, 33, 37, 45, 46, 50

[71] D. L. Griscom, "Diffusion of Radiolytic Molecular-Hydrogen As a Mechanism for the Post-Irradiation Buildup of Interface States in SiO_2-on-Si Structures," *Journal of Applied Physics*, vol. 58, pp. 2524, 1985. 27

[72] P. M. Lenahan and J. F. Conley, "A Physically Based Predictive Model of Si/SiO_2 Interface Trap Generation Resulting from the Presence of Holes in the SiO_2," *Applied Physics Letters*, vol. 71, pp. 3126, 1997. 27, 33, 33, 33, 84

[73] G. Ristic, M. Pejovic, and A. Jaksic, "Modelling of Kinetics of Creation and Passivation of Interface Traps in Metal-Oxide-Semiconductor Transistors During Postirradiation Annealing," *Journal of Applied Physics*, vol. 83, pp. 2994, 1998. 27, 34, 37

[74] M. Pejovic, G. Risic, and A. Jaksic, "Formation and Passivation of Interface Traps in Irradiated n-Channel Power VSMOSFETs During Thermal Annealing," *Applied Surface Science*, vol. 108, pp. 141, 1997. 27, 34, 37

[75] N. S. Saks, D. B. Brown, and R. W. Rendell, "Effects of Switched Gate Bias on Radiation-Induced Interface Trap Formation," *IEEE Transactions on Nuclear Science*, vol. 38, pp. 1130, Dec. 1991. 27, 37, 38, 39, 83

[76] T. R. Oldham, F. B. McLean, H. E. Boesch Jr., and J. M. McGarrity, "An Overview of Radiation-Induced Interface Traps in MOS Structures," *Semiconductor Science and Technology*, vol. 4, pp. 986, 1989. 27, 27

[77] K. L. Brower, "Kinetics of H_2 Passivation of P_b Centers at the (111) Si-SiO_2 Interface," *Physical Review B*, vol. 38, pp. 9657, 1988. 27

[78] N. S. Saks and D. B. Brown, "Interface Trap Formation Via the Two-Stage H^+ Process," *IEEE Transactions on Nuclear Science*, vol. 38, pp. 1848, 1989. 29, 31

[79] P. S. Winokur, H. E. Boesch Jr., J. M. McGarrity, and F. B. McLean, "Field- and Time-Dependent Radiation Effects at the SiO_2/Si Interface of Hardened MOS Capacitors," *IEEE Transactions on Nuclear Science*, vol. 24, pp. 2113, 1977. 30

[80] P. S. Winokur, H. E. Boesch Jr., J. M. McGarrity, and F. B. McLean, "Two-Stage Process for Buildup of Radiation-Induced Interface States," *Journal of Applied Physics*, vol. 50, pp. 3492, 1979. 30

[81] P. S. Winokur and Jr. H. E. Boesch, "Interface-State Generation in Radiation-Hard Oxides," *IEEE Transactions on Nuclear Science*, vol. 27, pp. 1647, 1980. 30

[82] P. S. Winokur, E. B. Errett, D. M. Fleetwood, P. V. Dressendorfer, and D. C. Turpin, "Optimizing and Controlling the Radiation Hardness of a Si-Gate CMOS Process," *IEEE Transactions on Nuclear Science*, vol. 32, pp. 3954, 1985. 30

[83] M. R. Shaneyfelt, J. R. Schwank, D. M. Fleetwood, P. S. Winokur, K. L. Hughes, G. L. Hash, and M. P. Connors, "Interface-Trap Buildup Rates in Wet and Dry Oxides," *IEEE Transactions on Nuclear Science*, vol. 39, pp. 2244, 1992. 30

[84] J. F. Conley and P. M. Lenahan, "Room Temperature Reactions Involving Silicon Dangling Bond Centers and Molecular Hydrogen in Amorphous SiO_2 Thin Films on Silicon," *Applied Physics Letters*, vol. 62, pp. 40, 1993. 33, 84

[85] N. Saks and R. Klein, "Effects of Hydrogen Annealing After Channel Hot Carrier Stress," *J. Microelectron. Eng., Proc. INFOS'93*, vol. 22, pp. 265, 1993. 33

[86] N. S. Saks, R. B. Klein, R. E. Stahlbush, B. J. Mrstik, and R. W. Rendell, "Effects of Post-Stress Hydrogen Annealing on MOS Oxides After Co^{60} Irradiation or Fowler-Nordheim Injection," *IEEE Transactions on Nuclear Science*, vol. 40, pp. 1341, 1993. 33

[87] L. Colalongo, M. Valdinoci, and M. Rudan, "An Efficient Numerical Method to Solve the Time-Dependent Semiconductor Equations Including Trapped Charge," *Simulation of Semiconductor Devices and Processes*, vol. 6, pp. 82, 1995. 43

[88] William H. Press, Saul A. Teukolsky, William T. Vetterling, and Brian P. Flannery, *Numerical Recipes in C: The Art of Scientific Computing*, Cambridge University Press, 2nd edition edition, 1992. 43

[89] R. Barrett, M. Berry, T. F. Chan, J. Demmel, J. Donato, J. Dongarra, V. Eijkhout, R. Pozo, C. Romine, and H. Van der Vorst, *Templates for the Solution of Linear Systems: Building Blocks for Iterative Methods*, SIAM, Philadelphia, PA, 2nd edition edition, 1994. 43

[90] B. S. Polsky and J. S. Rimshans, "Half-Implicit Difference Scheme for Numerical Simulation of Transient Processes in Semiconductor Devices," *Solid-State Electronics*, vol. 29, pp. 321, 1986. 43

[91] W. L. Warren, D. M. Fleetwood, J. R. Schwank, M. R. Shaneyfelt, B. L. Draper, P. S. Winokur, M. G. Knoll, K. Vanheusden, R. A. B. Devine, L. B. Archer, and R. M. Wallace, "Protonic Nonvolatile Field Effect Transistor Memories in $Si/SiO_2/Si$ Structures," *IEEE Transactions on Nuclear Science*, vol. 44, pp. 1789, 1997. 50

[92] H. E. Boesch Jr. and T. L. Taylor, "Charge and Interface State Generation in Field Oxides," *IEEE Transactions on Nuclear Science*, vol. 31, pp. 1273, 1984. 53

[93] J.-P. Colinge, *Silicon-On-Insulator Technology: Materials To VLSI*, pp. 96–97, Kluwer Academic Publishers, Boston, 1991. 54

[94] H. E. Boesch Jr., T. L. Taylor, L. Hite, and W. Bailey, "Time-Dependent Hole and Electron Trapping Effects in SIMOX Buried Oxides," *IEEE Transactions on Nuclear Science*, vol. 37, pp. 1982, 1990. 54, 65

[95] J.-P. Colinge, *Silicon-On-Insulator Technology: Materials To VLSI*, pp. 140–142, Kluwer Academic Publishers, Boston, 1991. 54

[96] SPAWAR Systems Center, San Diego, CA . 56

[97] D. J. Foster, "Subthreshold Currents in CMOS Transistors Made on Oxygen-Implanted Silicon," *Electronics Letters*, vol. 19, pp. 684, 1983. 56

[98] R. W. Dutton and Z. Yu, *Technology CAD: Computer Simulation of IC Processes and Devices*, Kluwer Academic Publications; Norwell, MA, 1993. 58

[99] SILVACO International, *SILVACO Virtual Wafer Fab (VWF), ATLAS, ATHENA, and Interactive Tools Users Manuals*, 1998. 58, 60, 60

[100] J. L. Leray, "Effet de la dose dans les componsants MOS," Short Course, Conference RADECS-La Grande Motte, USTL-CEM, BP 083, 34095 Montpellier cedex 05, France, 1989. 60, 61

[101] J. F. Conley, P. M. Lenahan, and B. D. Wallace, "Quantitative Model of Radiation-Induced Charge Trapping in SiO_2," *IEEE Transactions on Nuclear Science*, vol. 44, pp. 1804, 1997. 62, 62

[102] S. M. Sze, *Physics of Semiconductor Devices*, pp. 438–440, Wiley Eastern Limited, New York, 1981. 63, 63

[103] J. R. Adams and F. N. Coppage, "Field Oxide Inversion Effects in Irradiated CMOS Devices," *IEEE Transactions on Nuclear Science*, vol. 23, pp. 1604, 1976. 71

[104] S. H. Goodwin and J. D. Plummer, "Electrical Performance and Physics of Isolation Region Structures for VLSI," *IEEE Transactions on Electron Devices*, vol. 31, pp. 861, 1974. 72